Dissertation
submitted to
the Combined Faculties for
the Natural Sciences and for Mathematics
of the Ruperto-Carola University of Heidelberg, Germany
for the degree of
Doctor of Natural Sciences

put forward by
Dipl. Phys. Barbara Luise May
Born in Ochsenfurt
Oral examination: 02.12.2009

Radiocarbon microanalysis on ice impurities for dating of Alpine glaciers

Referees: Prof. Dr. Werner Aeschbach-Hertig
Prof. Dr. Augusto Mangini

Abstract

The main objective of this thesis is the deployment of radiometric dating on Alpine ice archives, where conventional, stratigraphical dating techniques fail. To this end a ^{14}C analysis of particulate and, in a novel attempt, also of dissolved organic carbon contained in the ice matrix is developed. Aimed at minimizing the required ice sample size, the designed ice processing line allows for handling of up to 700 g ice and is shown to involve blank levels small enough to ensure reliable ^{14}C analyses down to a modern carbon fraction of f_m = 0.33 at a minimum sample mass of about 20 μg carbon.
Deployment of the system at the high altitude drilling area Colle Gnifetti (Monte Rosa, 4 550 m.a.s.l.) and, in contrast, to an ice core at the low altitude Vadret dal Corvatsch ice cap (Upper Engadin, 3 433 m.a.s.l.) reveals a quite significant ^{14}C excess, not explained by any blank contribution and in contrast to the expected age range. The hypothesis that in situ produced ^{14}C might contribute to the ^{14}C content of dissolved organic carbon reveals strong short comings in applying this carbon fraction for radiometric dating of glacier ice, but also the new possibility to infer past accumulation changes.
The particulate fraction, mostly unaffected by excess ^{14}C, allows to connect an upper age limit of (7.5 $\pm$ 0.2) ka with the base of the Vadret dal Corvatsch, suggesting a minimal glacier extent during that time. For the Colle Gnifetti drill sites a tentative upper age constrain indicates pre-Holocene ice remains in the basal layer, while an enhanced ^{14}C profile in the dissolved organic carbon fraction at core bottom suggests a large in situ produced ^{14}C contribution most likely as a result of low accumulation during much colder periods.

Zusammenfassung

Ziel dieser Arbeit ist die Anwendung der Radiokarbon Datierungsmethode auf die Bereiche alpiner Eisarchive, in denen konventionelle, stratigraphische Datierungstechniken versagen. Zu diesem Zweck wird eine Methode entwickelt, um den in der Eismatrix enthaltenen partikulären, und zum ersten Mal auch den gelösten organischen Kohlenstoff für die ^{14}C Analyse zu extrahieren. Mit der auf möglichst kleine Eisprobenmengen ausgerichteten Extraktionsmethode können Eisproben bis zu 700 g aufbereitet werden. Es zeigt sich, dass der methodische Blank klein genug ist, um verlässliche ^{14}C Messungen bis zu einem modernen Kohlenstoffanteil von f_m = 0.33 an einer minimalen Probenmenge von etwa 20 μg Kohlenstoff zu ermöglichen.
Die Methode wird auf Eisbohrkerne des hochalpinen Colle Gnifetti Gletschers (Monte Rosa, 4 550 m.a.s.l.) und zum Vergleich auf einen Eisbohrkern der tiefer gelegenen Vadret dal Corvatsch Gletscherkappe (Oberengadin, 3 433 m.a.s.l.) angewendet. Dabei findet sich eine signifikante Menge an Exzess ^{14}C, welche nicht durch Blankbeiträge erklärt werden kann und im Gegensatz zum erwarteten Altersbereich steht. Die Hypothese, dass in situ produziertes ^{14}C zum ^{14}C Gehalt des gelösten organischen Kohlenstoffes beiträgt, erweist sich als starke Einschränkung für die Anwendung von ^{14}C in gelöstem organischen Kohlenstoff zur Datierung, bietet aber eine Möglichkeit auf Akkumulationsänderungen in der Vergangenheit zu schließen.
Die partikuläre Fraktion des organischen Kohlenstoffs ist nahezu unberührt von diesem ^{14}C Exzess und ermöglicht somit die Bestimmung einer oberen Altersgrenze von (7.5 $\pm$ 0.2) ka für das Basaleis des Vadret dal Corvatsch Kerns, welche einen minimalen Gletscherstand in dieser Zeit andeutet. Für den Colle Gnifetti Gletscher konnte eine vorläufige Altersgrenze festgelegt werden, welche Eis aus dem letzten Glazial andeutet. Ein Profil von überhöhten ^{14}C Konzentrationen im gelösten organischen Kohlenstoff des unteren Kernbereichs deutet auf eine große in situ Produktionsrate hin, welche höchstwahrscheinlich auf eine sehr viel geringere Akkumulationsrate in kälteren Zeiten zurückzuführen ist.

Contents

1 Introduction

The fourth assessment report on climate change states an increase of the global mean temperature in the last 100 years of on average 0.74 °C (0.56 °C to 0.92 °C) very likely due to anthropogenic causes. Palaeoclimatic studies furthermore suggest, that the second half of the 20th century was warmer than any other period in at least the last 1 300 years in the Northern Hemisphere. However, the maximum warmth period in the Holocene occurred in Europe and North America between 11 000 and 5 000 years ago. In this time, glaciers were in these regions smaller than today or even completely absent (IPCC, 2007).

To determine past climatic conditions, a variety of proxies can be measured in different climate archives, like ice cores, tree rings, stalagmites or sea sediments over different time intervals from 1 000 to several 1 000 000 years. Ice cores from polar regions allow the reconstruction of the past atmospheric composition and temperature changes in the last 800 000 years in Antarctica (EPICA, 2004) and 120 000 years in Greenland (NGRIP, 2004). Mid- and low-latitude, high altitude mountain glaciers cover less time, but are important for recording the local climate variability in a region close to the majority of human population. The close vicinity to human activities allows the study of the anthropogenic impact on climate forcing by short-lived atmospheric substances with a non-uniform global distribution and highest concentration close to the source (e.g. aerosol). Ice core records from mountain glaciers, i.e. from the Alps, being suspected to contain climate information of the last 10 000 years, have been investigated for several decades (Cecil *et al.*, 2004). The small scaled glaciers thereby challenge climate reconstruction, having complex ice flow dynamic especially at the bedrock and complicate deposition sampling behaviour. This complexity affects not only the record of climate proxies, but also the ability to date the ice.

Dating remains for most climate archives a challenge, and is especially difficult for ice cores from mountain glaciers. Standard dating methods for sedimentary archives, such as annual layer counting or the identification of absolute time horizons from e.g. volcanic eruptions, become, due to the the rapid flow induced layer thinning, highly uncertain after a few hundred years of age (Wagenbach and Geiss, 1989) and are limited to the upper 40 - 50 % of the core. Due to the complex bedrock geometry, theoretical ice flow model approaches can also not be applied to the lowest core sections. Finally, other non-sedimentary ice bodies, like small ice caps, ice wedges or cave ice, where ice formation processes are unknwon or disturb any seasonal signal, can not be dated at all.

Therefore, a dating technique is needed, which is independent of changes in climatic conditions and the ice formation process. Radionuclides, like ^{210}Pb, ^{39}Ar or radiocarbon (^{14}C),

offer here an ideal dating tool. ^{210}Pb allows dating only over the last 200 years, due to its short half life time. The ^{39}Ar concentration in ice is too low for dating ice masses of less than 1 kg. However, ^{14}C dating has been a standard dating method for archeology and geology and offers the best solution for dating ages up to at least 20 000 years (Lal *et al.*, 1990). Until now, the quality of ^{14}C analysis did not allow reliable ^{14}C measurements on the very small carbon masses required for ice core dating. Micro-graphitisation (Steier *et al.*, 2006) and gas ion source (Ruff, 2008) systems for Accelerated Mass Spectrometry (AMS) have only in the last years improved enough that ^{14}C analysis on carbon masses as low as 10 μgC became possible.

Concentrations of organic molecules in ice are extremely low and reservoir effects for organic matter might result in an overestimation of the surrounding ice age. Especially the particulate organic carbon (POC) fraction has extremely low concentrations (10 - 50 ppb) and may be biased by an inbuilt ^{14}C age from old soil or combustion of old organic matter (Jenk *et al.*, 2006). The dissolved organic carbon (DOC) fraction, being formed from secondary organic aerosols (SOA) is assumed to have a recent radiocarbon age at deposition, as SOA is mostly released by the living biosphere (Szidat *et al.* (2007); Gelencsér *et al.* (2007)) and is present in the ice in larger concentrations (50 - 100 ppb). DOC offers therefore the best chance to constrain the age of glaciers in their lower core sections by ^{14}C dating on ice masses < 1 kg, which is a reasonable sample size for analyses on ice cores.

Aim of the thesis is the development of a routine ^{14}C analysis of dissolved and particulate organic carbon fractions in ice dedicated to dating the lower sections of Alpine ice bodies. For this purpose, the present work comprises:

1. The development of a suitable extraction method for organic matter in the form of DOC and POC from ice sample volumes as small as possible.

2. The investigation of ^{14}C measurements on DOC (and POC) for different ice samples to determine the ability of DO^{14}C (and PO^{14}C) for dating Alpine ice by discussing problems and source contributions to the ^{14}C fractions and eventually the establishing of age constraints.

3. The testing and deploying of this radiometric dating method on ice cores from various Alpine glaciers distinguished by their depositional regime and depth age distribution.

2 Background

At present time about 10 % of Earth's land surface is covert with ice, but only 1%, like mountain glaciers, is in close proximity to humane activities. Ice cores from polar ice sheets and mountain glaciers provide a unique climate archive for temperature and precipitation rates through their isotopic composition (Dansgaard, 1964) as well as for atmospheric trace elements and trace gases within the enclosed air bubbles (Petit *et al.*, 2000). Depending on accumulation rate, ice thickness and flow dynamic of the ice, an ice core can cover a time period of 100 up to several 100 000 years.
While polar ice sheets cover a large time frame up to 800 000 years (EPICA, 2004), they are relatively detached from anthropogenic sources. Ice cores from mountain glaciers, e.g. from the Alps, are suspected to cover only time periods of $\approx$ 10 000 years, but are closer to human activities and thus can give detailed information on the anthropogenic impact on the late Holocene climate. However, the small scales, complex flow dynamics and heterogeneous accumulation of mountain glaciers makes climate reconstructions difficult (Wagenbach *et al.*, 1992) and especially determination of the age-depth relationship a big challenge. Dating techniques, which are relative successfully applied to polar ice cores, prove less effective for Alpine ice archives.

The following chapters will provide basic information about mechanics and dynamics of ice and mountain glaciers. Different dating techniques for Alpine ice cores are introduced and their advantages and disadvantages discussed. In order to illustrate the potential and problems of radiocarbon dating on organic matter in ice, the radiocarbon cycle is described and the different fractions of organic matter deposited in ice are discussed with respect to their sources and radiocarbon signatures.

2.1 Basics of ice and glaciers

For more details on the following subjects on ice and glacier physics reference is made to Paterson (1994) and Oeschger and Langway (1989).

2.1.1 Transformation processes of snow to ice

Mountain glaciers are called "cold" if the ice temperature is below 0°C all year round and "temperated" if the ice mass is at the melting point. Depending on the meteorological condi-

tions both types of glacier have different snow-ice transformation zones.

1. dry-snow zone: no melting occurs and the snow transforms into ice through settling, molecular diffusion, sublimation and coagulation of the snow flakes.

2. percolation zone: in summer, melt water penetrates a certain distance into the snow and refreezes, accelerating on its way the settling and coagulation of the snow flakes and forming ice layers and lenses.

3. wet snow zone: all snow since last summer is heated to 0°C.

4. superimposed ice zone: so much melt water is produced, that ice layer and lenses merge to a continuous mass at T < 0 °C.

5. ablation zone: in this area the glacier looses mass.

While cold glaciers can contain all of these zones (although not at once), temperated glaciers have per definition only superimposed ice and ablation zones. The transformation in dry-snow zones can take, depending on accumulation rates, up to a few hundred years. As soon as melt water is included, the ice formation process is much faster.

2.1.2 Mass balance of mountain glaciers

In time a glacier gains mass by accumulation processes, like snow deposition, avalanches or freezing of rain, while loosing mass by ablation processes, like melting, evaporation and removal of snow by wind. Investigating the gain and loss of matter on a certain area of a glacier and over a certain period of time Δt, the mass balance is given as:

$$b = \int_0^{\Delta t} (\dot{c} + \dot{a})\, dt \tag{2.1}$$

where b = local mass balance, $\dot{c} = \frac{\partial c}{\partial t}$ = accumulation rate and $\dot{a} = \frac{\partial a}{\partial t}$ = ablation rate within Δt. The area with b < 0 is called ablation zone of the glacier, while the area with b > 0 is called accumulation area. Both zones are separated by the equilibrium line. Integration over the whole glacier area gives the total mass balance:

$$B = \int_{A_c} b \cdot dA + \int_{A_a} b \cdot dA \tag{2.2}$$

with dA_c and dA_a being points in the accumulation and ablation areas. If B = 0 the glacier is in steady state and its geometry remains more or less the same. In steady state conditions a net-transport of ice from the accumulation to the ablation zone is required. This is achieved by combined flow and internal ice deformation processes.

2.2 Ice and glacier dynamics

In contrast to the large polar ice sheets of Antarctica and Greenland, mountain glaciers have small geometries, where their length and width is of a similar order to the total ice thickness. In addition, the location on a more or less steep bedrock leads to complex ice dynamic processes.

Being a viscous material, ice is deformed already at low stress values. The different directions of deformation ϵ_{ij}, one by normal stress (applied force and normal vector of the area are parallel) denoted by σ_{ii} and two by simple shear stress (applied force and normal vector of the area are perpendicular) denoted by τ_{ij} can be discussed separately.

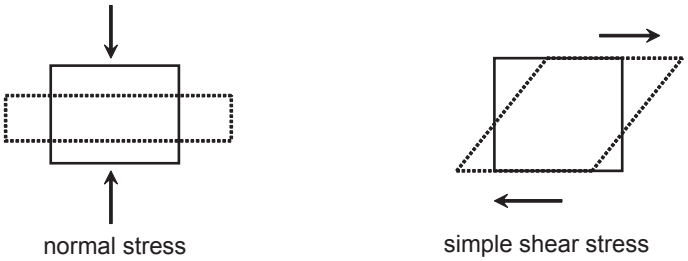

Figure 2.1: Deformation of an ice cube under normal und simple shear stress.

For all treatments of ice flow and deformation the constitutive relation between the amount and rate of deformation and the applied stress is necessary. This material property can be determined only empirically by experiments and is described by Glen's law giving the correlation between the deformation rate $\dot{\epsilon}_{ij}$ and the applied normal stress σ_{ii} and shear stress τ_{ij} respectively:

$$\begin{aligned} \dot{\epsilon}_{ii} &= C \cdot \sigma_{ii}^n \\ \dot{\epsilon}_{ij} &= C \cdot \tau_{ij}^n \end{aligned} \tag{2.3}$$

The first index gives the direction of the force, the second one represents the normal vector of the area. n is usually assumed a constant, while C depends on temperature, crystal size and impurity content. Empirical values for n are found to be between 1.5 and 4.2, but mostly n is set equal to 3. This law describes only a uni-axial compression or simple shear stress and its resulting strain or shear deformation. For the extension to the complex stress system in glaciers the law has to be generalised. Assuming ice is incompressible and an isotropic medium, the following final flow relation is found:

$$\begin{aligned} \dot{\epsilon}_{ii} &= C\tau^{n-1}\sigma_{ii} \\ \dot{\epsilon}_{ij} &= C\tau^{n-1}\tau_{ij} \end{aligned} \tag{2.4}$$

with τ being the effective deviator stress, a scalar entry independent of orientation and involving all 6 stress components. The deformation rate correlates with the velocity components by:

$$\dot{\epsilon}_{ij} = \frac{1}{2} \cdot \left(\frac{\partial v_i}{\partial r_j} + \frac{\partial v_j}{\partial r_i}\right) \tag{2.5}$$

To derive the velocity distribution of $\vec{v}(x, y, z)$, continuum mechanics yields the three fundamental equations for the conservation principal, which need to be closed by the flow law discussed above:

1. Conservation of mass

$$\frac{\partial \rho}{\partial t} + div(\rho \vec{v}) = 0 \tag{2.6}$$

2. Conservation of momentum

$$\underbrace{\frac{\partial \rho \vec{v}}{\partial t}}_{0} + div(\boldsymbol{\tau}) + \rho \vec{g} = 0 \tag{2.7}$$

3. Conservation of energy

$$\rho c \left(\frac{\partial T}{\partial t} \right) = div(K \cdot gradT) + \rho c \cdot \vec{v} \cdot gradT + trace(\boldsymbol{\tau} \dot{\boldsymbol{\epsilon}}) \tag{2.8}$$

The conservation of energy is usually neglected. The age-depth relationship in a glacier can be basically calculated from the velocity distribution through integrations along the flow lines, which in case of 1D reduces to the simple kinematic approach $dt = \frac{d\vec{r}(x,y,z)}{\vec{v}(x,y,z)}$ and is then given by:

$$t(z) = \int_0^z \frac{1}{v_z(z')} dz' \tag{2.9}$$

2.3 Dating of Alpine ice cores

In order to detect the climate change in ice cores drilled into glaciers, the age-depth relationship needs to be determined. The great ice sheets of Antarctica and Greenland can be well dated by annual layer counting. Dating of Alpine mountain glaciers is however due to the complex geometry, flow dynamic and accumulation regime more complicated and requires in most cases a combination of different methods.

2.3.1 Identifying time horizons

The first order of business in dating an Alpine ice core is the determination of absolute time horizons. The most prominent, the atomic bomb peak of 1963, is commonly identified by the enhanced tritium concentrations. Additionally, there are several well documented Saharan dust events during the 20th century, which can be easily identified in Alpine ice cores (Wagenbach and Geiss, 1989). The most common events are from 1971, 1947 and 1901/1902 AD and are often visible directly by an orange colouring of the firn. These absolute horizons allow a

reliable dating of the first 100 years and can be used to calibrate other dating techniques. They also provide a first estimate of the average surface accumulation rate.

Volcanic eruptions are often used as absolute time horizons. However, determination of a volcanic horizon in an ice core is a challenge and requires much care. Often dust, conductivity and ion records have to be combined to mark a possible volcanic signal in ice. There is a large record of historic eruptions available to date a volcanic horizon, but not every historically recorded volcano is recorded in an Alpine glacier. This leaves the problem of deciding, which eruption has been identified and results in large uncertainties. However, volcanic events may still be used to verify and tune an age-depth relationship derived by other dating techniques (Bohleber, 2008).

2.3.2 Annual layer counting

The main dating method used for sedimentary archives like the polar ice sheets and Alpine glaciers is the counting of annual layers visible in different records of the ice core. In the polar regions, seasonal variations are recorded in the water isotopes due to the strong temperature variations and can be counted down to large depth (Dansgaard, 1964). For Alpine glaciers, the accumulation varies during the year and precipitation is not uniformly sampled. A seasonal variation enclosed in the precipitation is thus not always distinguishable, especially for small accumulation rates. Other trace elements, like NH_4 or dust (e.g. Thompson *et al.* (1995); Maupetit *et al.* (1995)), contain a seasonal signal due to a seasonal source or the varying height of the tropospheric boundary layer. In winter, high Alpine glaciers lie in the free troposphere and are mostly cut off from any low level source regions, while in summer transport reaches high altitudes.
However, regardless which proxy is used for annual layer counting, the fast annual layer thinning in Alpine glaciers, the complex flow dynamic as well as natural variations in deposit and accumulation limit this dating method to the upper 40 - 50 % of the core and thus, depending on the accumulation rate, to 100 - 400 years. Also, counting of annual layers assumes that every year has been preserved and can be identified. Missing years or miscounting leads to a fast accumulating age error with depth.

2.3.3 Radiometric dating

There are mainly four radioactive elements with adequate half life times to allow dating in Alpine ice cores according to:

$$A = A_0 \cdot e^{-\lambda t} \tag{2.10}$$

λ is the decay constant and correlates with the half life time by $\lambda = \frac{ln2}{T_{1/2}}$ and A is the activity. The concentrations of ^{39}Ar ($T_{1/2}$ = 269 a) and ^{32}Si ($T_{1/2}$ = 276 a) in ice are both too low to allow reliable dating of ice samples smaller than 1 kg at present time. With a half life time of 22.3 years, ^{210}Pb can be used to date 200 years, if the initial concentration is known or can be estimated well enough (e.g. Gäggeler *et al.* (1983)).

Radiocarbon dating is the most promising radiometric dating technique for the lower core sections, having a half life time of $T_{1/2}$ = 5 370 a, which allows dating of up to 20 000 years. The low organic carbon concentrations in ice require now, due to the steady improvement of ^{14}C measurement precision over the last decades, ice sample sizes of less than 1 kg to obtain enough carbon mass for ^{14}C analysis, which prohibits a high time resolution, but would still help to constrain the age at the bottom of the core. While radiocarbon dating on organic matter in ice is not yet applied in a routine way, first successful analyses have been reported by Ruff (2008) and Jenk *et al.* (2009).

2.3.4 Ice dynamic modeling

Ice dynamic models are typically used to extrapolate the age-depth relationship down to larger core depth.

Nye's model

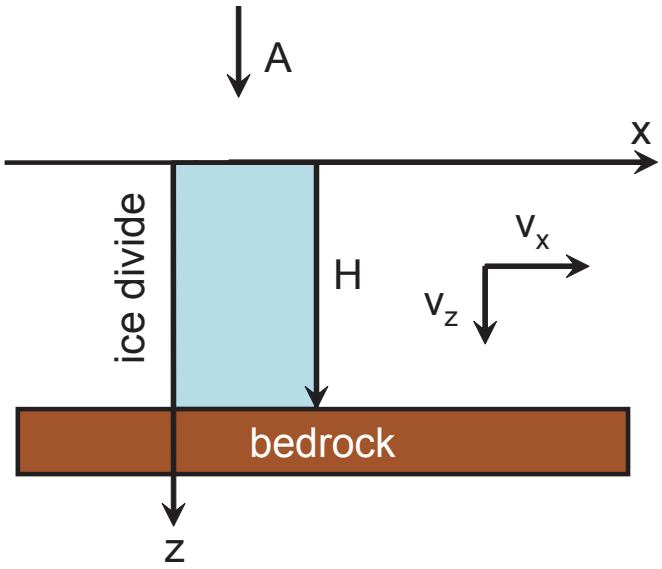

Figure 2.2: 2D Mye model on a flat bedrock: assumptions are (1) infinite extension in x-direction parallel to bedrock, (2) constant glacier thickness H (steady state) and (3) constant accumulation rate A.

Nye's model assumes a 2D ice slap with an ice thickness H(x,t) parallel to bedrock ($\frac{\partial H}{\partial x} = 0$). Since mass conservation has to be adhered, the mass added to the top of the ice-slap by accumulation A(x,t) has to be counteracted by a mass flow in x-direction over the complete ice thickness H. Integrating equation (2.6) over z from top (z = 0) to bedrock (z = H(t)) gives:

$$\int_0^{H(t)} \frac{\partial \rho}{\partial t}\, dz + \int_0^{H(t)} div(\rho \cdot \vec{v})\, dz = 0$$

For an incompressible medium follows:

$$\begin{aligned} \int_0^{H(t)} div(\vec{v})\, dz &= 0 \\ \int_0^{H(t)} (\frac{\partial v_x}{\partial x} + \frac{\partial v_z}{\partial z})\, dz &= 0 \end{aligned} \tag{2.11}$$

The system is assumed to be in steady state, meaning H(t) = H is constant in time. Also v_z(0) is given by the constant accumulation rate A(x,t) = A and v_z(H) = 0, since the ice is assumed to be frozen to the ground. Finally a mean horizontal velocity v_x(x,y,t) = $\bar{v}_x$(x) is assumed.

$$\begin{aligned} \frac{\partial \bar{v}_x}{\partial x} \cdot H &= A \\ \bar{v}_x &= \frac{A}{H} \cdot x \end{aligned} \tag{2.12}$$

Using this approximation, the dependence of v_z on z can be estimated for an incompressible medium as follows:

$$\begin{aligned} \frac{\partial v_x}{\partial x} + \frac{\partial v_z}{\partial z} &= 0 \\ \int_0^z \frac{\partial v_z}{\partial z} dz &= -\int_0^z \frac{A}{H} dz \\ v_z(z) - A &= -\frac{A}{H} \cdot z \\ v_z(z) &= A \cdot (1 - \frac{z}{H}) \end{aligned} \tag{2.13}$$

Together with equation (2.9) this gives the age-depth relation:

$$t_{Nye}(z) = -\frac{H}{A} \cdot ln(1 - \frac{z}{H}) \tag{2.14}$$

Ice-slab model

The ice-slab model assumes a parallel-sided slab of ice with the extension in x- and y-direction being large compared to the ice thickness H(x,y,t). In steady state H(x,y,t) = H is constant in time and space. The ice-slap is frozen to a rough plane with slope α, providing the only driving stress component. Considering a column of ice perpendicular to the plane with a constant ice density ρ, the gravitational force has a component parallel to the slope called the driving stress. In equilibrium this gravitational pull is balanced by the shear stress τ_{xz}.

$$\tau_{xz} = \rho g sin\alpha \cdot z \tag{2.15}$$

If τ_{xz} is the only non-zero stress component, the flow lines are parallel to the surface and the flow is called laminar. In this case the z-component of the velocity is zero and therefore

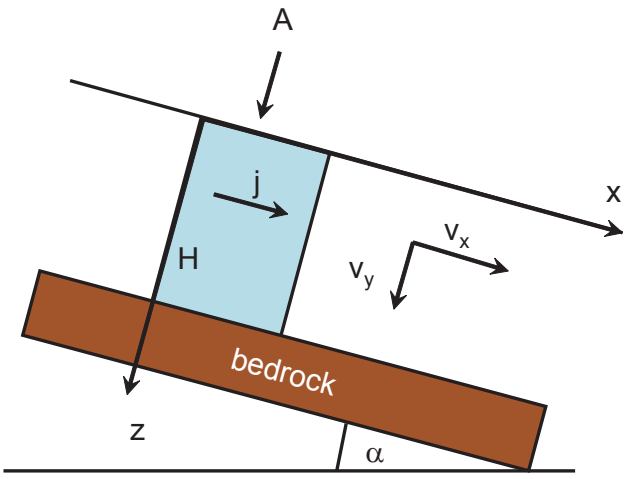

Figure 2.3: 2D ice slap model on an inclined bedrock: assumptions are (1) infinite extension in x-direction, (2) constant glacier thickness H (steady state) and (3) constant accumulation rate A.

$\dot{\epsilon} = \frac{1}{2}\frac{dv_x}{dz}$. Combining this relation with the general flow equation 2.4 and with Equation 2.15 and integrating over z, gives:

$$\begin{aligned}
\int_0^z \frac{1}{2}\frac{dv_x}{dz'}dz' &= \int_0^z C(\rho g sin\alpha)^n (z')^n dz' \\
v_x(z) - v_x(0) &= \frac{2C}{n+1}(\rho g sin\alpha)^n \cdot z^{n+1} \\
v_x(H) - v_x(0) &= \frac{2C}{n+1}(\rho g sin\alpha)^n \cdot H^{n+1}
\end{aligned}$$

Thus the vertical velocity v_x depends on z:

$$v_x(z) = v_x(0)\left(1 - \left(\frac{z}{H}\right)^{n+1}\right) \tag{2.16}$$

The velocity decreases with depth z and as n ≈ 3, most of the decrease takes place near the bedrock. Adhering to the boundary condition of the ice being frozen to the bedrock v_x(H) = 0 and integrating Equation 2.16 over the complete ice thickness gives the average velocity in x-direction $\bar{v}_x = \frac{1}{H}\int_H^0 v_x(z)dz$.

$$\begin{aligned}
\bar{v}_x &= \frac{2C}{n+1}(\rho g sin\alpha)^n \frac{1}{H}\int_H^0 \left(z^{n+1} - H^{n+1}\right) dz \\
\bar{v}_x &= \frac{2C}{n+1}(\rho g sin\alpha)^n \frac{1}{H}\left(-\frac{1}{n+2}H^{n+2} + H^{n+2}\right) \\
\bar{v}_x &= \frac{2C}{n+2}(\rho g sin\alpha)^n H^{n+1} \\
\bar{v}_x &= \frac{n+1}{n+2}v_x(0)
\end{aligned} \tag{2.17}$$

Note that up to this point the laminar solution does not require any accumulation since $v_x(0)$ does not vary with x. In a crude approach, however, the conservation of mass results in the dependence of v_x on x, given by $\bar{v}_x = \frac{A}{H}\, x$. From this follows:

$$v_x(x,z) = \frac{n+2}{n+1}\frac{A}{H} \cdot\ x\ \left(1 - \left(\frac{z}{H}\right)^{n+1}\right) \tag{2.18}$$

Assuming once again an incompressible medium, thus deploying Equation 2.6 in the form $\frac{\partial v_x}{\partial x} + \frac{\partial v_z}{\partial z} = 0$ and considering the boundary condition of $v_z(0) = A$:

$$v_z(z) = A\left(1 - \frac{n+2}{n+1}\left(\frac{z}{H}\right) + \frac{1}{n+1}\left(\frac{z}{H}\right)^{n+2}\right) \tag{2.19}$$

For n = 3 this is:

$$v_z(z) = A\left(1 - \frac{5}{4}\left(\frac{z}{H}\right) + \frac{1}{4}\left(\frac{z}{H}\right)^{5}\right) \tag{2.20}$$

This polynomial equation can not be integrated analytically to give age versus depth (see Equation 2.9) and therefore the age-depth relationship has to be obtained by numerical integration.

As can be seen, even the 2D modeling of ice dynamics is very complex and many assumptions are generally made, which do not represent real conditions. These problems result in strong uncertainties in the lowest core sections.

In conclusion, dating of Alpine ice cores is a challenge. While the first few hundred years can be dated well enough, although with some difficulty, the typical dating techniques fail for the lower core sections. Radiometric dating with ^{14}C seems at the moment the best solution to extend the age-depth relationship derived for the upper core section down to the bottom of the core.

2.4 Radiocarbon in organic matter

For radiocarbon dating, organic matter must be extracted from the ice archive. However, even if a sufficient amount of carbon is extracted, its ^{14}C signature might not correlate to the age of the surrounding ice, depending on the age of the organic matter at deposition on the glacier.

2.4.1 Organic matter in ice

Organic matter is incorporated into glacier ice either in the form of dissolved organic carbon (DOC) or as particulate organic carbon (POC). Both fractions origin from the atmospheric organic aerosol body.

Atmospheric aerosols are defined as the suspension of liquid or solid particles with a diameter of 10 nm to 100 μm in a gas, usually air (Junge, 1963). This definition covers many different aerosol species with a wide range of physical and chemical properties. One possible classification is through their production process:

1. Dispersion is the direct bulk-to-particle production from soils and liquid surfaces through raising up of dust from the ground or through bursting of bubbles on the ocean surface. These particles are called primary aerosol and have sizes of 1 - 10 μm.
2. Nucleation is the gas-to-particle production from the gaseous phase, where particles evolve from gas molecules through condensation in an over-saturated environment or on an already existing particle. These particles are called secondary aerosol and have radii under 0.1 μm.

DOC and POC are commonly distinguished by the particle size, POC being the fraction that can be filtered. POC is therefore dominated by the primary aerosol, while the DOC fraction origins from the secondary aerosol fraction.

Gelencsér (2005) summarises the different natural and anthropogenic sources of primary and secondary organic aerosol. Primary organic aerosol consists of plant debris, microorganisms (like bacteria) and soil particles as well as contributions from biomass burning. The gaseous precursors for secondary organic aerosol are emitted from the living biosphere as e.g. terpens as well as from the soil in the form of volatile organic carbon (VOC). Additionally, anthropogenic sources like fossil fuel combustion, land use change and wood combustion contribute to both fractions.

During their atmospheric lifetime, aerosols take part in various processes, that change their size and chemical composition. The small, secondary aerosol particles thus coagulate within hours to larger compounds with radii < 1 μm. Water vapour and other gaseous components condense on their surface and they are incorporated into water drops. The majority of particles has a size of < 0.1 μm, while the bulk of carbon mass is contained in the larger sizes.

Deposition of aerosol happens through sedimentation or rain-out. The larger particles have a relative short lifetime, since they are fast deposit through sedimentation and thus quicker

removed from the atmosphere. Small particles with a size < 1μm act as water condensation nucleii and are therefore deposit through precipitation.

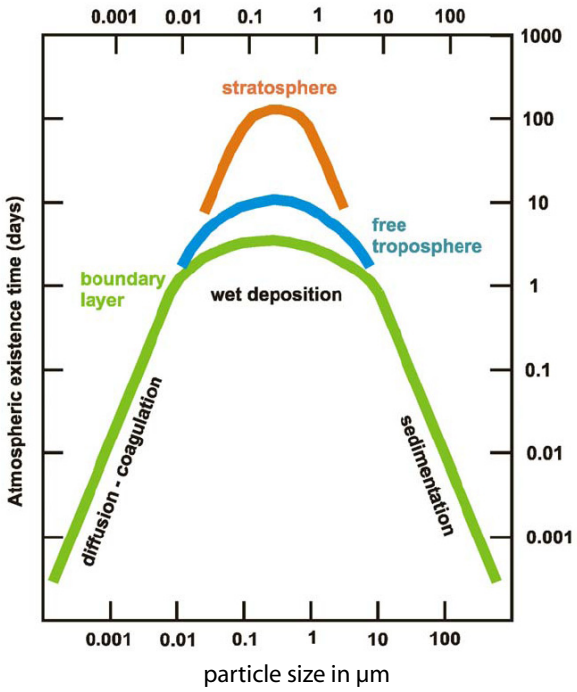

Figure 2.4: Typical lifetime of atmospheric aerosol depending on particle size and atmospheric height (altered from Jaenicke (1987)).

It follows, that organic matter accumulated on high altitude glaciers is dominated by particles in the smaller size mode. Since POC contains mainly the large, primary aerosol particles, its concentration in ice is relatively low at 10 - 50 ppb for pre-industrial ice. The DOC concentration, on the other hand, contains mainly secondary aerosol and for high Alpine glaciers, the pre-industrial DOC level is on average between 50 - 100 ppb.

2.4.2 The radiocarbon cycle

Carbon is a major element of life and can be found in a lot of different organic and inorganic components in the atmosphere, the biosphere and in ground soil. The most abundant components are the two stable isotopes, ^{12}C and ^{13}C, followed by the radioactive isotope ^{14}C with a natural atom ratio of $\frac{^{14}C}{^{12}C} = 10^{-12}$.

Radiocarbon is produce continuously mainly in the lower stratosphere through interaction of thermal (“slow”) neutrons with nuclei of atmospheric nitrogen (Libby, 1946):

$$^{14}\mathrm{N} + n \rightarrow ^{14}\mathrm{C} + p \tag{2.21}$$

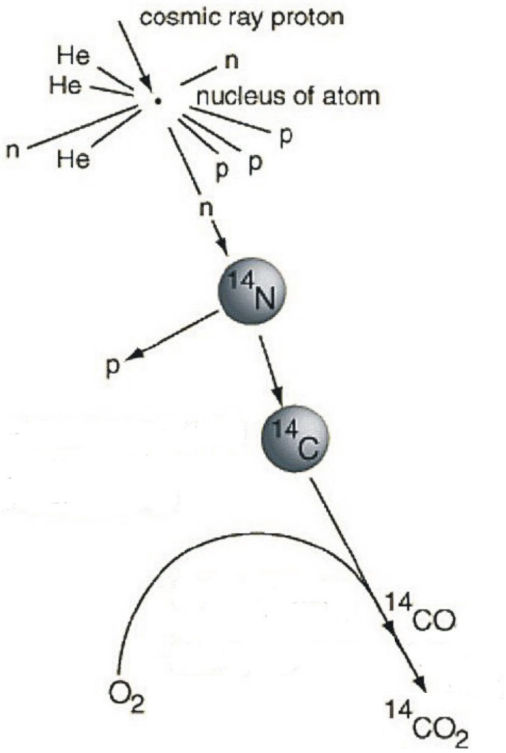

Figure 2.5: Sketch of the natural production of ^{14}C by cosmic rays in the upper atmosphere (Nave, 2005).

Thermal neutrons are produced naturally by primary high energy (1-10 GeV) GCR (**G**alactic **C**osmic **R**ay) having a global particle mean flux of 3 cm^{-2} s^{-1}. The GCR particles produce cascades of secondary particles by interacting with the air molecules (Masarik and Beer, 1999). Different studies calculated similar global production rates of ^{14}C in the atmosphere of 2.0 atoms cm^{-2} s^{-1} (10 % uncertainty). As the magnetic field diverts the particles toward the magnetic poles, ^{14}C production is largest at high latitudes. (Lal and Peters (1967); Masarik and Beer (1999)). The GCR particle flux is modulated by the solar magnetic field, depending on the solar activity, and Earth's magnetic field, resulting in a natural variation of the atmospheric ^{14}C concentration with time (Usoskin, 2008).

After the production in the atmosphere, ^{14}C is rapidly oxidised to ^{14}CO and then to $^{14}CO_2$. As $^{14}CO_2$ it takes part in the global carbon cycle and is mixed and transported in the atmosphere, exchanged with the carbon inventory of the ocean and the biosphere and stored in sediments and soil (Figure 2.6).

The eventual sink for ^{14}C is the radioactive β^- decay, with a half-life time of 5 730 years:

$$^{14}C \rightarrow {}^{14}N + \beta^- + \bar{\nu} \tag{2.22}$$

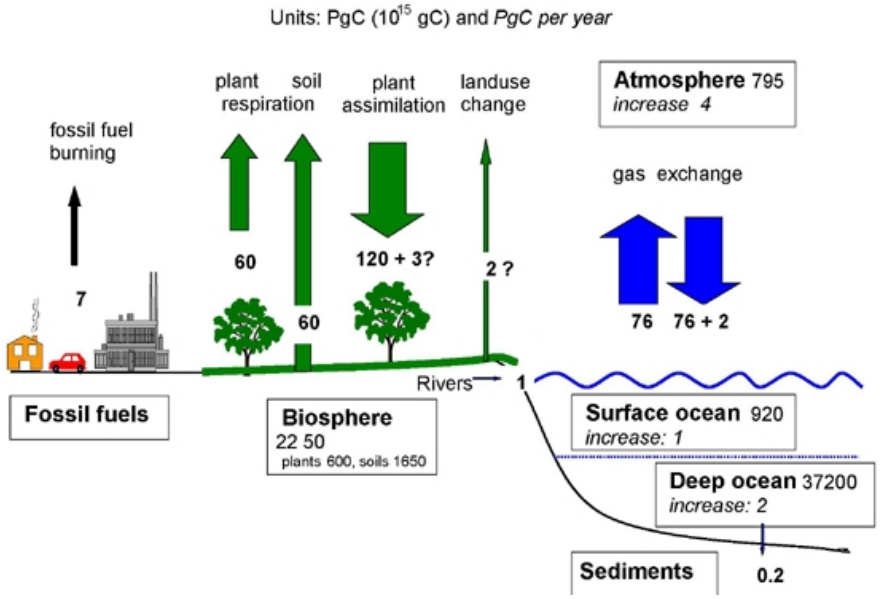

Figure 2.6: The global carbon cycle together with its different reservoirs (PgC) and exchange fluxes (PgC/year) for CO_2 (2000-2005) (pers. com. I. Levin, 2009)

2.5 Radiocarbon dating

As discussed previously, the common dating techniques in ice are limited to maximal a few hundred years, whereas radiocarbon provides the possibility to date ice ages up to 20 000 years.

Reporting ^{14}C ratios

The procedure on reporting ^{14}C concentrations is standardised by Stuiver and Polach (1977). A more detailed description is given in Appendix A, however summarising, two important conventions have been defined:

1. Correction for isotope fractionation:

Chemical and physical fractionation occurs whenever carbon is transported within the carbon cycle, e.g. from the atmosphere into the biosphere. More importantly however, significant fractionation can occur during sample preparation, combustion and graphitisation in the laboratory and thus falsify the $^{14}C/^{12}C$ ratio. Since carbon has two stable isotopes, ^{13}C can be used to indicate fractionating processes, as it is expected, that any fractionation is twice as strong for ^{14}C as for ^{13}C, due to the two times larger mass difference. To make samples from different sources and different sample preparations comparable, all ^{14}C ratios are corrected for fractionation according to:

$$^{14}R_{sample,norm} = {}^{14}R_{meas} \cdot (1 - 2 \cdot \frac{\delta^{13}C_{meas} + 25}{1000}) \tag{2.23}$$

Per international convention, ^{14}C ratios are referenced to a δ^{13}C value of -25 ‰, which is the postulated mean value for wood.

2. Reference year 1950:

To allow an easy comparison of samples measured in different years, 1950 AD was agreed on as reference year. The ^{14}C concentration is therefore measured relative to the absolute radiocarbon standard value of 1950. The absolute standard material is wood grown in 1890, age corrected for the reference year 1950. The commonly used radiocarbon standard today is an oxalic acid standard normalised to δ^{13}C = -19 ‰, which correlates to the absolute radiocarbon standard by:

$$^{14}R_{absolute} = 0.95 \cdot \ ^{14}R_{Ox} \cdot (1 - 2 \cdot \frac{\delta^{13}C + 19}{1000}) \cdot e^{\lambda(t-1950)} \tag{2.24}$$

where t is the year of measurement.

In the present work, ^{14}C concentrations are reported as **fraction modern carbon f$_m$**, where the term "modern" refers to the standard value of 1950:

$$f_m = \frac{^{14}R_{sample,norm}}{^{14}R_{absolute}} \tag{2.25}$$

f$_m$ is dimensionless, but is equal to the pmC (percent modern Carbon) notation (pmC = f$_m$ · 100 [%]) reported by Stuiver and Polach (1977).

Calibration of ^{14}C ages

The atmospheric $^{14}CO_2$ is constantly incorporated and exchange between the atmosphere and the different carbon reservoirs. As soon as the reservoir stops exchanging carbon with the atmosphere, either by being no longer in contact or in case of living organisms by dying, the radiocarbon clock starts. The activity A at a time t is then:

$$A = A_0 \cdot \ e^{-\lambda t} \tag{2.26}$$

where $\lambda = \frac{ln2}{T_{1/2}}$. In case of radiocarbon the ^{14}C/^{12}C ratio can be used instead of the activity A, because $^{14}CO_2$ is homogeneously mixed in the atmosphere. t gives the age, at which carbon exchange with the atmosphere stopped. A$_0$ is the initial ^{14}C concentration, which is needed to determine the age of the sample.

Serious effort has been put into the determination of the calibration curve, which relates ^{14}C concentrations to a dendrochronological time scale. Figure 2.7 shows the newest calibration curve IntCal04 combining six chronologies of different sampling sites and materials in the northern hemisphere. For detailed information on the calibration curve see Bard *et al.* (2004).

Several software programs convert a measured ^{14}C fraction f$_m$ into a calibrated age based on this IntCal04 curve. In this work the OxCal 4.1 program was used (Bronk Ramsey, 2009)

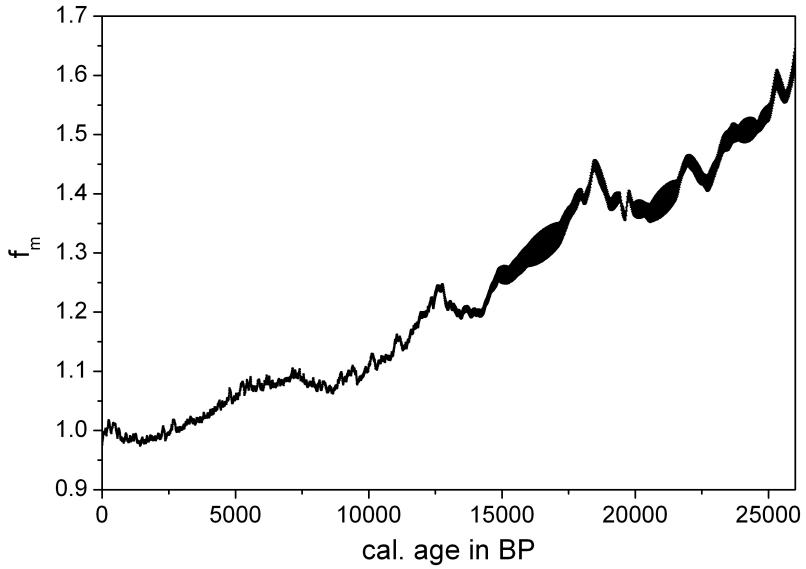

Figure 2.7: The IntCal04 calibration curve giving the initial atmospheric ^{14}C fraction as f_m at a calibrated age derived from tree rings (data taken from Bard *et al.* (2004)).

to derive calibrated ages from single ^{14}C concentrations through Monte Carlo simulation. The program uses the probability distribution of the ^{14}C concentration given by ($f_m \pm \Delta f_m$), looks for intersections with the IntCal04 curve and calculates a probability distribution of the calibrated age. Depending on the characteristics of the curve, e.g. small variations (plateaus) or strong variations (wiggles), the age distribution can cover a larger or a smaller time period, and even splitting into several time spans is possible (see Figure 2.8).

In this work, calibrated radiocarbon ages are given as 1σ time periods in years before 2000. The reported "central" value is the age with the larges probability.

Reservoir effect for organic aerosol

While the initial ^{14}C fraction is well known and allows a relative precise determination of the radiocarbon age, a problem still remains. Radiocarbon dating quantifies the age, at which the investigated reservoir stops exchanging carbon with the atmosphere. If a carbon reservoir contains a mixture of carbon from an "old" and a "young" source, the calibrated radiocarbon age overestimates the true age. This is called "reservoir effect". Well known, natural reservoir effects, are e.g. mixing of deep ocean water with surface water (marine reservoir effect) (Wagner, 2005) or solving of ^{14}C free carbonate in soil and ground water (hard water effect) (Deevey *et al.*, 1954).

For carbonaceous aerosols in the atmosphere, the sources and source strengths contributing to the respective aerosol fraction define the apparent age of the organic matter. Organic compounds released by the living biosphere either as primary or secondary aerosol can be assumed to have the same radiocarbon fraction f_m as the atmospheric $^{14}CO_2$ at the time. Since the at-

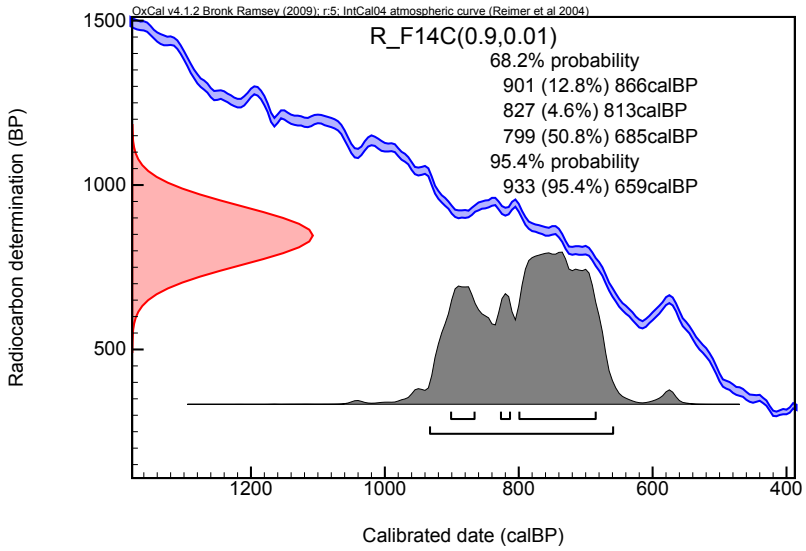

Figure 2.8: Example for an age calibration using OxCal 4.1. Given are the 1σ (68.2 %) and $2\,\sigma$ (95.4 %) time intervals.

mospheric lifetime of aerosols are in the order of days, the deposit of these aerosols onto the ice, would provide a direct information of the ice age. However, organics released from soil or from decomposing matter are already several years up to several thousand years old (Cherkinsky (1996); Tegen and Dörr (1996); Pessenda *et al.* (2000)) and the incorporated radiocarbon has already decayed. This reservoir effect, would result in a severe overestimation of the ice age.

The problem of the reservoir effect might be avoided by measuring ^{14}C on the secondary organic carbon fraction, which main source is the living biosphere. For the two carbon fractions in the ice core, this translates into ^{14}C analysis of DOC rather than POC. Soil may be a significant source of POC, resulting in too large radiocarbon ages, while the DOC fraction should be dominated by the biogenic SOA source.

Next to the natural source mix, anthropogenic activities resulted since industrialisation in two strong reservoir effects:

1. Fossil fuel combustion

Because of the relatively short half life time of radiocarbon compared to geological time scales, fossil carbon like coal and petroleum (millions of years old) is free of radiocarbon. Input of carbon through combustion of fossil fuels thus leads to a depletion of the ^{14}C concentration in the atmospheric CO_2, which is called the Suess-effect (shown in Figure 2.9). The depleted $^{14}CO_2$ signal is incorporated into the biosphere resulting in the release of ^{14}C depleted organic aerosols.
However, more importantly, fossil fuel combustion is also a direct source for organic aerosol, emitting gaseous organic compounds and soot, which then contributes to the atmospheric aerosol body and thus to both the POC and DOC fraction, although it is assumed, that it con-

tributes less to DOC than to POC. The ^{14}C signature of the atmospheric organic aerosol has been strongly depleted since beginning of the industrialisation (Jenk *et al.* (2006); Szidat *et al.* (2004)) prohibiting the use of this component for radiocarbon dating.

2. Nuclear fission and fussion bombs

In addition to the natural ^{14}C source, high-energy neutrons were produced through atmospheric tests of fission or fusion bombs and "slowed down" to the thermal level by collisions with nuclei in the atmosphere (Naegler, 2005). Atmospheric nuclear bomb tests have been carried out only between 1945 and 1980, the majority during 1954-1958 and 1961/1962, and thus resulted in a peak of the radiocarbon concentration in the atmosphere in the late 1950's and the early 1960's. The highest ^{14}C concentration at $f_m = 2$ in the atmosphere was reached in 1963. After the stop of the bomb tests, the radiocarbon concentration decreased due to the uptake of ^{14}C by the ocean and the biosphere. Since the atmosphere, the ocean and the biosphere are at present almost in a steady state again regarding their radiocarbon signatures, the Suess-effect is at the moment the main reason for the still decreasing atmospheric $^{14}CO_2$ concentration. Today the atmospheric radiocarbon signature has again nearly reached its pre-bomb value. Figure 2.9 shows the ^{14}C concentration of atmospheric CO_2 over the last 50 years.

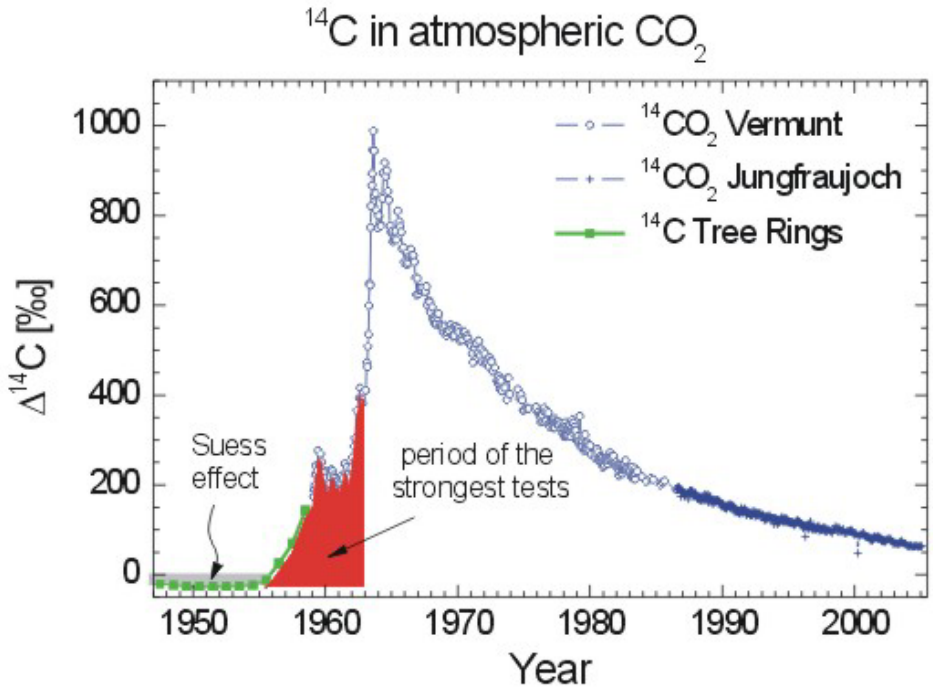

Figure 2.9: $\Delta^{14}C = (f_m - 1) \cdot 1000$ [‰] in atmospheric CO_2 in the Northern Hemisphere over the last 50 years, showing the Suess-effect (data from Stuiver and Quay (1981)) and the bomb-peak (data from Levin and Kromer (2004); Levin *et al.* (2008)).

The organic aerosol is influenced by this increase in atmospheric ^{14}C through the incorpora-

tion of the CO_2 into the biosphere, which then releases organic aerosol with an enhanced ^{14}C signature. In this case the ^{14}C signature changes while the organic aerosol mass remains constant. However, since the atmospheric $^{14}CO_2$ signal during the bomb peak is well documented, the well known bomb profile might still be used to determine how a fast changing atmospheric $^{14}CO_2$ signal is recorded in the carbonaceous aerosol fraction in ice.

3 Methodology of ^{14}C analysis in glacial DOC and POC

Aim of this work is the radiocarbon dating of Alpine glaciers by measuring ^{14}C on the dissolved and particulate organic carbon fraction on ice samples as small as possible.
Since the ice mass available for ^{14}C analysis is limited, e.g. by the geometry of the ice core, and the samples should cover a preferably small time period, i.e. being as short as possible, the extracted carbon masses can be, due to the low carbon concentrations in ice, extremely small. To still allow reliable ^{14}C measurements, an extraction system for

(1) small DOC and POC concentrations must be developed requiring
(2) a minimal and stable blank
(3) and a good extraction efficiency.

A large efficiency assures that the maximum of organic carbon contained in the ice sample is extracted and a small blank allows measurement of smaller carbon masses. The focus rests on the dissolved fraction, which is present in the ice in larger concentrations then POC and therefore allows extraction from smaller ice sample volumes. Additional analysis of POC could be used to confirm the DOC ages and the comparison of both fractions may give information about the sources of the two carbonaceous fractions and the respective age of the material at deposition. In the following, ...

- ... the concept and decision-making process for the DOC oxidation (3.2.2) and CO_2 degassing (3.2.1) method, as well as for the ideal POC filtration medium (3.2.3) is explained.

- ... the final set-up of the extraction system is described, giving information about the extraction procedure and which ice samples can be processed (size, organic carbon concentrations, etc.) (3.3).

- ... the developed system is characterised with regard to the blank, the minimal carbon sample size and the overall uncertainty of the measured ^{14}C concentrations (3.4).

- ... the performance of the system is tested on real ice samples to verify that the decontamination procedure and the determined blank apply to real samples as well and to investigate the repeatability of the extraction system.

3.1 State of the art

Measuring radiocarbon

Since its discovery in 1946 by Willard Frank Libby, the radioactive isotope ^{14}C has become a fixture in several research fields. The radiocarbon dating of organic matter through radioactive decay with a half life of 5730 a is a standard technique used mainly in archeology and geology (Arnold and Libby, 1949). Conventionally, the ^{14}C content of a carbon sample is measured by counting the β^- decay activity of a CO_2 or CH_4 gas using a Geiger counter (Kromer *et al.*, 1987) or liquid scintillation (Pringle *et al.*, 1955). These methods have the disadvantage of requiring carbon masses in the order of 1 g to allow for a sufficient counting statistic. With the invention of Accelerator Mass Spectrometry (AMS) and the possibility of directly counting ^{14}C atoms relative to the stable isotopes ^{12}C and ^{13}C without having to wait for their decay, the precision of ^{14}C analysis was increased and the necessary carbon mass reduced to 100 - 200 μgC (Suter *et al.*, 1981).
Conventional AMS measurement of ^{14}C on organic carbon requires for the organic matter to be oxidised to CO_2 and subsequently reduced to solid carbon targets by graphitisation. Gas ion sources, allowing the direct injection of the CO_2 gas into the AMS, have been proposed already 25 years ago (Middelton, 1984), but have been improved only in the last years enough to allow successful application for sample sizes of 30 μgC (Ruff, 2008).

For the present study, AMS measurement were carried out on graphite targets at the VERA laboratory (Vienna Environmental Research Accelerator, Institut für Isotopenforschung und Kernphysik, University of Vienna). The VERA graphitisation setup is designed for small carbon samples in the range of 5 - 100 μgC and allows graphitisation of three samples simultaneously in one day. Procedure blank was found to be 0.4 μgC with a ^{14}C signature of about f_m = 0.4 (Steier *et al.*, 2006). The AMS measurement returns reliable values for sample masses larger than 10 μgC, while for lower masses the error increases.

As the measurement of ^{14}C by AMS improves and allows exploration of new areas of research (Beukens, 1992), the extremely small sample sizes challenge the quality of sample preparation procedures.

Extraction of dissolved organic carbon - DOC

Dissolved organic carbon (DOC) has been measured for over 30 years in seawater samples (Grasshoff *et al.*, 1999) and more recently in freshwater and ice samples (Legrand *et al.*, 2007). Different techniques have been used, all eliminating first the inorganic carbon fraction, before the organic carbon is oxidised to CO_2. The gas is then extracted, e.g. by diffusion through a semi-permeable membrane or purging of the liquid sample with gas and quantified, e.g. by manometry, gas chromatography or infrared absorption.

In the present study, an infrared absorption CO_2-detector (Licor Bioscience: LI820) was used to monitor the oxidation and CO_2 degassing processes. The detector measures the strength of the IR signal that passes through a certain optical path length. The ratio of the CO_2 absorption band signal at 4.26 μm and a reference signal at 3.95 μm indicates the amount of light

absorption by CO_2, and thus, the gas concentration (Biosciences, 2002). In the present study, CO_2 concentrations in the gas stream reached seldom over 100 ppm and a high accuracy is needed in the ppb concentration range. However, the main concentration range of the LI820 lies in the order of 100 to 20 000 ppm and has a relative unstable baseline. The detector was still adequate enough for the simple task of identifying problems during as well as the end of the oxidation and extraction process. A new CO_2 online detector was purchased (Teledyne Instruments, API M 360EU), but could not be installed within this thesis.

Collection of the CO_2 gas for graphitisation and AMS ^{14}C analysis is commonly done by freezing it out from a carrier gas stream in cold traps with liquid nitrogen. A setup for sampling of CO_2 and manometric quantification of the carbon mass was already available (see Section 3.3.2), although designed for slightly larger carbon masses in the range > 50 μgC. However, the manometric quantification was easily adapted to allow the determination of smaller carbon masses (see Section 3.4.1).

The most difficult and controversial step remains the oxidation of the organic carbon fraction, which is a complex mix of organic molecules. Over time, mainly three different methods have been developed and improved:

- wet chemical oxidation (WCO): Liquid samples are oxidised in ampoules by autoclaving at 100-170°C with oxidants (e.g. $K_2S_2O_8$) (Menzel and Vaccaro (1964); Sharp *et al.* (1995)).

- high temperature combustion (HTC): Liquid samples, that are directly injected into a combustion line, or dry samples, retrieved by either evaporation (MacKinnon, 1978) or ultra-filtration (Benner and Hedges, 1993) of a liquid sample, are combusted at high temperatures in a stream of pure oxygen. The combustion is carried out with or without the aid of a catalyst (Menzel and Vaccaro (1964); Sugimura and Suzuki (1988)).

- UV-induced oxidation: Liquid samples are oxidised by irradiation with UV light and the addition of an oxidant (e.g. a peroxid solution or pure oxygen) (Collins and Williams (1977); Oppenländer and Gliese (2000)).

Several inter-comparisons have shown that all methods can be improved to have very small blank contribution and good agreement with each others. The largest controversy remains the unknown oxidation efficiency for different samples. The HCT method is commonly supposed to achieve complete oxidation, while the WCO procedure gives significantly lower values, and the UV method might also fail to oxidise more complex molecules (Gershey *et al.* (1977); Sharp *et al.* (1995); Sharp *et al.* (2002)).

Extraction of particulate organic carbon - POC

Particulate organic carbon (POC) from ice samples has been extracted by filtration through a carbon free, heat resistant filter medium (Steier *et al.*, 2006) or recovered onto any chosen surface by sublimation of the ice (Biegalski *et al.*, 1998). After removal of inorganic carbon, the POC is commonly combusted to CO_2 at high temperatures over 750°C.

Usually, filtration is used for POC extraction (Chýlek *et al.* (1995); Weissenbök *et al.* (2000); Jenk *et al.* (2007)) being a simple and quick procedure applied successfully in seawater studies (Grasshoff *et al.*, 1999), but often carries the shortcoming of a poor particle collection efficiency. In comparison, sublimation of ice may provide the better recovering efficiency, but the melt water is irretrievably lost.
Grasshoff *et al.* (1999) outlines the quantification of POC in seawater and recommends the use of either glass fibre or metal foil filters. However, most POC studies on ice cores report use of quartz glass filters, that can be pre-heated at 1000°C for carbon decontamination (Weissenbök *et al.* (2000); Steier *et al.* (2006)).
Combustion of the POC samples to CO_2 can be done either in a closed off quartz-tube with copper oxide (CuO) as oxygen donator (Weissenbök *et al.*, 1998) or in an open system under a stream of oxygen (Szidat *et al.*, 2004). The combustion in a closed-off quartz tube with CuO is a standard method for converting organic matter to CO_2.

3.2 Concept of the extraction line

Careful consideration of the information found in the literature about the extraction of organic carbon from liquid or solid samples, following conclusions were reached:

DOC: Aiming to extract DOC from sample masses of 300-500 ml, the wet HTC method was immediately disregarded, as such large water masses can not be combusted in a prudent way. The dry HTC technique is very susceptible to contamination and loss of organic compounds during the evaporation. The WCO method, while being suitable for large sample volumes, suffers from the necessity of large amounts of oxidants, which induces a significant blank, while evidently not achieving complete oxidation. The UV induced oxidation technique seems therefore the most reasonable choice, allowing oxidation of a large sample volume with both large and small DOC concentrations within a suitable time frame (see Section 3.4.2).

This leaves the decision about the UV oxidation system being (1) “dynamic”, i.e. the melt water is led in a stream past the UV lamp or (2) “static”, i.e. the melt water is sampled and irradiated with UV in a glass vessel, as well as the decision about the best method for CO_2 gas extraction from the water. The different possibilities are investigated and compared in the following sections.

POC: Since in this study the dissolved organic carbon fraction is to be analysed preferential, the sublimation method was no option and POC extraction by filtration the only logical conclusion. As glass fibre filters can only be heated to about 500°C, but combustion temperatures are over 750°C, they were disregarded as filter medium. The suitability of silver filters versus quartz filters is investigated in Section 3.2.3.
For the subsequent conversion of POC to CO_2, the closed-off combustion with CuO as oxygen donator was chosen, based on the fact, that a suitable setup of a stream combustion system requires significant work especially regarding the blank. On the other hand, the closed-off combustion is found to allow a relative homogeneous and time efficient combustion process of several samples at once, has a minimal blank contribution and was successfully used, as

described in Section 3.3.3, on previous occasions.

3.2.1 CO_2 degassing

Before deciding on a dynamic or static DOC extraction system, it should be investigated, what method of degassing the CO_2 from water, be it the inorganic carbon fraction or the oxidised DOC fraction, is more suited for an effective extraction of a 500 ml sample, with a minimum risk of contamination.
Mainly, two methods for complete CO_2 degassing of a water sample were investigated and tested:

1. flow extraction through a semi-permeable membrane
2. static extraction by bubble degassing

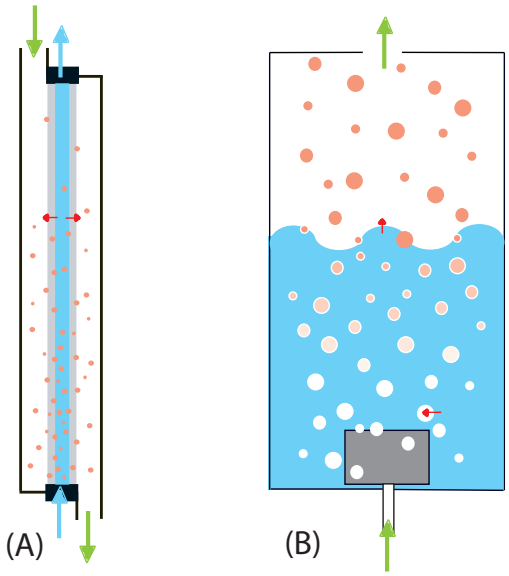

Figure 3.1: Degassing CO_2 from water: (A) dynamic degassing by flow through a semi-permeable membrane, (B) static degassing by purging with clean air bubbles. The green/blue arrows show the gas/water flow, the red arrows signify the concentration gradient and consequently the direction of CO_2 flow.

Theory of air-water exchange

CO_2 is dissolved in water in the forms of gaseous CO_2, hydrogen carbonate HCO_3^- and carbonate CO_3^{2-}. Acidification to a pH of about 2 results in a shifting of the equilibrium, so that all CO_2 is present in gaseous form.

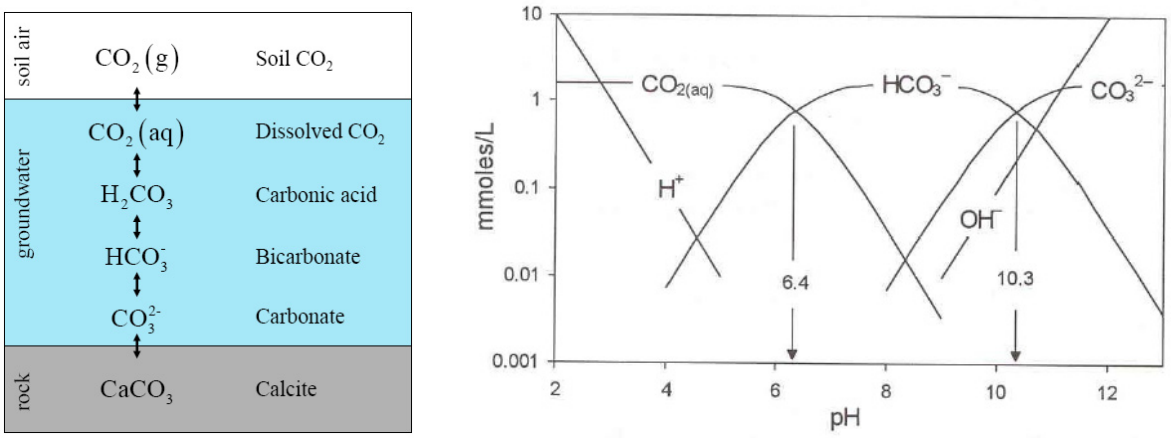

Figure 3.2: The carbonate system and its pH dependence (Clark and Fritz, 1997).

Bringing CO_2 free gas in contact with the solution, the concentration gradient Δc between water and air results in a netto transfer flux j of CO_2 out of the water into the gas stream. The mass transfer is controlled by molecular diffusion in a thin boundary layer, where $\frac{\partial c}{\partial z}$ can be assumed to be constant.

$$\begin{aligned} j &= D \cdot \frac{\partial c}{\partial z} \ (Fick's\ law) \\ &= \frac{D}{z} \cdot \Delta c \end{aligned} \tag{3.1}$$

D is the diffusion constant of the gas in water. z is the thickness of the boundary layer and depends on different parameters, most importantly the degree of turbulence in the water and the air. $\frac{D}{z}$ has the dimension of a velocity and is therefore called transfer velocity. If the gas obeys Henry's law depends Δc on the solubility $h_{cc} = c_{water}/c_{air}$ of the respective gas in water conditioned on temperature, pressure and salinity according to:

$$\Delta c = (c_{water} - h_{cc} c_{air}) \tag{3.2}$$

Table 3.1 summarises some of the parameters for different gases and organic compounds.

Since in the present case, the gas in contact with the water sample is CO_2 free and constantly replaced, the concentration c_{air} is zero. The change in concentration with time of degassing within a sample volume V is given as the mass flux j through the area A:

$$j \cdot A = V \cdot \frac{\partial c}{\partial t} \tag{3.3}$$

The resulting evolution of concentration c in the volume with time and the characteristic time constant τ is:

$$c = c_0 \cdot e^{-t/\tau} \tag{3.4}$$

$$\tau = \frac{Vz}{DA} = \frac{V}{kA} \tag{3.5}$$

Table 3.1: Solubility h_{cc} and diffusion constant D for different gases at 293 K. (1) Sander (1996); (2) Broecker and Peng (1974)

molecule	h_{cc} [dim.less] (1)	D [cm^2/s] (2)
CO_2	0.832	$1.64 \cdot 10^{-5}$
CO	$2.32 \cdot 10^{-2}$	$1.75 \cdot 10^{-5}$
CH_4	$3.43 \cdot 10^{-2}$	$1.75 \cdot 10^{-5}$
HCHO	$7.58 \cdot 10^{4}$	$\approx 10^{-5}$
CH_3OH	$5.38 \cdot 10^{3}$	$1.28 \cdot 10^{-5}$ (288 K)

Extraction by semi-permeable membrane

The liquid sample is led through a semi-permeable membrane tube. The material of the tube allows CO_2 to pass through the pores, while water is retained. The membrane tube is contained in another tube, which is flooded with a clean carrier gas. The gas flows contrary to the water flow and takes up the CO_2 diffusing through the membrane (see Figure 3.1 (A)). In this case, z can be set equal to the radius of the tube. The surface area of the tube is $2\pi rl$.
Two types of membrane tubes were available for testing: a single acurel membrane tube and a membrane contactor (Liqui-Cel) with 1100 parallel polypropylene tubes. Table 3.2 gives the characteristics for these two setups, including the theoretical characteristic time τ, after which the CO_2 concentration in a 500 ml liquid sample is reduced to e^{-1} of the initial concentration and the maximum water flow rate necessary to allow for a complete degassing over the length of the tube.

Table 3.2: Characteristics of the single membrane tube and the membrane contactor setup: tube radius r, tube length l, number of tubes n, total area A and volume V of the tube(s). j gives an upper limit for the water flow rate necessary to assure, that all CO_2 is extracted in one passage of the membrane. τ_{water} gives the characteristic time after which the concentration in a 500 ml sample is reduced to e^{-1} of the initial concentration.

type	single membrane tube	membrane contactor
r [cm]	0.025	0.011
l [cm]	10	15
n	1	1100
A [cm^2]	1.6	1140
V_{tube} [cm^3]	0.02	6.3
j [ml/min]	< 0.01	< 20
τ_{water} [min]	8000	4.9

Test measurements with a carbonate solution supported the theoretical considerations presented in Table 3.2. For the single membrane tube, the amount of extracted CO_2 depended strongly on the water flow rate, which could not be reduced enough to achieve complete extraction in one flow-through. Additional, problems arose from the diffusion of the carrier

gas into the water stream. The created bubbles hindered the flow pattern and disturbed the diffusion process (Mommert, 2007). Complete extraction within an acceptable time was no problem for the membrane contactor, however the housing is made of polycarbonate and the fixed setup makes decontamination difficult.

Extraction by bubble degassing

The water sample is contained in a vessel with a gas in- and outlet and is directly purged with CO_2 free gas. A frit is used to produce bubbles, which take up the CO_2 on their rise to the water surface. Furthermore, the bubbles create a strong turbulence at the air-water interface, influencing the layer thickness z. The degassing process is therefore twofold: diffusion into the bubbles and direct diffusion through the sample surface. While the sample surface is fixed, the total effective exchange area depends on the number and size of the bubbles and through this also on the gas flow. This complexity makes a calculation of the characteristic extraction time τ difficult.
instead, the CO_2 extraction method was tested by degassing a carbonate solution and measuring the CO_2 concentration in the carrier gas with the LI820 CO_2 detector. Figure 3.3 shows the normalised CO_2 concentration profile for three different gas flows. The larger the gas flow through the sample, the faster is the CO_2 extraction.

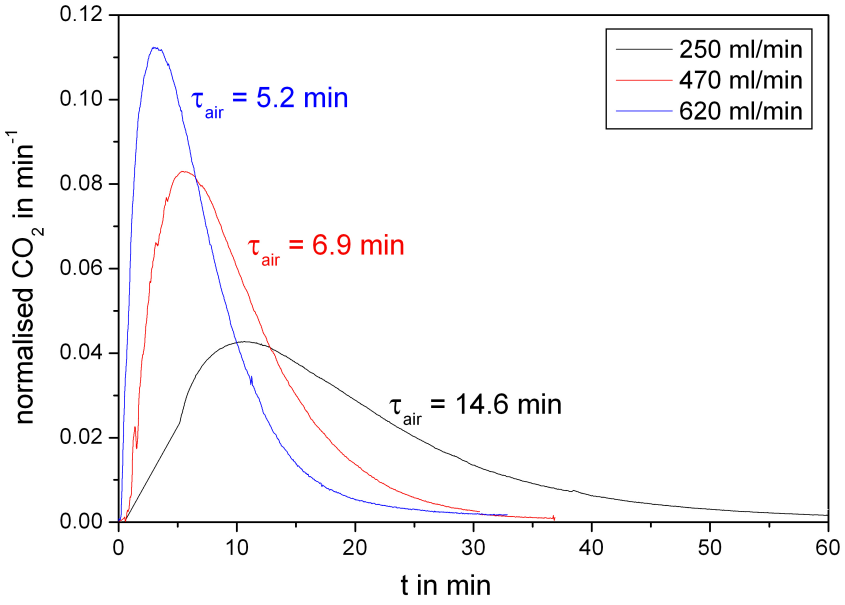

Figure 3.3: Degassing of a carbonate solution using three different gas flows. τ_{gas} gives the characteristic time after which the CO_2 concentration in the gas stream is e^{-1} of the maximum concentration: $c = c_{max} \cdot e^{-t/\tau_{gas}}$.

It should be noted, that τ_{gas} characterises the extraction process from the gaseous side, while τ_{water} represents the liquid side. The two parameter are therefore not exactly equal, but closely correlated and while a direct comparison is not possible, the order of magnitude is sufficient.

Conclusion

Concluding, both degassing with the membrane contactor as well as bubble degassing are fast and efficient extraction methods. Both methods posses a potential for contamination due to either the polycarbonate housing of the contactor or the large surface of the pot required for the bubble degassing. Since both methods proved effective, the final decision rests on UV oxidation being “dynamic” or “static”.

3.2.2 DOC oxidation

UV-induced oxidation of organic molecules was found to be the most logical method for the extraction of DOC for ^{14}C analysis. However, it remains to be decided, if a dynamic or static oxidation is more suitable in handling ice samples of 500 ml, has the last chance of contamination and allows an efficient degassing and trapping of the produced CO_2 for ^{14}C analysis.

The UV-induced oxidation method converts DOC to CO_2 by hydroxyl-radicals (OH), that are formed through various processes by UV light of 185 nm and 254 nm (Figure 3.4). Although, OH production might be achieved purely through the break-up of H_2O, an oxidant is normally added to enhance the process. This oxidant can either be oxygen gas or a liquid oxidant, like hydrogen- oder ammonium-persulfate.

There are two possible ways for setting up a UV-induced oxidation system.

1. dynamic: a constant water flow is led past the UV lamp
2. static: the water is sampled and irradiated within a glass vessel

Past experiences with two DOC quantification systems for small samples used at the Institut für Umweltphysik (IUP)(WALTER = dynamic and DOCster = static; see Appendix B for more detailed information), led to the following conclusions:
The dynamic system needs a constant addition of a liquid oxidant, which can induce a large blank contribution. Even with the oxidant, DOC was not always completely oxidised in one passage of the UV lamp, resulting in the setup of a sample loop. Time of analysis, including waiting for basline and IC extraction, for a 5 ml sample was about 20 min at a water flow of 5 ml/min.
For the static system, the liquid oxidant can be foregone by purging the sample with synthetic air or oxygen gas to produce OH. While the DOC oxidation and extraction time is in the order of 5 min, several intermediate steps are necessary to allow a quantitative extraction of DOC, resulting in a total analytical time for a 5 ml sample of 17-20 min.

Based on these findings for small sample sizes, considering the findings for optimal degassing of the CO_2 and taking into account, that the extracted CO_2 must be frozen out in a cold trap, different extraction scenarios were envisioned.

1. a completely dynamic system: extraction of IC from the melt water flow with a membrane contactor; oxidation of DOC in the water flow passing the UV lamp using persulfate as oxidant; CO_2 extraction from the water flow with a membrane contactor

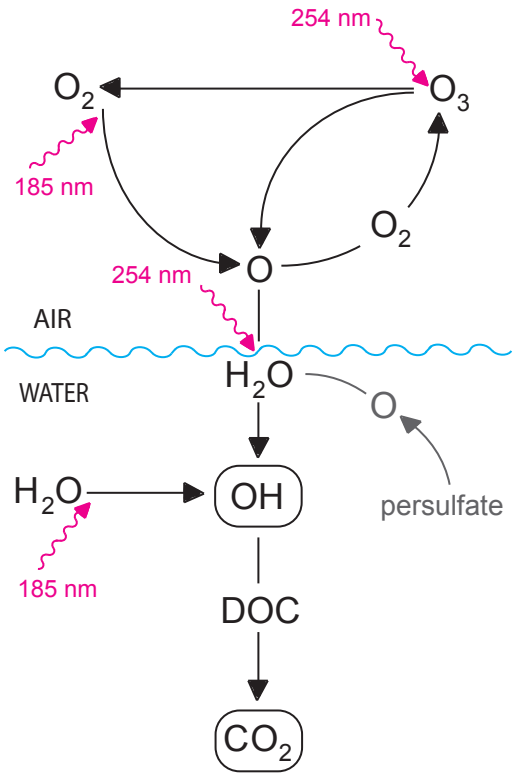

Figure 3.4: Schema of different oxidation mechanism of dissolved organic carbon.

2. a semi-dynamic system: extraction of IC from the melt water flow with a membrane contactor or sampling the melt water in a glass vessel and extracting the IC with bubble degassing; static UV oxidation in the glass vessel; CO_2 extraction from the water flow with a membrane contactor

3. static system: sampling of the melt water in a glass vessel; extraction of IC with bubble degassing; static UV oxidation; static CO_2 bubble degassing

The first method has the advantage of no waiting time, because the melt water may be instantaneously processed. The system allows minimal surface contact of the melt water thus minimizing the blank. However, the melting velocity (≈ 3 ml/min) might be to low resulting in a non-continuously water flux. Also, depending on the DOC concentration, one passage by the UV lamp might not be enough to assure complete oxidation. A solution would be the setup of a sample loop, including a storage pot, in which the processed water is constantly mixed with the new melt water. However, the additional pot and the constant circling might increase the total blank mass.
The second method allows to adjust the time of UV irradiation assuring total oxidation, but similar to the circling method above, the risk of contamination is high. Another problem is the loss of CO_2 during the static oxidation to the air volume above the water sample.

The third setup has the advantage that sampling of the melt water, extraction of IC, oxidation and extraction of DOC can be achieved in one vessel and the UV irradiation time can be adjusted as necessary. The large surface of the pot might result in a large blank, but a liquid oxidant can be forgone.

Conclusion

Based on these considerations, it was decided that the static oxidation and extraction method is preferable, since it allows the necessary flexibility in irradiation time to assure complete oxidation and extraction of IC and DOC with one setup, thus reducing the chances of contamination. Also, in order to monitor the extraction process for the dynamic method, the gas flow would have to be very small (in the order of 20 ml/min) to achieve a distinct CO_2 concentration. Such a low gas flow makes the trapping in the CO_2 cold traps difficult. On the other hand, the gas stream should be as large as possible for bubble degassing. A gas flow of 580 ml/min was finally determined to be ideal for an efficient degassing and an efficient cleaning and trapping of the CO_2 gas.

3.2.3 POC filtration

For the POC extraction, filtration was the only possible extraction method, however two filter media could be considered as filter medium: quartz microfilter (Whatman) and silver membrane filter (SPI Supplies). The silver filters have a pore size of 0.2 μm, while the quartz filters have no defined pore size, but are commonly used for particle filtration < 10 PM in air. Requirements for the filter medium are the easy filtration of large and small particle concentrations with an adequate extraction efficiency and a minimal blank contribution.

All filter were pre-cleaned before sample processing. Quartz filters have been pre-heated at 750 °C for 4h and placed under a water saturated atmosphere for cool down to reduce adsorption of organic compounds from the laboratory air. Silver filters have been washed in mQ water in an ultrasonic bath (low intensity), dried at 60 °C and also stored under a water saturated atmosphere. The filter holder is described in Section 3.3.3.

Blank

The POC filtration blank value combines (1) the blank of the filter, (2) the blank derived from processing of the sample and (3) the blank added by the combustion. The closed off combustion process has been found to be blank free. Table 3.3 summarises average masses for the filter blank and sample process blank for both filter media. Silver and quartz filter exhibit no significant difference in their blank contribution. A more detailed discussion on the sources of these blank masses is given in Section 3.4.

Table 3.3: Filtration mass blank for quartz and silver filter: "filter" = filter material, "mQ" = processing a liquid blank sample, "DOC" = processing a liquid dissolved organic carbon standard, "blank ice" = processing a artificial blank ice sample. The number in brackets gives the number of blank measurements averaged in the blank value.

	quartz [μgC]	silver [μgC]
filter	2.3 (1)	2.9 (1)
mQ	6.2 ± 0.8 (4)	6.1 (1)
DOC	4.1 (1)	3.8 (1)
blank ice	6.4 ± 2.5 (5)	-

Filtration efficiency

The filtration efficiency of both filter media was determined by measuring the particle concentration before and after filtration for (1) clean water and (2) a granite powder solution. The granite solution does not necessarily reflect a true POC sample size composition, but may provide an upper limit to the filtration efficiency. For both filter media a filtration efficiency of only 80 % was determined. (see Appendix C).

Filtration velocity

To determine an upper value for the filtration velocity, mQ water (pre-treated ultrapure, DOC free water) was filtered through the medium and the filtered volume versus time was measured. Figure 3.5 shows that the filtration velocity of the quartz filter was for a sample volume of 700 ml constant at v = (373 ± 3) $\frac{ml}{min}$. The filtration velocity of the silver filter, however, started at a significantly lower value of 38 $\frac{ml}{min}$ and decreased rapidly. For samples actually containing particles the silver filter was blocked rapidly and, more often than not, complete filtration was not possible.

Conclusion

Filtration of POC should be possible for large and small concentrations and should be completely achieved within a reasonable time frame. The significant difference in filtration velocity for quartz and silver filter and the fact, that for silver filters even filtration of 500 ml mQ water was nearly impossible, led to choosing quartz over silver filter as filtration medium, especially since all other relevant parameters showed seemingly no advantage for the use of silver filter.

3.3 Final setup of the DOC and POC extraction system

In the following the final setup and procedure for POC and DOC extraction is described and the resulting limitations and consequences for the minimal sample size discussed. Both units

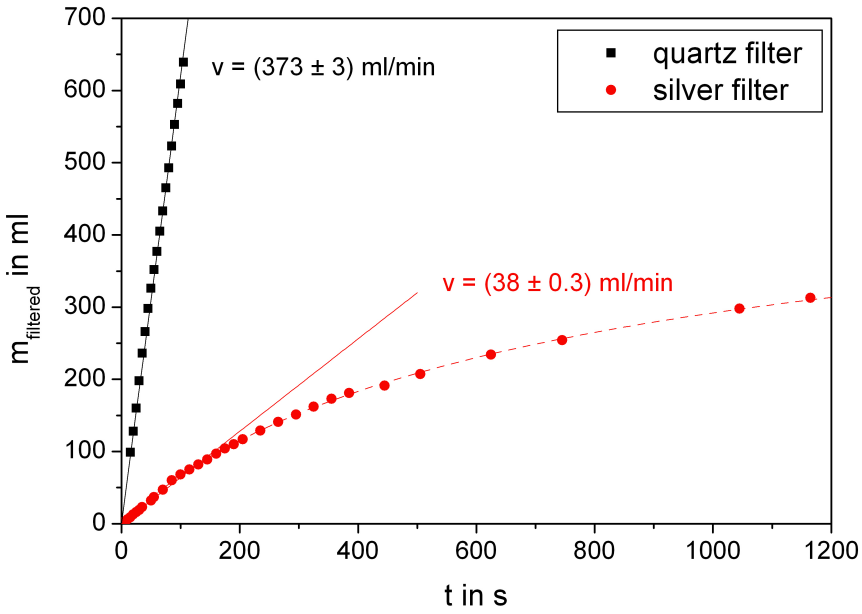

Figure 3.5: Filtration velocity for quartz (black) and silver (red) filter at 2 bar.

are flexible and can be used separately as well as consecutively, if both fractions are desired from the same sample (Figure 3.6). All pots are prior to sample processing cleaned with mQ water. Synthetic air, which is led through soda lime and charcoal to remove any residual CO_2 and hydro-carbons is used to flood the different vessels and as carrier gas for the CO_2 extraction.

3.3.1 Sample preparation line

Ice decontamination

The ice sample is cut and then sealed up in a PFE-foil. Assuming that a maximum of half an ice core can be made available for radiocarbon dating, the upper limit of the sample cross-section is 20 cm^2 (3") to 40 cm^2 (4"). A minimum area of 2.5 x 2.5 cm is necessary to allow for a sufficient decontamination.
For decontamination, the sample is slowly tempered at room temperature for 20-40 min. This precaution prevents cracking of the ice and subsequent infiltration of contaminated water into the inner part of the ice sample. Then the sample is cleaned under running mQ water from all sides, before being put into the melting pot. The pot is sealed and flooded with clean synthetic air, before the sample is again washed with mQ water inside the melting pot. Afterward the first 20 - 30 ml of melt water are discarded. The decontamination factor $\frac{m_{after\ decon}}{m_{before\ decon}}$ for the whole procedure is between 50 and 75 %. This mass loss has to be considered when deciding on the size of the ice sample.
Stricker (2008) showed this decontamination technique, omitting the second cleaning step within the melting pot, is very efficient and fast for small blank ice samples containing few air

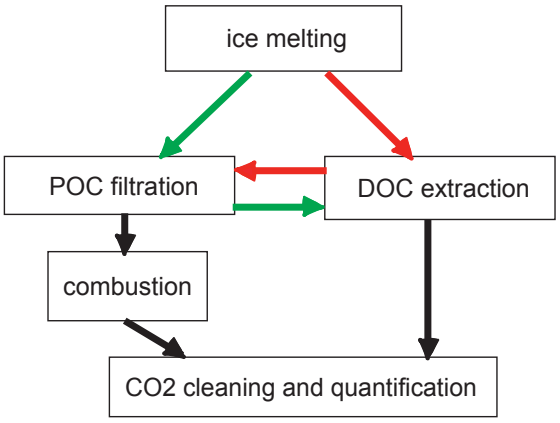

Figure 3.6: Schema of the POC and DOC extraction system: the POC and the DOC unit can be used on their own as well as consecutively and it is possible to filter POC before (green) or after (red) DOC extraction.

bubbles (Figure 3.7(a)). Test measurements using the DOCster (see Appendix B.1) showed the same for large blank ice samples (Figure 3.7(b)).

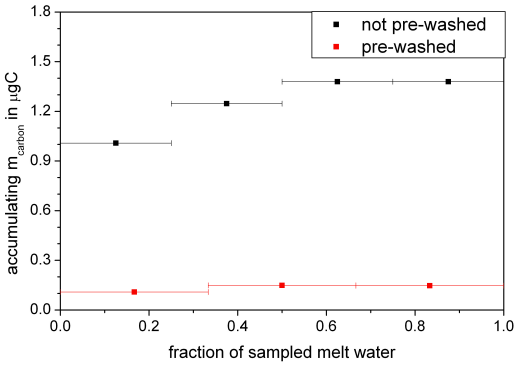

(a) Small blank ice samples (30-100 cm^3) melted in udder vessel.

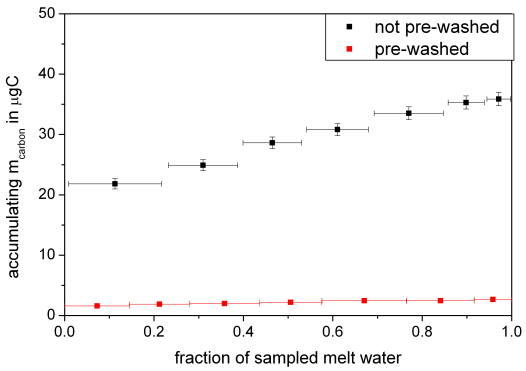

(b) Large blank ice samples (200-300 cm^3) melted in melting pot and sampled in PFA pot.

Figure 3.7: Illustration of the decontamination efficiency for small (data from Stricker (2008)) and large blank ice samples. Shown is the accumulating carbon mass relative to the fraction of sampled melt water with and without the described decontamination procedure as stepwise measured with the DOCster.

In essential, this decontamination procedure reduces the time of decontamination as the otherwise stepwise melting of the outer sample part is now simply washed away. In addition the protraction of contamination by refreezing on the surface or infiltration into the inner parts of

the ice sample of the contaminated melt water is significantly reduced.

Ice melting

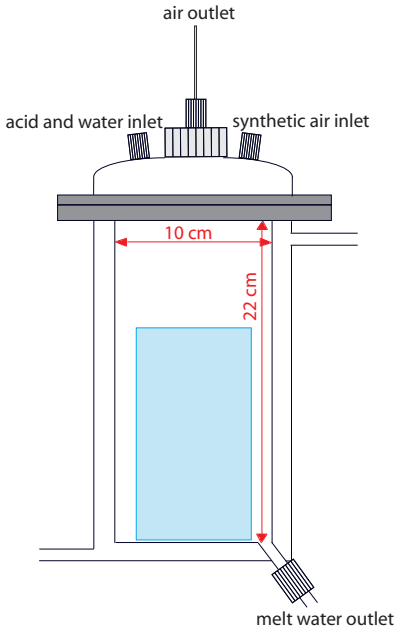

Figure 3.8: Illustration of the melting pot.

The melting unit consists of a glass pot with an inner diameter of 10 cm and a removable cover, allowing for a maximum ice sample geometry of 6.5 x 6.5 cm and a maximum height of about 22 cm. Thus samples with 900 cm^3 or a mass of 800 gr can be melted. Using two infrared lamps, the ice is usually completely melted in two to three hours. The melt-water is directly discharged to reduce contact with the melting pot surface and the ice sample itself and is transfered either into a PFA pot for POC filtration or to the DOC extraction unit.

3.3.2 DOC - Extraction

DOC oxidation and degassing

The melt water is transfered either directly after melting or after POC filtration into the DOC glass pot (Figure 3.9). The DOC pot has an inner diameter of 7 cm and a fill height of about 20 cm. In its center is a Suprasil quartz-glass tube with an outer diameter of 2.5 cm. Thus the maximal sample volume is about 750 ml. While the ice sample is melted, the inorganic carbon fraction is extracted as clean air is continuously led through the collected melt water.
Suprasil is a synthetic quartz glass, which allows transmission of short wavelength light. The quartz glass tube holds a specific UV lamp (Heraeus Noble Lights: NIQ40-18), which radiates

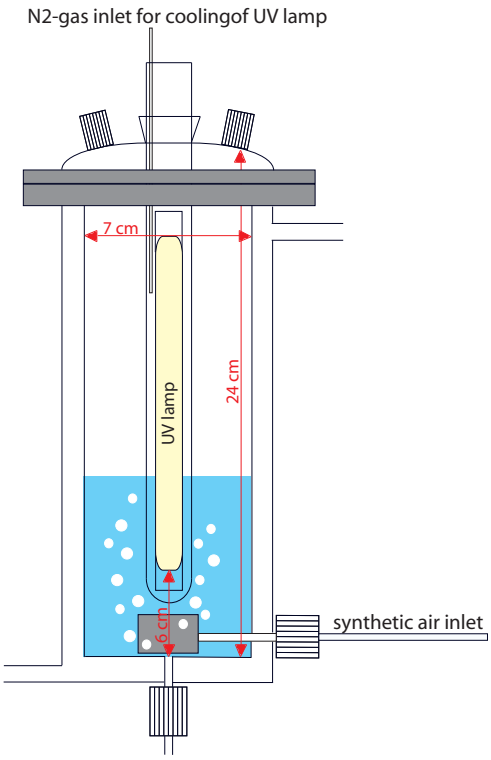

Figure 3.9: Illustration of the DOC extraction pot.

mainly in the for oxidation of DOC needed wavelengths 254 nm (10 W) and 185 nm (4 W). The carrier gas for the CO_2 degassing is induced in small bubbles through a stainless steel frit with pore size 2 μm at 580 ml/min.
Due to the 6 cm offset between the UV-lamp and the bottom of the vessel, the minimum sample volume must be 300 ml for the radiation length being sufficiently insert in the water.

The DOC pot is pre-cleaned by filling it with mQ water adding 30 - 40 ml 21% phosphoric acid and turning on the UV light and the gas stream for half an hour. 300 ml of this DOC-free acid water is then left in the pot and the sample melt water added onto it, in order to enhance the oxidation efficiency by increasing the UV radiation length covered by water.

It should be noted, that the UV lamp has its maximum power at 90 - 100°C and is destroyed at temperatures over 130°C. Since the lamp is placed inside a tube, heat accumulation can easily result in exceeding this limitation and a cooling of the lamp is necessary. For the present setup, cooling has been achieved by a continuous stream of N_2 around the lamp, effectively removing the heat and preventing the production of ozone in the laboratory air.

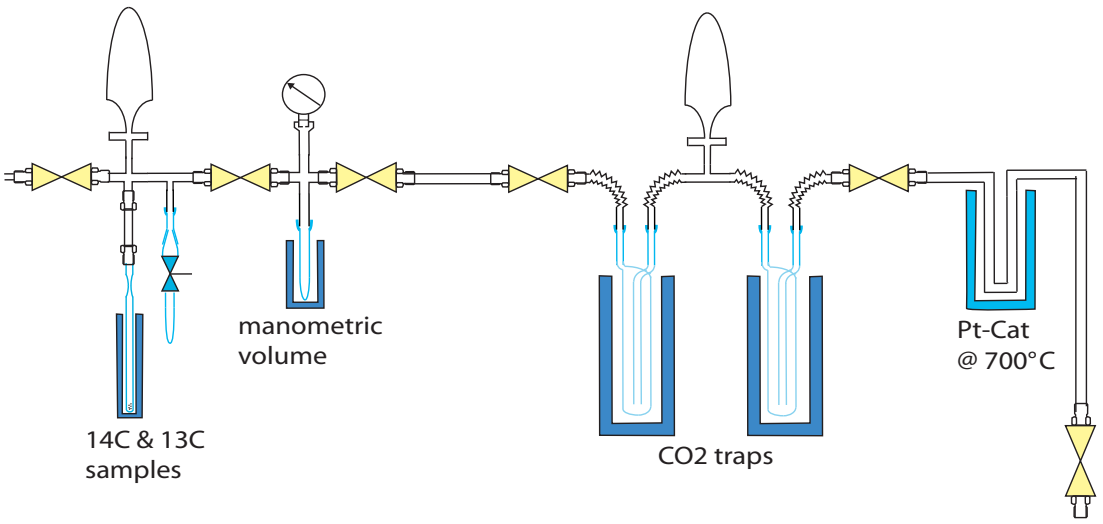

Figure 3.10: Illustration of the extraction line.

CO_2 online monitoring and trapping

After DOC oxidation and degassing, water vapour is removed from the gas stream by a cryogenic trap at -78 °C, before it is led through the CO_2 detector for online monitoring of the extraction to determine, when the process is complete.

The gas is then led over a platinum catalyst at about 700°C for the oxidation of remaining ozone, before being frozen into two CO_2 cold traps with liquid nitrogen and quantified manometrically. With a volume of (3.265 $\pm$ 0.019) ml and a pressure sensor with a maximum pressure of 1000 mbar, sample masses between 2.5 to 1 500 μgC can be measured. Finally the CO_2 gas is sampled for ^{14}C analysis, whereby part of the gas can be sidelined for a separated ^{13}C measurement.

3.3.3 POC - Extraction

Filtration

For POC filtration the melt water is either directly or after DOC extraction transferred into a PFA pot with a diameter of 10 cm and a cylindric bottom (Figure 3.11(a)) and a total volume

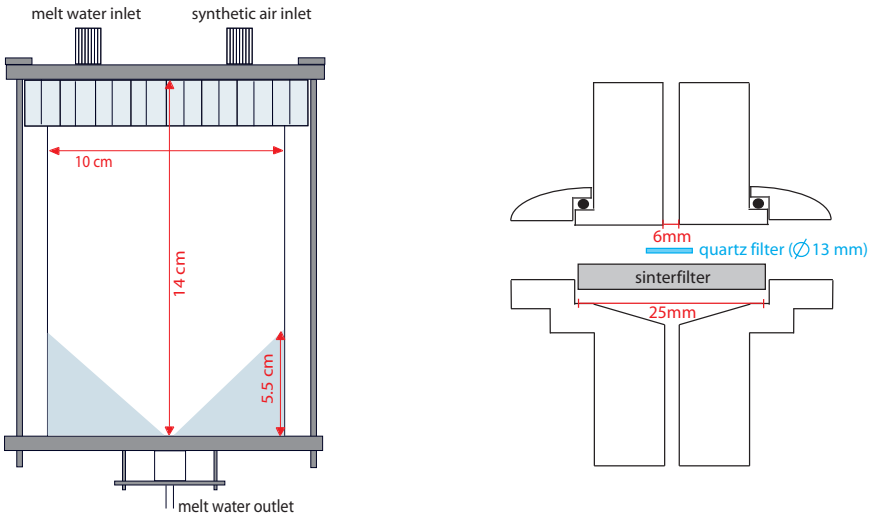

(a) The PFA pot for filtration.

(b) The filter holder for filtration.

Figure 3.11: Illustration of the filtration unit.

of 700 cm^3. The melt water is pressed in regular steps with 1 to 5 bar through the filter, that is contained in a stainless steel filter holder (Figure 3.11(b)) and stabilized by a stainless steel sinter filter.
Filtration is normally done on an area of about 0.28 cm^2 or in cases of very large POC concentration on 4.9 cm^2. After filtration, about 80 ml of a water-acid mixture is used to wash remaining POC from the melting and the PFA pot onto the filter and to remove inorganic carbon from the filter.

The filter holder is cleaned with mQ water and dried at 60°C. The quartz filter is pre-heated at 750°C for 4h before placed under a water saturated atmosphere along with the sinter filter. Due to the high humidity during cool down the filter surface is "blocked" by water and adsorption of organic compounds from the laboratory air is prevented.

Filter combustion

After filtration, the quartz filter is dried under vacuum with an infrared lamp, before transfered into a pre-heated quartz glass tube with an inner diameter of 7 mm. 1-5 mg silver wool is added for halogen reduction and 1-2 gr copper oxide (CuO) as oxygen donator. The sample tube is then evacuated while heated to (80-110)°C for about half an hour to remove any water remains. The tube is melted off and the sample combusted at 750°C for 4 hours.

An illustration of the complete DOC and POC extraction system is shown in Appendix B.3

3.4 Characterisation of sample preparation line

In order to determine the overall uncertainty of the radiocarbon results and the minimal sample size, the carbon extraction methods have to be characterised regarding mass blank, ^{14}C blank, extraction efficiency and the uncertainty of the manometric quantification needs determination.

3.4.1 Carbon mass quantification

For blank corrections of the measured ^{14}C values, the carbon mass of the sample must be determined. The uncertainty of this quantification contributes to the overall uncertainty of the final ^{14}C results.

Manometric quantification at IUP

The extracted CO_2 is quantified manometrically, i.e. the sample is frozen into a known volume of (3.265 $\pm$ 0.019) ml and its pressure and temperature are determined.
The temperature is measured on the outside surface of the volume with a normal mercury thermometer with a reading uncertainty of 0.2°C. The pressure sensor (Omega: PX72-015AV) gives a voltage output between 0 - 10 V, which is transformed into a pressure signal using a two point calibration at vacuum and at atmospheric pressure. Specifications state that the sensor is linear within 0.5% of full scale and has a nominal repeatability of 0.3% of full scale. The sensor is temperature compensated between -15°C and 85°C.

The calibration drifts over time, which has a significant impact on the small sample sizes being quantify. Starting with (1) p[mbar] = 96.9$\frac{mbar}{V}\cdot$ U[V] + 0.7 mbar, five months later, three recalibrations within two weeks gave (2) p[mbar] = (97.0 $\pm$ 0.5)$\frac{mbar}{V}\cdot$ U[V] + (2.6 $\pm$ 0.3) mbar. As can be seen, the drift within a week is relatively small compared to the significant drift over several months.
Concluding, if the sensor is recalibrated at least once a week, the pressure reading has a relative uncertainty of 0.5 % for pressures larger than 100 mbar. For smaller pressures, an absolut uncertainty of 0.5 mbar is assumed to be a sufficient constrain.
Based on these parameters, the relative overall quantification uncertainty is shown in Figure 3.12(a). It is less than 10 % for sample masses larger than 8 μgC. Also, for sample masses up to 40 μgC an absolute uncertainty of about 0.8 μgC is found, leading to a minimal sample size of three times this uncertainty of about 2.5 μgC.

Manometric quantification at VERA

During the graphitisation process done at the VERA laboratory, the sample mass is again quantified manometrically using a volume of around 0.9 cm^3, which is determined for each sample specifically with an uncertainty of 0.02 cm^3. The pressure is measured with the same pressure sensor as at the IUP, however calibration is done prior to each measurement, resulting

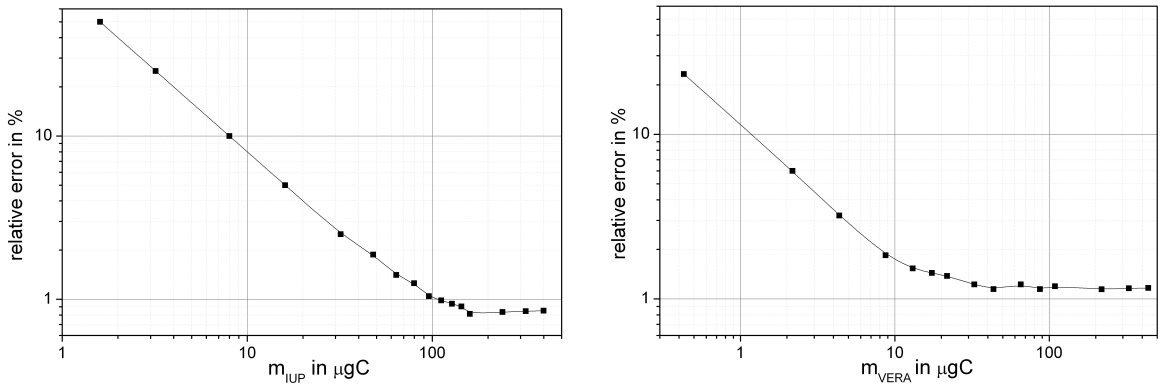

(a) ...at IUP. (b) ...at VERA.

Figure 3.12: Overall uncertainty of manometric quantification...

in an absolute uncertainty of around 0.3 mbar.
Figure 3.12(b) shows the relative overall uncertainty of the VERA mass quantification, being less than 10 % for sample masses larger than 1.5 μgC.

Comparison of the two manometric quantifications

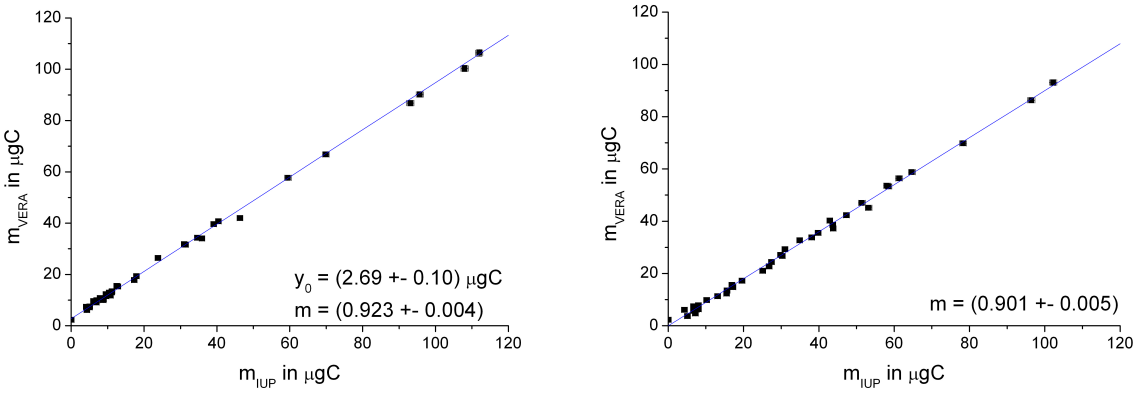

(a) IUP pressure sensor calibration (1) (b) IUP pressure sensor calibration (2)

Figure 3.13: Comparison of IUP and VERA manometric quantification for the IUP pressure calibration (1) and (2).

Figure 3.13(a) shows that for carbon masses, quantified with the old IUP pressure calibration (1), were about $(2.69 \pm 0.10)\,\mu gC$ smaller then determined at VERA. Sample masses determined with the newer IUP calibration (2) show no such offset. However, in both cases the VERA sample masses are only 91 % of the ones previously determined at IUP. These lower values can be explained by the additional cleaning step at VERA, which removes remaining water vapour and non-condensable gases.

Concluding, the IUP manometric quantification is sufficiently good, if the pressure sensor is calibrated regularly. A regular quantification of the manometric volume might also be advisable. Regarding the removal of water vapour and non-condensable gases, a refining of the cleaning steps, especially the sizes of CO_2 and water traps, should be considered.
Overall, the values from the quantification at VERA will be used for evaluating the radiocarbon measurements, as they give the carbon masses used for the ^{14}C AMS measurement, have a smaller uncertainty and an additional cleaning step for other gases.

3.4.2 DOC extraction

The DOC extraction procedure has to be characterised for its blank and extraction efficiency, to determine the minimal sample size, necessary for a reliable ^{14}C analysis, and the overall ^{14}C uncertainty. Furthermore, the UV oxidation velocity should be investigated to give an estimate of the time necessary for complete extraction. Since the LI820 IR CO_2 analyser is relatively inexact for very small concentrations, it should be assured that the oxidation is indeed complete, when the CO_2 concentration in the gas stream suggests the end of extraction.

DOC extraction blank

The blank of the DOC extraction differs depending on the order of preparation, thus both cases (I) “POC-before-DOC” and (II) “DOC-before-POC” have to be investigated.

(I) POC filtration before DOC extraction:
To determine if the POC filtration has any influence on the DOC blank, mQ water was filtered through a pre-heated but otherwise not specifically treated quartz filter. In comparison, a decontaminated blank ice sample as well as a TOC standard solution (1000 ppb) was filtered through a pre-heated quartz filter, which was additionally washed with 1000 ml mQ water prior to filtration. The filtrate was stepwise measured with the DOC analysator DOCster.

As can be seen in Figure 3.14, even a pre-heated quartz filter contains a large amount of water soluble organic carbon - most likely adsorbed onto the filter surface during cool down - which is washed out into the filtrate and significantly contributes to the DOC blank. This contamination can be reduced first by placing the filter under a clean, water saturated atmosphere for cool down, as well as washing the filter prior to filtration with mQ. However, even this procedure may not always completely eliminate contribution to the DOC blank. Considering that the filtration of mQ water may possibly add to the POC blank, a compromise will have to be found, to assure the reduction of the DOC blank contribution without unnecessarily increasing the POC blank. Looking at the filtration of mQ water in Figure 3.14 suggests that 90 % of the DOC may be already washed out with 200 ml.

Three DOC extraction measurements were done to determine the blank of this sample procedure: (1) filtration of a blank ice sample through a not pre-washed filter, (2) filtration of a blank ice sample through a filter, previously washed with about 150 ml mQ and about 10 ml

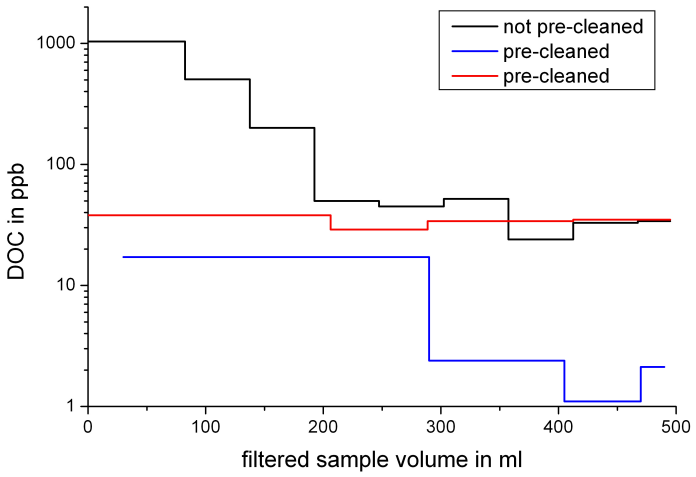

Figure 3.14: Stepwise measurement of DOC after filtration: black = filtration of mQ water through an untreated quartz filter, blue = filtration of a blank ice sample after washing the filter with 1000 ml mQ water, red = filtration of a TOC standard solution (shown is the excess of the expected 1000 ppb) after washing the filter with 1000 ml mQ water. The added up amount of DOC measured was 109 μgC for the mQ sample, 6 μgC for the ice sample and 11 μgC excess DOC for the standard solution.

21% phosphoric acid, and (3) filtration of an oxalic acid standard solution (121 ppb) through a not pre-washed filter. Table 3.4 summarises the results.

Table 3.4: Extracted DOC blank mass and ^{14}C value after filtration. Note that the value for (3) gives the excess oxalic acid carbon mass to the expected mass of 36 μgC and the necessary blank ^{14}C concentration to reduce the expected $f_{OxalicAcid}$ = 1.04 to the measured f value.

	m [μgC]	f_m	decontamination factor [%]
(1)	31.4	0.703 ± 0.006	82
(2)	34.0	0.365 ± 0.004	72
(3)	+25.6	0.076 ± 0.130	-

The extracted DOC blank was very large and the pre-washing with only 150 ml did not reduce the DOC blank as expected. Following these test measurements, extracting DOC before filtration of POC seemed more reasonable, as the DOC extraction does not affect the POC filtration blank.

(II) POC filtration after DOC extraction:
One major blank source of the DOC extraction procedure is the large surface of the melting and DOC pot. The most efficient cleaning process was to keep the pots filled with mQ water, when not used, and rinsing them with mQ water several times before extraction. Additionally,

the DOC pot is pre-cleaned with UV light prior to each sample processing (see Section 3.3.2). This pre-treatment reduced the DOC extraction blank by a factor of 3.

Analysing carbon free water and ice samples, the blank masses and ^{14}C concentrations summarised in Table 3.5 were determined. In addition, standard measurements were carried out using different concentrations of a liquid oxalic acid ^{14}C standard solution with a ^{14}C signature of f_m = (1.042 $\pm$ 0.005) (provided by the Radiocarbon Laboratory, IUP). The expected carbon concentrations of the standard samples were measured before sample processing with the DOCster. The blank mass derived from the standard measurements by linear regression of measured versus expected mass is also given in Table 3.5 along with the corresponding ^{14}C signature derived by the method described below. All blank and standard samples were measured over the course of 5 month (Dec-Apr) parallel to the real samples reported in Chapter 5.

Table 3.5: DOC blank derived from processing carbon free mQ water and artificial blank ice as well as ^{14}C oxalic acid standards. The number in brackets give the number of measurements determining the respective value.

sample	mass [μgC]	f_m
mQ	7.1 $\pm$ 1.9 (5)	0.553 $\pm$ 0.101 (5)
blank ice	9.7 $\pm$ 2.5 (4)	0.750 $\pm$ 0.095 (4)
oxalic acid standard blank	6.5 $\pm$ 0.7 (13)	0.646 $\pm$ 0.050 (4)

As can be seen, all mass blanks seem to agree within their uncertainties, however it might be that for a decontamination factor of 70 - 76% surface contamination of the ice still contributes to the blank with about 3 μgC on average and increases the ^{14}C signature of the ice black compared to the liquid blank.

Combining all 21 blank and standard measurements, the average blank mass is (6.7 $\pm$ 1.0) μgC and the extraction efficiency 96 % (Figure 3.15).

To determine the ^{14}C signature of this DOC blank, the measured ^{14}C value f_{meas} is plotted versus the inverse of the measured mass, following:

$$\begin{aligned} f_{meas} \cdot\ m_{meas} &= f_{expected} \cdot\ m_{expected} + f_{blank} \cdot\ m_{blank} \\ &= f_{expected}(m_{meas} - m_{blank}) + f_{blank} \cdot\ m_{blank} \\ f_{meas} &= f_{expected} + [m_{blank} \cdot\ (f_{blank} - f_{expected})] \cdot\ \frac{1}{m_{meas}} \end{aligned} \tag{3.6}$$

The ^{14}C value of the blank can then be derived from the slope S of the linear correlation and the blank masses presented in Table 3.5:

$$f_{blank} = \frac{S}{m_{blank}} + f_{expected} \tag{3.7}$$

Figure 3.16 shows this correlation for the water and ice blank measurements (here $f_{expected}$ is not known and a free parameter of the linear correlation) as well as for the reliable oxalic acid

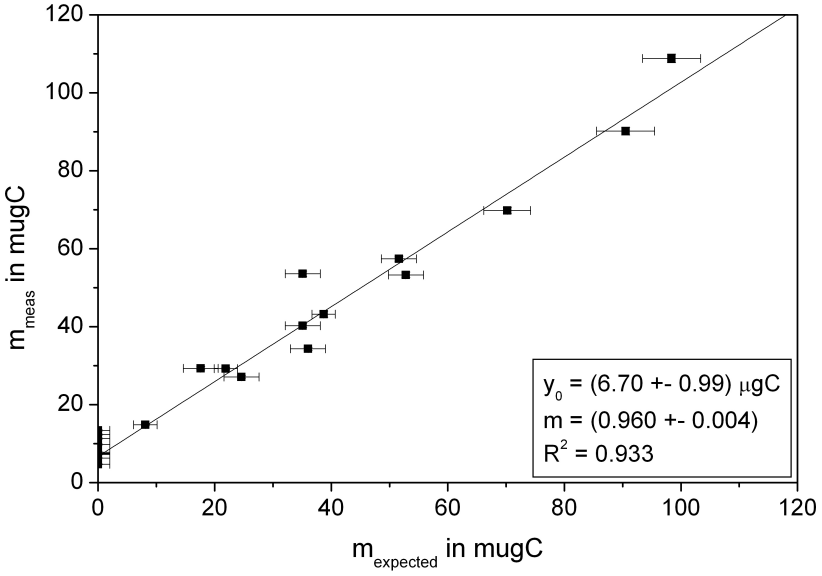

Figure 3.15: Blank mass for DOC extraction derived from 21 mQ water, artificial ice and oxalic acid standard measurements.

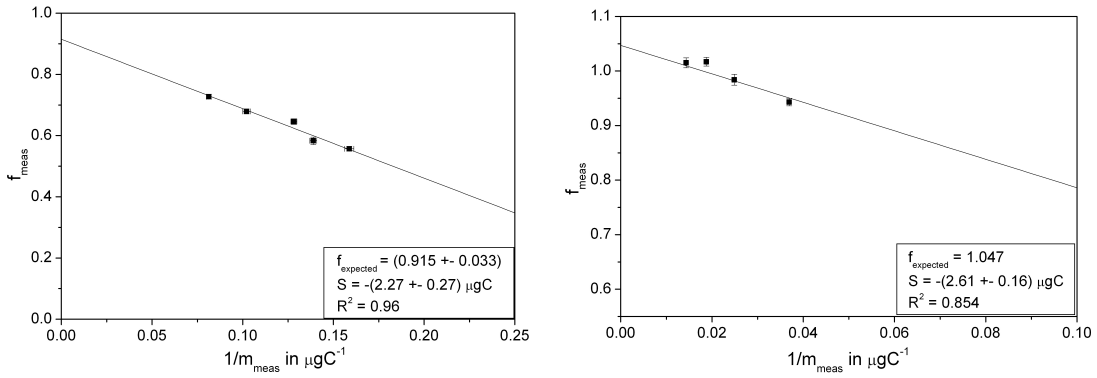

(a) ... water and ice blank measurements. (b) ... oxalic acid ^{14}C standard measurements.

Figure 3.16: Determination of the DO^{14}C blank from...

^{14}C standard measurements.

The resulting f_{blank} according to Equation 3.7 is for Figure 3.16(a) (0.63 ± 0.10) and for Figure 3.16(b) (0.65 ± 0.05), giving an average value of f_{blank} = (0.64 ± 0.07).

Extraction velocity and efficiency

At the beginning, the ideal gas flow for a fast CO_2 extraction was analysed by degassing a carbonate solution for different gas flows. The larger the gas flow through the sample, the faster is the extraction of CO_2 (see Section 3.2.1).

Having decided on a gas flow of 580 ml/min for a time efficient degassing, the time needed for a complete oxidation of different organic carbon compounds was determined by measuring the remaining DOC in the sample with the DOCster (Figure 3.17(a)). As can be seen, the oxidation time depends on the type of organic matter.
Looking at the extraction time needed for different carbon concentrations of oxalic acid, no correlation was found (Figure 3.17(b)) in the measured concentration range of 25 - 200 ppb. The apparent differences in the extraction time can be attributed to a difference in the pH value of the sample and the slight variation of the gas flow from sample to sample.

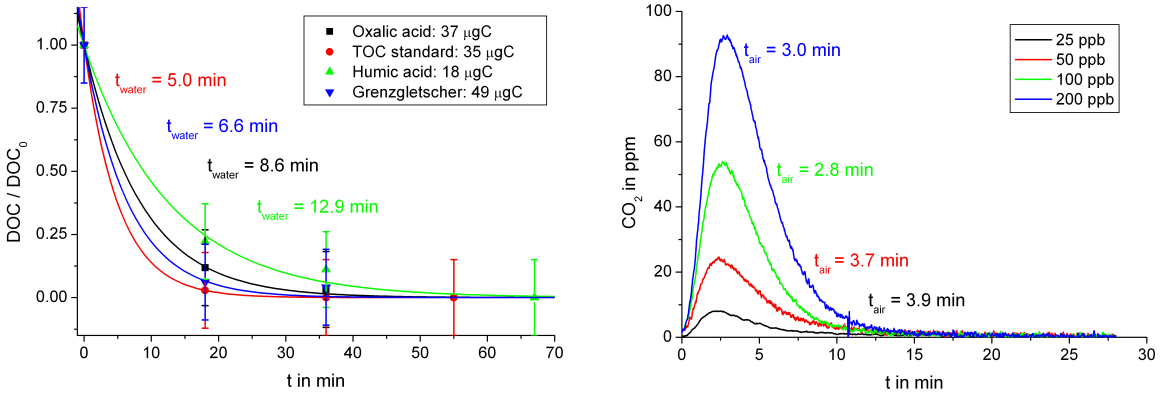

(a) Remaining DOC concentration in different organic carbon samples normalised to the start value measured with the DOCster.

(b) CO_2 concentration in the carrier gas stream measured with the LI820 for the extraction of different oxalic acid concentrations.

Figure 3.17: DOC oxidation and degassing time: the characteristic time t_{gas} gives the time after which the CO_2 concentration in the gas stream is e^{-1} of the maximum concentration and t_{water} gives the time after which the concentration in the water volume is reduced to e^{-1} of the initial concentration.

Note that the characteristic times t discussed here, are not directly equal to the values discussed in Section 3.2.1, but represent now the combination of oxidation and degassing process.

A problem now arises. The monitoring of the CO_2 concentration in the gas stream should allow to determine the completion of the DOC extraction. However, the LI820 is not precise enough in the ppb range. Therefore, if the degassing is faster than the oxidation - as is the case for the presented oxalic acid measurements - a complete extraction of DOC may be seemingly concluded by the CO_2 profile, while DOC still remains in the sample.

Overall, it was found, that an extraction time of 40 min. is sufficient to convert and extract more than 96 % of the DOC for most samples, except humic acid (89 %).

3.4.3 POC filtration

For the POC filtration, a good determination of the blank is necessary, since the small particulate carbon masses extracted form ice samples, react especially sensitive to blank contribution. A small and well defined blank is therefore desirable.

The different contributions to the POC filtration blank, being (1) the blank of the filter, (2) the blank from sample processing and (3) the combustion blank, were investigated. The combustion procedure was found to be blank free. Table 3.6 gives then the respective mass and ^{14}C blank values for different blank sample types.

Table 3.6: Mass and ^{14}C blank for POC filtration with quartz filter: "filter" = filter material blank = (1)+(3), "mQ" = processing a liquid blank sample = (1)+(2)+(3), "blank ice" = processing an artificial blank ice sample = (1)+(2)+(3). The number in brackets gives the number of measurements defining the respective value.

	m [μgC]	f_m
filter	2.3 ± 0.1 (1)	0.610 ± 0.016 (1)
mQ	6.2 ± 0.8 (4)	0.644 ± 0.017 (2)
blank ice	6.4 ± 2.5 (9)	0.596 ± 0.124 (5)

As can be seen, both mQ and ice blanks have a comparable blank mass and ^{14}C signature, indicating that ice decontamination does obviously not contribute to the POC blank. For those 5 quartz filters measured for their ^{14}C content the average mass blank is $(5.2 \pm 1.0)\,\mu$gC with an average ^{14}C signature of (0.61 ± 0.10).

Possible sources for the POC blank may be:

- POC in the laboratory air
- WSOC (water soluble organic carbon) in the laboratory air
- DOC contained in the sample
- POC contained in the "blank" sample

Point one and two may explain the filter blank. E.g. assuming a total carbon concentration in the laboratory air of $6\,\mu$gC/m^3 the filter blank would equal about $0.5\,$m^3 air. This contamination could be reduced by handling the filters only in dust free environment. However concerning the process blanks, it was determined that any WSOC adsorbed onto the filter surface is washed out in the filtrate (see 3.4.2, (I) POC filtration before DOC extraction), thus making a significant contribution arguable. Furthermore, even if the blank samples might contain traces of dissolved organic carbon, filtration of a DOC standard sample showed that it would not be retained by or adsorbed in the filter matrix, thus not contributing to the blank. Notable is that after subtracting the filter blank from the process blanks, a carbon concentration of 7 ngC/ml might be found for the sample, which seems however unbelievably large for mQ water.

Summarising the origin of the blank remains questionable and even the determined amount may not represent a true blank for real samples. However, the determined mass and ^{14}C signature gives the POC blank to the best of knowledge and although rather large, is sufficiently constrained, remaining relative constant over the course of 5 month (Dec-Apr). However, further work is needed in the future, to determine and reduce the blank sources.

3.4.4 Overall analytical uncertainty of the ^{14}C results

Finally, the overall uncertainty for the ^{14}C values after blank correction according to Equation 3.6 has to be determined for POC and DOC containing (1) the measurement uncertainty for the mass and the ^{14}C concentration of the sample as well as (2) the amount and uncertainty of the blank mass and its ^{14}C signature. The uncertainty of the measured sample mass and f_m value can be mostly neglected. Figure 3.18 shows the resulting overall relative uncertainty for different sample masses and f_m values calculated by error propagation of Equation 3.6. Illustrated also are estimates for the corresponding ages and 1σ age uncertainties derived with OxCal. It should be noted however, that these age values give only a rough notion of the order of magnitude and can vary due to the variations in the IntCal04 inventory curve depending on the combination of f and Δf.

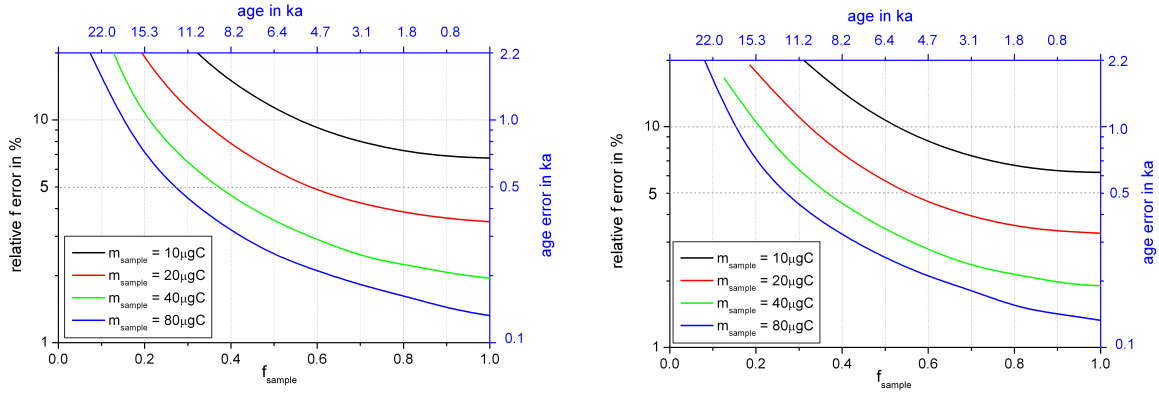

(a) Overall uncertainty for POC

(b) Overall uncertainty for DOC

Figure 3.18: Overall uncertainty of the ^{14}C fraction f_m for different sample masses derived by error propagation of Equation 3.6 and estimates of the corresponding ages and $1\,\sigma$ uncertainties given by OxCal 4.1.

Due to the similar blanks for POC and DOC the overall uncertainty for both fractions is nearly equal. However, while most sample masses for POC reported in this study are in the range of 10 to 20 μgC, DOC sample masses range between 20 to 100 μgC sometimes even larger.

Concluding, a DOC sample of 40 μgC can be dated up to an age of 8000 years with a $1\,\sigma$ uncertainty of less than 500 years, while a POC sample of 20 μgC can be dated only up to 4000 years with the same uncertainty.

3.4.5 Testing the extraction system with real samples

After characterising the DOC and POC extraction using blank and standard samples, the performance of sample processing was investigated for real samples. The focus was on the decontamination quality, sample sizes and the repeatability of ^{14}C analysis for DOC and POC, as well as the ability to reconstruct a recent atmospheric ^{14}C signal in ice. Additionally, first insights into the source mix of DOC and POC (see Section 2.5) may be gained.

Reconstruction of the bomb peak decline from DOC in ice

Three well dated ice samples from a high accumulation ice core of the Col du Dôme (CDD) glacier in the Mont Blanc massif were used to investigate the ability to reconstruct a recent atmospheric ^{14}C signal incorporated in ice with $DO^{14}C$ analysis. All samples contained summer snow and were lying in the declining period of the bomb peak. Table 3.7 shows the sample parameters.

Table 3.7: Sample parameters for three CDD ice samples from the bomb peak era. The ice mass gives the sample size before decontamination. The carbon mass gives the expected VERA derived value according to $m_{VERA} = 0.9\ m_{IUP}$, but without blank correction.

name	date	ice mass [mg]	decon. factor [%]	carbon mass m [μgC]
CDD 86a	1975	570	64	82.2 ± 0.9
CDD 95	1972	540	70	107.1 ± 1.0
CDD 105a	1966	320	56	49.5 ± 0.9

A problem arose during graphitisation. The transfer of the CO_2 sample gas into the graphitisation reactor was hindered by foreign gases reducing the diffusion of the CO_2 leading to only about 50 % of the sample gas being transfered into the reactor. However, there is no reason to discarde the determined ^{14}C values, since ^{14}C values are per definition corrected for any fractionation. However, since any contamination contributed to the total sample mass extracted, the carbon mass quantified at the IUP was corrected according to $m_{VERA} = 0.9 \cdot m_{IUP}$ (see Section 3.4.1) and used for blank correction.

The $^{14}CO_2$ concentration during the bomb peak is well documented (Levin *et al.* (1985); Levin and Kromer (2004); Levin *et al.* (2008)) and can be used to interpret the quality of the measured $DO^{14}C$. The $DO^{14}C$ shows as expected a decrease with time, however contains only about 80 % of the ^{14}C concentration measured in atmospheric CO_2.

Table 3.8: Blank corrected ^{14}C fraction measured in DOC from ice samples compared to atmospheric CO_2 from the Austrian Vermunt station (Levin *et al.*, 1985).

date	$DO^{14}C$		$^{14}CO_2$	$\frac{DO^{14}C}{^{14}CO_2}$
	f_m	f_{corr}	f_m	[%]
1975	0.976 ± 0.013	1.010 ± 0.017	1.37 ± 0.02	74 ± 2
1972	1.176 ± 0.015	1.216 ± 0.018	1.47 ± 0.02	82 ± 2
1966	1.185 ± 0.020	1.280 ± 0.031	1.69 ± 0.03	76 ± 3

In order to explain the reduced $DO^{14}C$ fraction by contamination, the blank mass would have to be either significantly larger, which is unlikely considering the good decontamination factor, or its radiocarbon signature has to be a great deal lower, which contradicts the finding, that the blank ice samples showed rather a higher ^{14}C signature.

May *et al.* (2009) report ^{14}C fractions for total organic carbon (TOC) aerosols sampled between 2002 and 2004 and gives summer TO^{14}C to $^{14}CO_2$ ratios for three mountain site stations of 81 % at Puy de Dôme (France, 1450 m.a.s.l.), 80 % at Schauinsland (Germany, 1200 m a.s.l.) and 74 % at the high Alpine site Sonnblick (Austria, 3106 m a.s.l.). Similar findings are reported in various works by Szidat *et al.*, e.g. Szidat *et al.* (2007) or Szidat *et al.* (2004). Although, these values include the water insoluble aerosol fraction, while the ice sample measurements apply only to the dissolved carbon fraction, the findings show, that the ^{14}C values obtained from the ice samples correspond well to the atmospheric organic aerosol signal.

The analysis shows clearly the problem arising from the different ^{14}C source signatures contributing to the atmospheric carbonaceous aerosol and consecutively to the dissolved organic carbon fraction. The bomb ^{14}C is incorporated into the biosphere and from there released into the atmospheric aerosol body leading to an increased ^{14}C signature. At the same time, the combustion of ^{14}C free fossil fuels leads to the 20 % smaller DO^{14}C values compared to $^{14}CO_2$. While for the presented samples, the falsification of the ^{14}C signal is due to anthropogenic activities, there is no garanty, that pre-industrial DOC sources have no "old" ^{14}C signature (see Section 2.5), which would disturb the age signal. Nonetheless, the recent atmospheric ^{14}C carbonaceous aerosol signal could be reconstructed from DOC in Alpine ice cores for sample volumes of 200-300 ml and high carbon concentrations.

Testing the repeatability on cold ablation zone ice

In order to determine the quality of the decontamination process as described in Section 3.3.1 and the repeatability of ^{14}C analyses for real ice samples, several samples from the Grenzgletscher ablation zone were investigated.

The Grenzgletscher is a polythermal glacier (Suter *et al.*, 2001), which flows down from the Colle Gnifetti firn sattle on the northwesterly flank of the Monte Rosa massif. In its upper accumulation area, the glacier is cold throughout and frozen to the bed. In the region around the equilibrium line ($\approx$ 2800 m.a.s.l.), temperate ice covers the cold ice. In the ablation area, the temperate ice layer is melted away and cold ice origin from the upper accumulation area resurfaces. In 1992 several large ice blocks were taken from the emerging cold ice at two sites in the ablation zone of the Grenzgletscher (see Figure 3.19). Low ion, ^{210}Pb and tritium concentrations indicate preindustrial ice (mentioned in Pichlmayer *et al.* (1998); Steier *et al.* (2006)). The Grengletscher provides thus an easy access to pre-industrial ice in large quantities, which allows the measurement of two similar samples of any sample size to test the ^{14}C extraction system.

It should be noted, that it could not be determined from which of the two sampling sites marked in Figure 3.19 the two sample blocks # 19 and # 21 were taken.

The decontamination of these Grenzgletscher samples is due to the high bubble concentration of the ice more difficult, then for the bubble free blank samples. Thus, while blank ice represents an ice sample, where decontamination would be ideal, the Grenzgletscher represents a sample type, where decontamination might be the most problematic.
Figure 3.21 shows DOC measurements done with the DOCster on small ice samples from

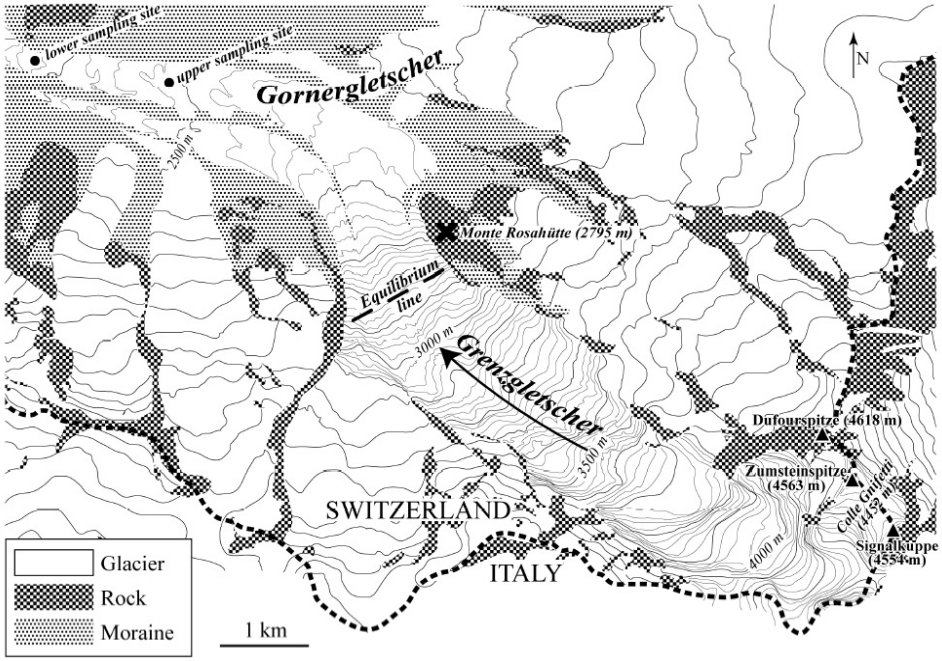

Figure 3.19: Map of the Grenzgletscher flowing down from the Colle Gnifetti and merging below the equilibrium line with the Gronergletscher (taken from Steier *et al.* (2006)). The two sampling sites have been marked in the lower ablation zone.

19 (DOC concentration ≈ 10 ppb) and # 21 (DOC concentration ≈ 120 ppb) with and without washing of the samples prior to melting. The decontamination factor $m_{after\ decon}/m_{before\ decon}$ for the pre-washed samples was around 50 %. Shown is the accumulating carbon mass in the sampled melt water.

For both samples, the excess carbon mass added to the true carbon mass of the sample by contamination of the ice surface, is reduced by decontaminating the sample through washing with mQ. The decontamination procedure seems, however, less efficient for samples with lower DOC concentration. Overall it can be concluded, that although all ice samples contain high bubble concentrations, the decontamination procedure with pre-washing of the sample proves similar effective than for the blank ice.

Following the measurements on small samples, the quality of the decontamination procedure and the DOC / POC extraction system was tested for large ice volumes. POC was extracted from two and DOC extracted from one ice sample taken from block # 19. Additionally, two ice samples were extracted for DOC from ice block # 21. The two POC and DOC samples were cut from the same position within the block and dimensioned in a large and a small ice volume respectively, to allow the investigation of blank contribution, since the larger the sample size, the smaller the influence of the blank. Table 3.9 contains the parameters and results of the extraction process.

POC: The extracted POC mass is very similar for both samples, although the extracted ice volume differs by almost a factor of five. The δ^{13}C (not shown in Table 3.9) is equal for both

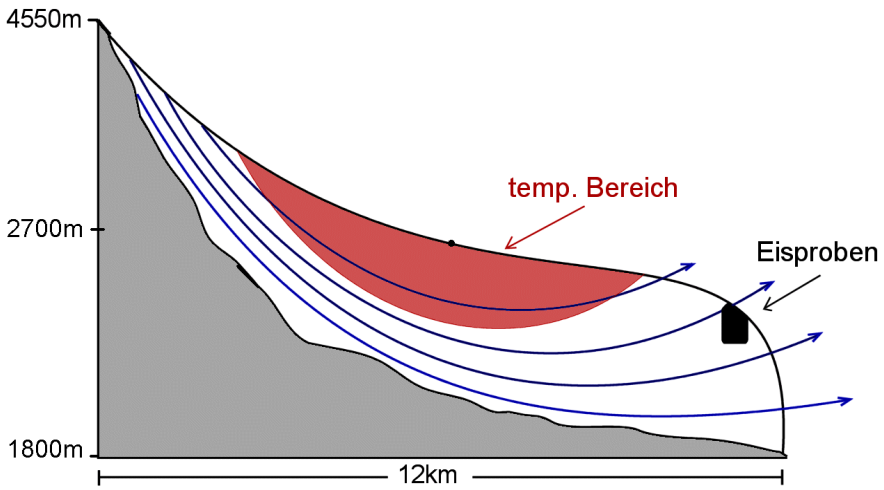

Figure 3.20: Schema of the Grenzgletscher taken from (Friedrich, 2003). Shown in red is the temperated ice region.

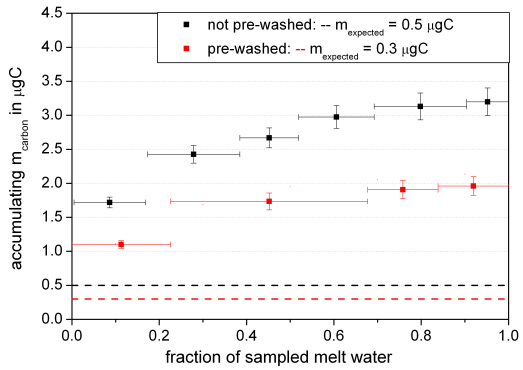

(a) Ice samples from block # 19: the determined DOC concentration for # 19 is ≈ 10 ppb.

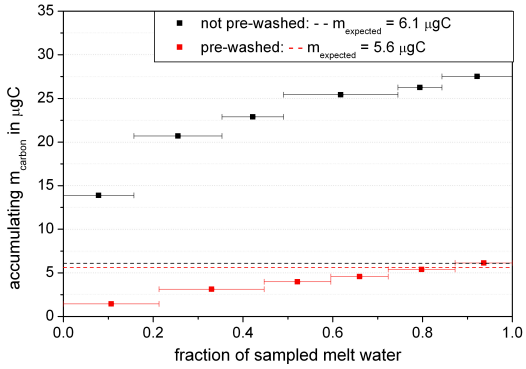

(b) Ice samples from # 21: the determined DOC concentration for # 21 is ≈ 120 ppb.

Figure 3.21: Accumulating amount of carbon in melt water for small (50 - 100 cm^3) Grenzgletscher ice samples melted in the udder vessel. Black = measurement without decontamination of the samples, red = measurement with decontamination by previous washing of the sample.

at +4.5 ‰, whereas the ^{14}C signatures differ significantly. Assuming that this difference is due to a contamination of the small sample, nearly all of its carbon mass, i.e. 9.8 μgC, would have to be due to contamination and would have to carry a ^{14}C signature of f_{blank} = 0.48, in order to achieve accordance of the ^{14}C values for the small and the larger POC sample.
However, Grenzgletscher POC samples analysed from the upper sampling side of the ablation zone by Steier *et al.* (2006) ranged also between 16 - 62 ppb and ^{14}C fractions of f_m = 0.44 - 0.9, showing a strong variation in the POC age mix found in the Grenzgletscher ice. Therefore

Table 3.9: POC and DOC extraction from Grenzgletscher samples. The ice mass gives the sample mass before decontamination. Blank correction is done according to the determined blank parameter in 3.4.2 and 3.4.3.

	ice mass [mg]	decon. fraction [%]	m_{meas} [μgC]	f_{meas}	f_{corr}
# 19 POC_{small}	200	50	10.8 ± 0.2	0.511 ± 0.013	0.419 ± 0.106
# 19 POC_{large}	590	85	9.9 ± 0.2	0.697 ± 0.009	0.792 ± 0.124
# 19 DOC_{small}	480	66	15.9 ± 0.8	0.885 ± 0.026	1.063 ± 0.077
# 21 DOC_{small}	550	55	35.9 ± 0.4	0.938 ± 0.023	0.998 ± 0.031
# 21 DOC_{large}	820	73	57.8 ± 0.7	1.063 ± 0.009	1.117 ± 0.015

the mass and ^{14}C values found for the two POC samples here may also be correct. Further measurements would be required to determine the truth and thus no final conclusion on the quality of decontamination and the repeatability of the POC filtration process can be given at this point.

DOC: The first DOC sample was from the same ice block as the POC samples. The extracted mass concentration is slightly larger, than expected from DOC measurements of small samples of the same ice block, but still within the range given by all Grenzgletscher DOC measurements (unpublished data, M. Schock). The blank corrected ^{14}C value shows modern concentrations, indicating present-day or at least very young ice.

For the DOC samples from block # 21, the DOC concentrations are in the order of previous DOC measurements, although they differ from each other. The ^{14}C fractions are similar to # 19 very high.

All three DOC samples have therefore atypical high ^{14}C fractions, partly lying over the modern reference value. The imminent assumption, that the blank correction is not adequate for real samples, presents the dilemma of determine the correct blank for real samples.

All possible blank contributions during the DOC extraction, like pollution through the carrier gas, glass surfaces, mQ water and acid, are contained in the determined extraction blank. If there is an additional contamination for real samples, it must origin before the sample melting and DOC extraction.

Comparison of mQ water and ice blanks indicated already a possible contribution to the overall blank from the decontamination and melting procedure. Additional contamination sources reach from exposure to the atmosphere during drilling, storage in PE foil and exposure to laboratory air and different materials during prior core analysis. However, assuming simply a larger blank mass does not solve the problem. Crucial for the blank correction is the ^{14}C signature of the blank.

PE foil is typically produced from petroleum and can be assumed to have a low ^{14}C content. Exposure of the ice to large concentrations of acetone or ethanol used in the laboratory can be ruled out as a significant contamination source, since the contact of the sample with the laboratory air is too short and the sample is washed under a clean atmosphere afterward. Contamination of the laboratory air with radiocarbon is unlikely and the ^{14}C concentration in air would have to be extremely large, to explain the contamination during the short atmospheric

exposure of the ice surface. Such a contamination would also be seen in the blank. During storage, the samples are inside the PE foil and in a styrofoam or metal box, so that even a continuous exposure to a radiocarbon source would have limited effect.

A contamination through exposure to the atmosphere either during sampling or later during sample preparation could have a relative high ^{14}C ratio. The average $^{14}CO_2$ value for 1992, the time of sample taking, was measured to be f_m = 1.13 at the tropospheric background station Jungfraujoch (Levin and Kromer, 2004) and 1.03 for 2009 in Heidelberg (I. Levin, 2009, unpublished data), the time of sample processing. These values thus represent the uppermost justifiable limit for any ^{14}C contamination of the Grenzgletscher samples. They do however not necessarily reflect the real contamination of the ice by atmospheric contact, since the extracted DOC sample contains not contamination by atmospheric CO_2 but by carbonaceous aerosols. The ^{14}C signature of the carbonaceous aerosol is in most cases lower than the CO_2 value by 10 to 20 %, as shown above for the bomb peak signal and as apparent from different atmospheric aerosol studies (e.g. Szidat *et al.* (2007); May *et al.* (2009)).
However, even if contamination with a high ^{14}C concentration takes place, it should be superficial and the surface of the samples, which might have been in contact with the atmospheric air, is cut off and a simple surface contamination should be negligible.

Identifying or determining an additional contamination blank proves difficult, as neither the blank mass nor the ^{14}C value of the contamination is known. However, the following facts can be given regarding the process blank of the DOC extraction:

- The blank mass and ^{14}C concentration as determined in Section 3.4.2 summarises all carbon and ^{14}C contributions added during the DOC extraction process by the carrier gas, the mQ water or the acid. These blank contributions are independent of the sample type and contribute to all samples equally. The extraction blank must therefore be subtracted from all samples.

- It was expected that the small and large DOC sample from # 21 should have both the same DOC concentration and ^{14}C signature. However, the small sample has a larger DOC concentration and a lower ^{14}C value. Consolidation of the two samples indicates an increased blank contribution of + 7.3 μgC for the small sample. There was indeed a problem during the decontamination of the small sample, which could explain the additional blank mass. However, this additional blank is a singular occurrence and should not be ad hoc attributed to all samples.

- An additional contamination of the Grenzgletscher samples from exposure to atmospheric air, storage and sample handling can not be completely rejected. However, only a large carbon mass contamination with a ^{14}C signature f_m > 1.11, would reduce the measured and extraction blank corrected ^{14}C concentration of the large DOC sample to a value around or below the reference value and even then the ^{14}C concentration would be still larger than expected for pre-industrial ice.

Disregarding for the moment the high ^{14}C values, it can be concluded, that after the additional correction of the small ice sample from block # 21, all three DO^{14}C values lie in the same

range. The additional correction of the small ice sample is justified by the adaption of the determined DOC concentration and the fact, that there was a problem during decontamination of the sample. The remaining difference between the samples from # 19 and # 21 could be due to a true age difference. Not knowing, how strong the natural variation of DOC in the Grenzgletscher ice is, it must be concluded, that the DOC extraction seems to allow reproduction of ^{14}C values within 5-10 %.

3.5 Summary of the extraction system performance

Aiming at ^{14}C analysis on ice samples as small as possible, the major requirements for the DOC and POC extraction system were a minimal blank and a good extraction efficiency. A large extraction efficiency assures that the maximum of organic carbon contained in the ice sample is extracted and the smaller the blank and its absolute reliability the smaller the minimal carbon mass required for a reliable ^{14}C analysis.

System concept and setup:

After careful considerations of previous investigations, a system was developed to extract DOC and POC from ice samples. DOC extraction is achieved by static UV-induced oxidation with synthetic air and bubble degassing of the evolved CO_2. This method was determined to be the most adequate for the extraction of DOC from 300-500 ml samples for ^{14}C analysis. POC filtration should be done on quartz filter, which were then combusted at 750 °C in a closed-off quartz tube with CuO as oxygen donator. Filtration after DOC extraction was found to be preferable, to avoid a relative large blank contribution from the filtration process to the DOC analysis.

The final setup allows to process ice samples with an area between 2.5 x 2.5 cm and 6.5 x 6.5 cm, a length up to 22 cm and a sample volume between 200 ml and 700 ml. For a sufficient decontamination, a mass loss of more than 25 % should be accounted for. The system is well suited for sample volume of 300-500 ml, which was the aim for ice sample size.

Carbon mass quantification:

Sophisitcated graphitisation allows reliable AMS ^{14}C analysis of carbon masses between 10 and 200 μgC. The manometeric quantification at the IUP allows credible determination of carbon masses between 2.5 and 1500 μgC. With an overall uncertainty of less than 10 % for sample masses larger than 8 μgC, this quantification system seems sufficient for the envisaged sample masses.

The manometric quantification at VERA is at the moment more precise allowing quantification of sample masses larger than 1.5 μgC with less than 10 % uncertainty. Furthermore, the carbon masses determined at VERA are on average 10 % smaller then the masses determined at the IUP most likely due to additional removal of remaining water vapour. This leads to the conclusion, that the trapping and quantification system in Heidelberg needs further improvement. For the cleaning steps better adapted cold trap geometries should be considered and with respect to the quantification precision, the pressur sensor of the manometric unit should be calibrated regularily with the reference volume further reduced.

Since the VERA carbon values give the very masses used for AMS measurement, they are

deployed as well the evaluation of the presented data.

Blank contributions and minimal sample sizes:

The DOC extraction process has a blank of (6.7 $\pm$ 1.0) μgC (based on 21 standard and blank samples) and a ^{14}C signature of (0.64 $\pm$ 0.07) (based on 9 blank and standard samples), if the POC filtration is done after DOC extraction, otherwise the filtration process contributes greatly to the DOC blank. The blank determination was done over the course of 5 month (Dec-Apr) parallel to the sample measurements discussed in Chapter 5. Blank sources are most likely the large surfaces of the melting and the DOC pot. In less than 40 min 96 % of the organic compounds are oxidised and extracted, except for humic acid, were the efficiency is only 86 %. The minimal carbon sample mass given as three times the blank mass would then be 20 μgC.

POC filtration is done on a quartz filter of 0.28 to 4.9 cm^2 with a filtration efficiency of 80 %. The filtration blank (based on 5 blank samples) is (5.2 $\pm$ 1.0) μgC with a ^{14}C signature of f_{blank} = (0.61 $\pm$ 0.1). The blank sources could not be identified, but the exposition of the filter to laboratory air might contribute significantly and requires further work. Minimal samples size for the POC filtration are therefore 15 μgC.

Based on this blank values is the overall uncertainty of the blank corrected ^{14}C fraction of a of 20 μgC sample for both the DOC and the POC fraction less then 10 % for ^{14}C values larger than f_m = 0.3. This translates roughly into the ability of dating 11 000 years with an 1 σ uncertainty of 1 000 years.

Testing the system performance with real ice samples:

Testing the extraction system with real ice samples, the bomb peak $^{14}CO_2$ signal can be reproduced in the DO^{14}C fraction of the high accumulation ice core Col du Dôme with 80 % of the $^{14}CO_2$ signal. The difference in DO^{14}C and $^{14}CO_2$ is similar to the ratio of TO^{14}C / $^{14}CO_2$ measured on recent atmospheric aerosol samples. The reconstructed DO^{14}C signal can therefore be assumed to be equal to the atmsopheric ^{14}C signal of organic aerosol and it can be concluded that the sample extraction works well for real ice samples with large DOC concentrations.

The decontamination procedure was tested on large ice block samples from the Grenzgletscher. No significant problem was detected despite the large bubble concentration of the ice. The decontamination is therefore adequate even for bubble rich ice. However, reproducing PO^{14}C and DO^{14}C values proved difficult.

The extracted POC concentrations were very small and therefore sensitive to the blank contribution. No consens could be found for the ^{14}C fractions of the two POC samples, but according to Steier *et al.* (2006) PO^{14}C seems to vary greatly within the Grenzgletscher ice blocks anyway. The non-consent has therefore very likely nothing to do with the filtration method, but is of natural origin, indicating the problem arising from possible reservoir effects in the organic aerosol source mix.

For DOC, a problem during decontamination of one sample, makes the interpretation of the measurement repeatability unclear. The extracted carbon concentrations differed, but were still in agreement with previous measurements. The ^{14}C values of the three samples agreed within 10 %, which is either the natural variation within the Grenzgletscher ice or due to the

decontamination problem for one of the samples.
The biggest problem is presented by the high $DO^{14}C$ values after blank correction, lying above the modern reference value. However, no reasonable contamination source can be identified, that would cause such high ^{14}C concentrations. Therefore, the extraction blank is assumed to be applicable to real samples and no other contamination takes place.

At this point, the DOC and POC extraction system is expected as being characterised well enough to allow first interpretation of Alpine ice samples.

4 The investigated area - Two types of Alpine glaciers

4.1 Colle Gnifetti

4.1.1 Glaciological and meteorological setting

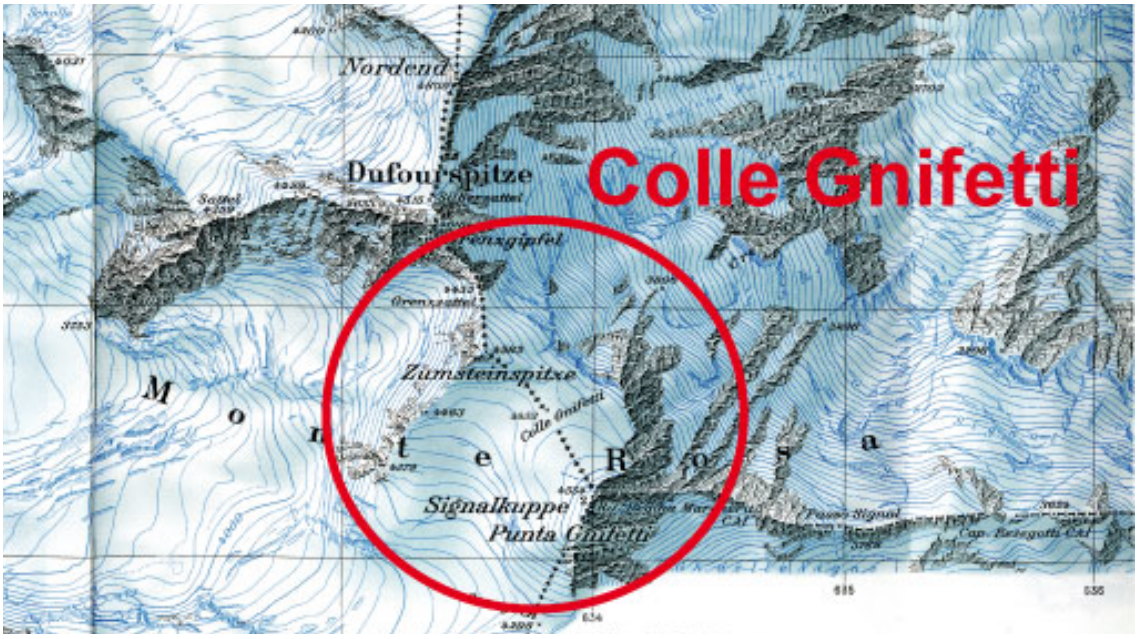

Figure 4.1: Geographic map of the Colle Gnifetti glacier in the Monte Rosa Massif on the Swiss-Italian boarder.

The Colle Gnifetti (CG) glacier, situated at an altitude of 4 550 m a.s.l. in the Monte Rosa massif, forms a firn saddle between Zumsteinspitze and Signalkuppe (see Figure 4.1). The ice flows from these peaks to the main outflow of the Grenzgletscher or breaks off over a steep cliff at its north-eastern edge. Temperatures well below melting point at bedrock cause the glacier to be frozen to the ground prohibiting sliding motions. The CG is a “cold” glacier having ice and firn temperature below zero degree throughout the year, being on average -15°C (Haeberli and Alean, 1985). This condition is a prerogative for the chronological preserving of climate

signals and makes the Colle Gnifetti one of few Alpine glaciers providing the possibility to serve as a mid-latitude climate archive. However, the small horizontal dimensions compared to the ice thickness of about 100 m, the complex bedrock topography and ice flow dynamics, the exposed location and the varying meteorological conditions challenge the interpretation of the climate archive (Wagenbach *et al.*, 1992).

The accumulation rate varies over the glacier surface depending on the exposure to wind and aspect systematically increasing from about 0.1 m w.e. (meter water equivalent) at the north-west slope of Signalkuppe to 1.2 m w.e. at the south slope of Zumsteinspitze (Alean *et al.*, 1983). While on a large scale the CG has been shown to be in steady state over the last hundred years, variations of the surface topography on small scales can cause a temporal change in accumulation at one position. Furthermore, although air temperatures are below zero throughout, the glacier samples snow not homogeneously over the year. The winter snow being drier and lighter is often blown off by strong winds, while the more heavier, wet summer snow sticks to the underlying firn. The amount of sampled winter and summer snow may change from year to year and even loss of a complete annual layer is possible. This sampling behaviour makes interpretation of the isotopic signal exceedingly difficult (Bohleber, 2008). The temporal changes in accumulation rate at one position on the glacier as well as the inflow of ice to that position from up-stream regions with significantly different accumulation rates, called the up-stream effect (Wagner, 1996), also disturbs the age-depth relationship.

4.1.2 The available ice cores

Several ice cores have been drilled in collaboration of IUP and KUP (Klima und Umweltphysik, Physikalisches Institut, Universität Bern) at the Colle Gnifetti, their position being shown in Figure 4.2(a). Table 4.1 combines the most important details about the four down to bedrock climate ice cores analysed and in store at the IUP.

Table 4.1: Main core characteristics of the four deep Colle Gnifetti ice cores analysed at the IUP. Given are the core depth in absolute m and m w.e., the year of drilling t_0, the position of the tritium peak, the accumulation rate averaged over 30-40 years derived by the identification of the tritium peak A_0 and the firn-ice transition.

core abbrevation	CC	KCS	KCH	KCI
H [m]	64.10	100	60.30	61.84
H [m w.e.]	49.85	78.65	45.02	48.44
t_0 [year AD]	1982	1995	1995	2005
^{3}H [m w.e.]	4.1	16.18	7.34	5.75
$A_0(^3H)$ [m w.e./a]	0.22	0.51	0.23	0.14
firn ice transition [m w.e.]	20	28	22	17

KCH, CC and KCS lie on the same surface flow line, while the newest KCI core has been drilled in direction of the cliff, at a position with small accumulation rate as the ice cliff acts as a sink for the wind blown snow (see Figure 4.2(b)).

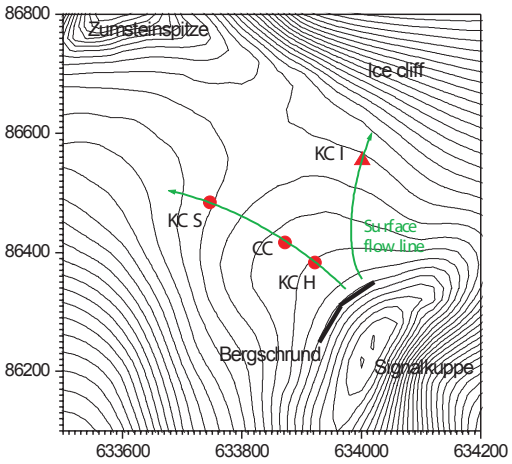

(a) Positions of main Colle Gnifetti ice cores analysed and in store at IUP. Figure taken from Bohleber (2008).

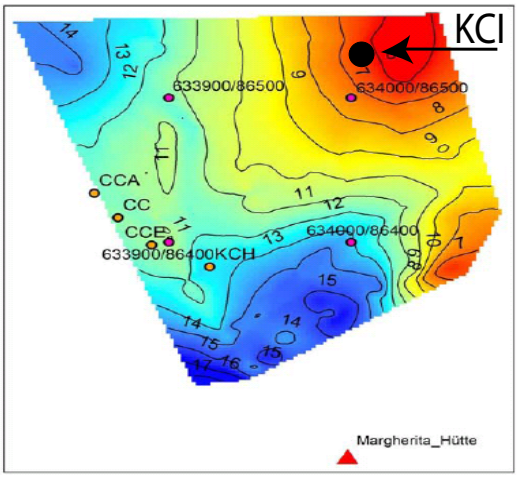

(b) Spatial distribution of accumulation rate: red = small accumulation, blue = large accumulation. The position of the KCI core is marked. (based on ground penetrating radar data from Boehlert (2005))

Figure 4.2: Surface flow lines and accumulation rates at Colle Gnifetti. Note that Figure 4.2(b) shows only a part of the surface covered by Figure 4.2(a).

The accumulation rate A_0 varies considerably for the different core positions. However the flow dynamics of the glacier saddle make it clear, that all lower core sections obey a common surface accumulation regime. Thus A_0 converges in the lower core sections toward the typical value of the upper catchment area contained by the Bergschrund, a deep crevass separating the flowing from the stagnant part of the glacier (Keck, 2001). Nevertheless, the annual layer thickness is still not homogeneous between the cores, since while the KCH core exhibits a mean horizontal flow direction downslope of the Signalkuppe, the KCI is influenced by a two dimensional flow pattern.

4.1.3 Previous dating attempts

Dating of the Colle Gnifetti ice cores has been undertaken by Armbruster (2000), Keck (2001) and especially Bohleber (2008) using:

- identification of absolute time horizons in the last 100 years, like the tritium bomb peak and Saharan dust events.
- establishing of a volcano chronology.
- continuous and discrete annual layer counting especially of NH_4^- and other major ions or dust records.
- ice model extrapolation for the lower core sections.

Bohleber (2008) dismisses the establishing of a volcano chronology as dating technique, as the identification of a volcanic horizon in an ice core and the determination of the eruption event in history it represents is very difficult. A volcano chronology may therefore at best be used to validate other dating scenarios. The Colle Gnifetti core dating is mainly based on annual layer counting of the NH_4^- concentration record for CC and KCS and the particle concentration record for KCH and KCI as well as model extrapolation in the lower core sections. Table 4.2 summarises some parameters of the preliminary age-depth relationship of the four cores shown in Figure 4.3.

Table 4.2: Core dating characteristics for CC, KCH, KCS and KCI derived from Armbruster (2000), Keck (2001) and Bohleber (2008) (SS = Saharan dust event; n.i. = not identified).

dating parameter	CC	KCH	KCS	KCI
surface date AD	1982	1995	1995	2005
SS 1947 AD [m w.e.]	1.0	4.4	10.0	4.7
^{3}H 1963 AD [m w.e.]	4.1	7.3	16.2	5.8
SS 1947 AD [m w.e.]	7.8	n.i.	n.i.	7.7
SS 1936 AD [m w.e.]	n.i.	12.6	26.7	n.i.
SS 1901 AD [m w.e.]	16.0	20.0	37.3	11.5
1000 AD [m w.e.]	-	42	60.7	34
dating uncertainty at 1900 AD	$\pm$ 5 a	$\pm$ 3 a	-	$\pm$ 2 a
dating uncertainty at 1600 AD	$\pm$ 18 a	$\pm$ 75 a	$\pm$ 10 a	$\pm$ 42 a
dating uncertainty at 1000 AD	-	$\pm$ 200 a	$\pm$ 52 a	$\pm$ 80 a

Figure 4.3 shows that as expected, the KCI core exhibits, compared to the other cores, same ages at lower depth. Following this dating, the oldest ages would be found in the KCI or the KCS core.

4.2 Vadret dal Corvatsch (Piz Murtèl)

4.2.1 Glaciological and meteorological conditions

The Vadret dal Corvatsch is a small ice cap on top of the Piz Murtèl (3 433 m a.s.l.) in the Upper Engadin. At the beginning of the 20th century, the ice crest was part of a larger glacier, which has "broken up" since then. The Corvatsch consists now of a northern and a southern part and is about 500 m long (see Picture 4.4). The southern part exhibits an asymmetric geometry, with a cornice running from the peak of Piz Murtèl in northern direction separating a 45 m high, very steep slope (30 - 45°) on the north-west from the smoother decline on the south-eastern slope (Haeberli *et al.*, 2004).

Busarello (2002) determined the topography of the bedrock and the glacier surface via georadar measurements in 2000 AD and quantified the glacier thickness. These measurements were repeated 2007 revealing that since then the glacier lost on average 5 m of its thickness, which also changed the surface topography (see Figure 4.6).

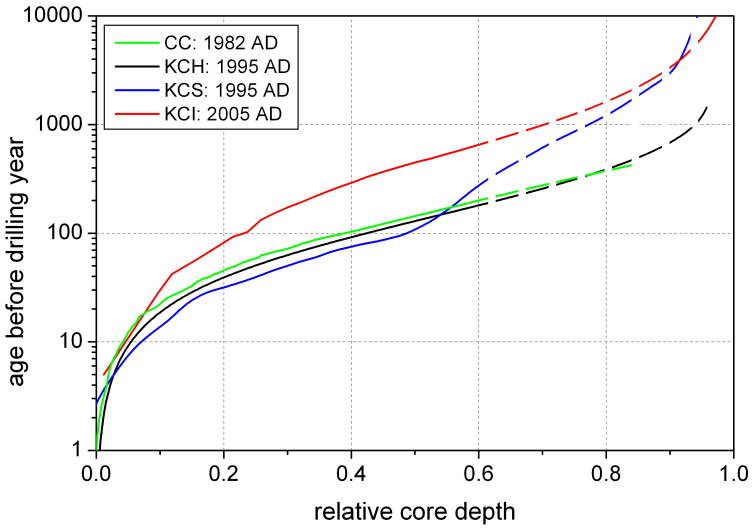

Figure 4.3: Comparison of all four Colle Gnifetti ice core chronologies. The dashed line indicates, where the age-depth relationship becomes no longer reliable. Plot taken from Bohleber (2008).

Haeberli *et al.* (2004) reported, that during the hot summer of 1998 snow on Piz Murtèl melted back to the crest and the subjacent ice was exposed, revealing a striking sequence of crest parallel layers on the leeward slope, strongly resembling annual layering (see Figure 4.5(b)). Furthermore, during the summer 2003, snow and firn disappeared and ice loss of at least 3 m was observed.

Investigating the meteorological conditions in the last 28 years, the average air temperature measured at the Corvatsch station at 3 315 m a.s.l. is -(5.3 $\pm$ 0.6)°C and the mean annual precipitation sum (880 $\pm$ 130) mm/a, both showing no significant changes since 1980. However, the years 1998, 2003 and 2006 are exceptional with very high summer temperatures and low precipitation.
Due to the relative low altitude of the glacieret, air temperatures always reach positive values in summer: 22 % of the monthly mean temperatures since 1980 are > 0°C, only 29 % of the months have maximal temperatures not exceeding zero and 42 % of the months have more than 10 days with temperatures above 0°C. These positive temperatures result in melting of the surface snow cover. Therefore ice formation happens through melting and refreezing (superimposed ice) rather than sedimentation. As the accumulation is converted into ice over the course of two or three years, the glacier can still chronologically preserve climate information.

Although the ice cap lies today in the altitude range where temperated firn is typically observed, measurements revealed sub-zero ice temperatures over 3 300 m a.s.l. and an average of -3°C for the basal layer (Hager, 2002). These findings indicate that the small ice cap contains in parts cold ice frozen to the bedrock and thus may contain several thousand years old ice. As the ice mass is very sensitive to climate change, dating of the bedrock ice may give information about minimal glacier extension (Haeberli *et al.*, 2004).

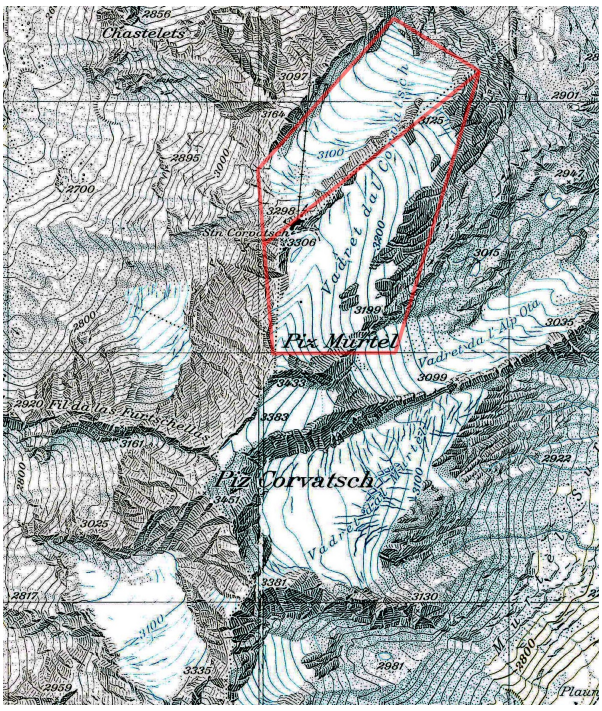

Figure 4.4: Geographical map of the Piz Murtèl area. The red line indicates the north and south part of the Vadret dal Corvatsch glacier (map from Swisstopo).

4.2.2 Previous studies on the ice composition and the glacier age

The Vadret dal Corvatsch has been the focus of decided research for about 10 years. During the EU-ALPCLIM project (Wagenbach (2001), Haeberli *et al.* (2004)), the ice temperature, ice formation and mass balance have been investigated to determine the utility of small glacierets as climate archive. In 1999 a 6 m long ice core was drilled at the crest and analysed for i.e. ice density, δ^{18}O, conductivity, ion content and tritium. The visual inspection of air bubbles, the average density of 0.85 g cm^{-3} and the high ion content indicated superimposed ice formation. The tritium peak of 1963 was found in a depth of about 4 m thus giving an idea about the age of the recovered ice.
In 2005 a surface profile of the north-western slope was taken and analysed for various parameters by Bengel (2005). The dust and age profile revealed, that melting processes and subsequent run down of melt water, makes interpretation of the data nearly impossible.

A first attempt at modeling the age-depth profile was made using a 2D finite element model for two glacier geometries (Wagner, 1996). Assuming plain strain, steady state, a homogeneous ice density of 0.9$\frac{g}{cm^3}$, incompressibility of the ice and no basal melting and sliding, the results for a symmetric (a) and a asymmetric (b) triangle geometry are shown in Figure 4.7.

For the symmetric geometry, ice emerging at the lower half of the slope has been accumulated in a narrow zone at the summit and thus under more or less the same topoclimatic conditions. Flow velocities are extremely slow in such symmetric and steady-state conditions and therefore result in very large ice ages of several thousand years even reaching into the last glacial.

(a) Summer 1998: strong melting of the complete snow and firn cover revealed the subjacent ice (Picture by M. Hoelzle).

(b) Winter 2007 during the VCL drilling campaign (Picture by B. May)

Figure 4.5: Vadret dal Corvatsch glacier as seen from the Corvatsch Cable Car Station.

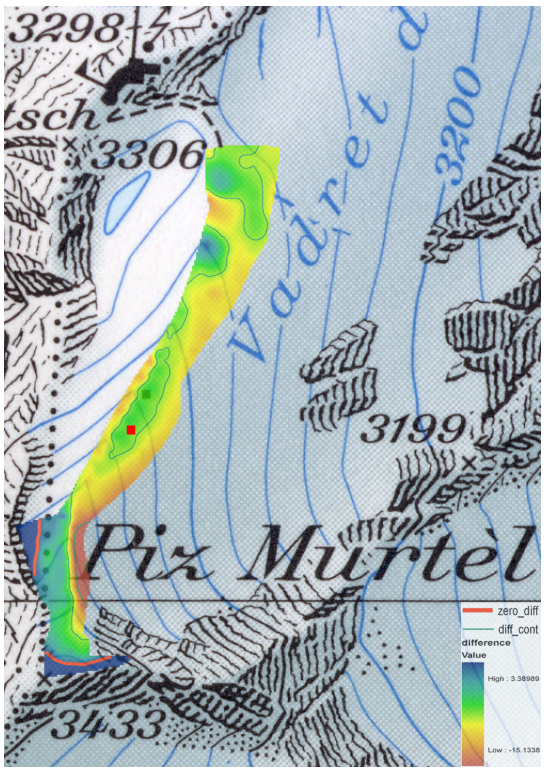

(a) Change in ice thickness between 2000 and 2007

(b) Change in surface topography between 2000 (red) and 2007 (blue)

Figure 4.6: Change in the Vadret dal Corvatsch glacier thickness and surface topography (data by M. Hoelzle, map from Swisstopo). The red square indicates the position of the VCL ice core.

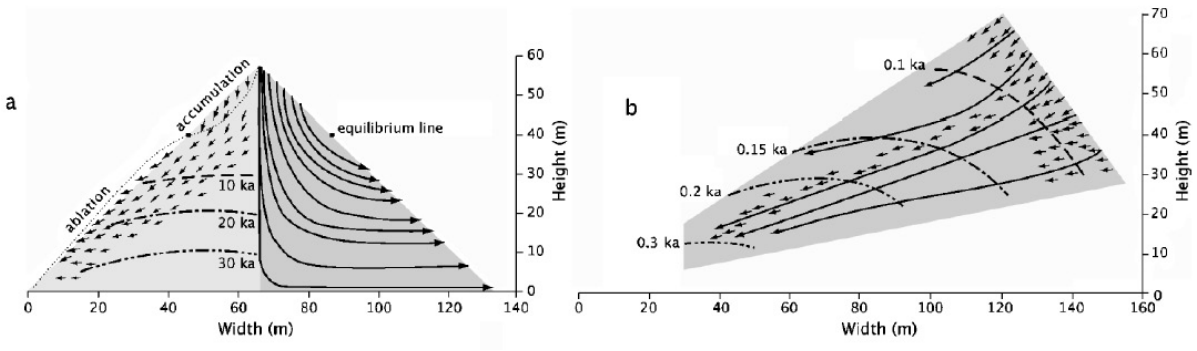

Figure 4.7: 2D finite element modeling of a (a) symmetric triangle with horizontal bed and an (b) asymmetric triangle with an inclined bed (Wagner, 1996).

For an asymmetric geometry, accumulation takes place in the direct summit zone and in the whole area of the steep leeward slope. The ice flows away from the slope with far larger velocities than for the symmetric case. The resulting ice ages are in the order of centuries, with older ice in an extremely thin layer at the bottom of the ice body (Wagenbach (2001); Haeberli *et al.* (2004)).

4.2.3 The VCL ice core

In January 2007 an ice core (VCL) was drilled in cooperation with the Department of Geography, University of Zurich down to bedrock about 3 - 4 m from the ridge on the south-eastern flank at an altitude of 3 340 m a.s.l. about 100 m below the peak. The core has a diameter of 3” and a total length of 27.46 m starting about 0.6 m below the top surface of 2007. The core contains 0.4 m.w.e of snow/firn layer, followed instantaneously by ice with an average density of 0.85 g cm^{-3}. The ice core was analysed by Rau (2008) with Continuous Flow Analysis (CFA) for particle concentration and conductivity and an δ^{18}O and D-profile was determined on discrete aliquots. The tritium peak of 1963, found in the short ice core from 1999 by Frauenfelder (Wagenbach, 2001), was no longer found in the VCL core. Maximum tritium values exceeding the natural values were however measured at the top of the ice core and were attributed to the year 1962 (Rau, 2008).

4.3 The bottom part of the available ice cores

Two of the four CG cores, CC and KCS, as well as the VCL core are drilled down to the bedrock. All three show the distinct yellow silt indicating basal ice, which has to be regarded carefully with respect to dating, since it does not reflect the age of the glacier ice. The colouring indicates the influence of the bedrock on the ice matrix and impurity contents, seen e.g. in a characteristic increase of particle concentration, conductivity and organic carbon. For the other two cores, KCH and KCI, increases in particle concentration and conductivity have been observed too, but no silt was encountered, suggesting that the basal layer was not reached, but

is probably not far off.

The stable water isotope δ^{18}O records show for all CG cores the strongest signal at the bottom of the core through a significant shift of δ^{18}O below the 20th century mean of -13 ‰. It seems obvious, that this signal indicates Pleistocene ice. However the different preliminary dating give different ages for the δ^{18}O transition in the different cores. Thus, the question remains, if the transitions seen in the CG cores, indicates indeed Pleistocene ice, or if diffusional processes, as discussed by Keck (2001), are responsible.

For the VCL, no extraordinary signal can be seen in the δ^{18}O signal of the basal layer. Also, contrary to the CG cores, the variation of the particle concentration and the conductivity signal does not diminish, as would be expected due to a rapidly decreasing annual layer thickness. This difference sets the small ice cap apart from the typical cold glacier and indicates, that the age distribution in this glacieret may behave quite differently than for the CG.

Since the annual layer thickness in the lowest part of the ice core becomes infinitesimal thin, the age in the bottom of the core explodes making theoretical as well as traditional, experimental dating impossible. The bottom of any ice core is therefore a sensitive region and needs to be paid special attention. Since all other dating methods fail here, ^{14}C may finally be able to put an age constrain on this difficult area.

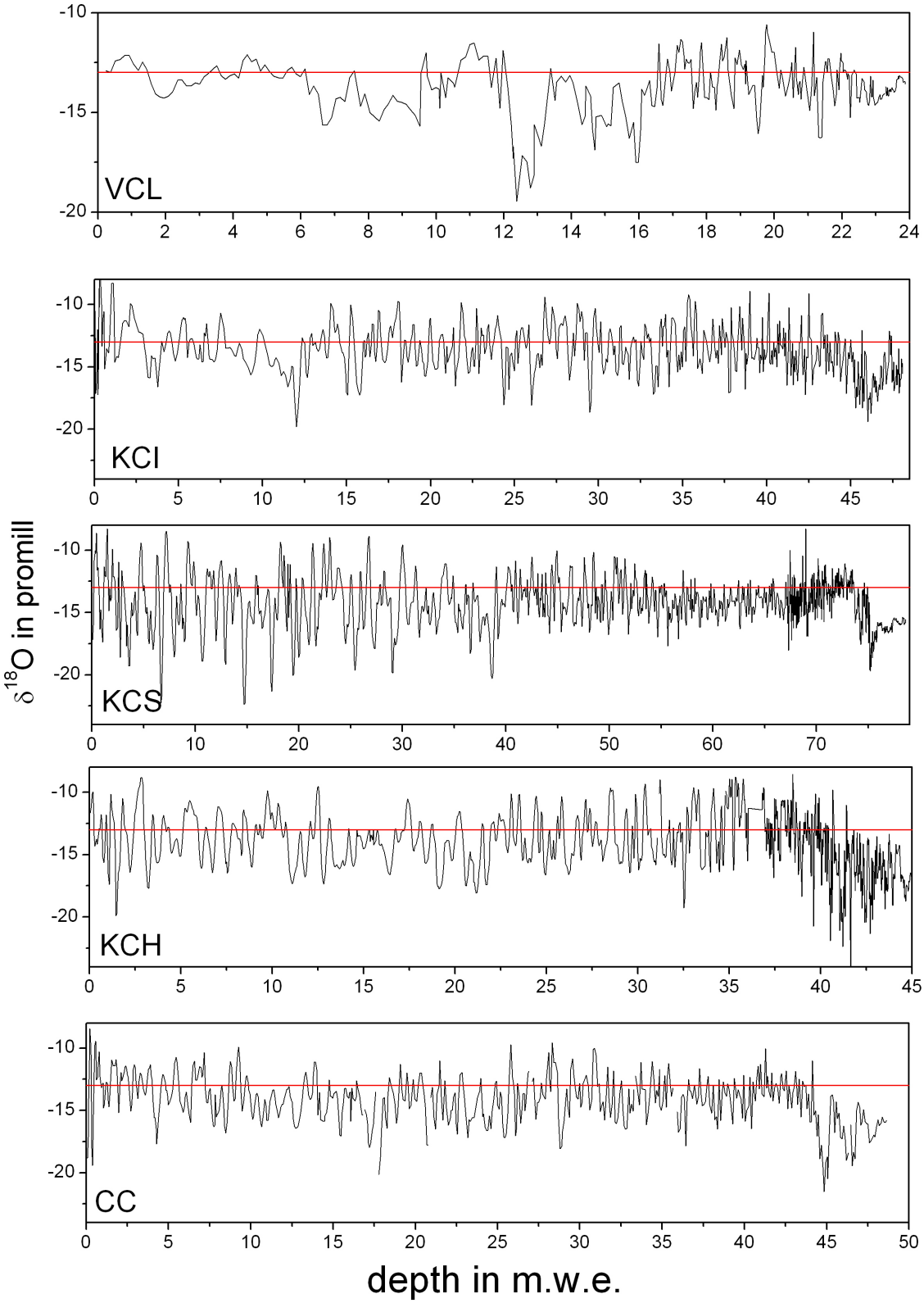

Figure 4.8: δ^{18}O record of the CC, KCH, KCS, KCI and VCL ice core down to near bedrock. The red line indicates the 20th century mean δ^{18}O. Note the different scale of the y-axes for the VCL core.

5 Presentation and discussion of ice core ^{14}C data

5.1 Sample selection, blank correction and data presentation

The focus of this work was the dating of mainly two ice cores: (1) the VCL from the Vadret dal Corvatsch and (2) the KCI from the Colle Gnifetti. In addition, some samples were measured for the other two CG cores, KCH and KCS, to allow a comparison of the radiocarbon ages derived for different cores from the same glacier.
The following chapter contains the presentation of the ^{14}C data set, including characteristics of and reasoning for the different samples, followed by a first perusal, where obviously biased values are discarded. Finally, artificial and natural input of excess ^{14}C into the organic carbon sample masses are discussed.

5.1.1 The data set

Mainly there were three rounds of sample preparations and ^{14}C measurements: (A) January 2009, (B) February - April 2009 and (C) June - July 2009. At the time of sample preparation for round (A), the (I) "POC-before-DOC" method was still envisioned for the extraction of both fractions, but the blank could not be sufficiently reduced. Even without prior POC filtration, the DOC blank was at the beginning not yet sufficiently small enough to attempt DO^{14}C measurements. For the samples prepared in round (B) and (C) all DOC samples were extracted with POC still present in the sample ((II) "DOC-before-POC").

Sample selection for the Vadret dal Corvatsch

The lower altitude of the Vadret dal Corvatsch yields higher particle concentration in the ice than found in a higher glacier. ^{14}C analysis could, therefore, easily be carried out on POC, returning enough carbon mass for small ice volumes (100 - 200 ml). The POC samples were analysed in the first round (A) of ^{14}C measurements and no DOC was extracted parallel to the POC. In the second sample charge (B), six DOC samples were prepared for comparison, but POC was not extracted due to sample limitation of ^{14}C analysis. Additionally, six POC samples are reported, that were obtained during Countinuous Flow Analysis (CFA) (see Rau

(2008)). Although, these samples were more a byproduct of the CFA, great care has been taken with decontamination of the filter to make ^{14}C analysis possible. After filtration, the CFA filters have been treated like all other POC samples.

All POC and DOC samples were selected to ensure coverage of the whole core. As the VCL contains no firn, the whole ice core was available for sampling without concern for decontamination. Strong dust layers and exceptional high particle concentrations were avoided, to evade singular deposition events, which might carry an atypical ^{14}C signature.
The whole core was previously cut as seen in Figure 5.1 and all ^{14}C samples were simply taken from part B.

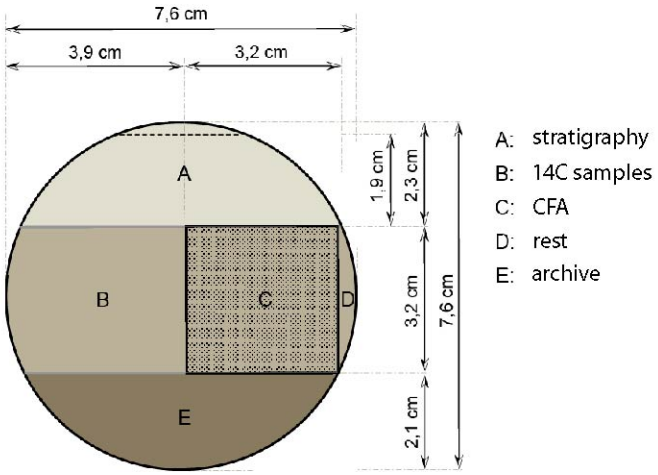

Figure 5.1: Illustration of the cutting into different parts of the VCL core.

Sample selection for the Colle Gnifetti

The particle concentration in the high Alpine Colle Gnifetti cores are far lower than for the Vadret dal Corvatsch. Therefore, ^{14}C analysis was mainly focused on the DOC fraction.
The first ^{14}C samples from the Colle Gnifetti were extracted in the first round (A) from three ice samples of the KCS core. The preliminary dating of the KCS core suggested large ages and there was still enough core material available for reasonable sample sizes. Regardless of the blank problems for DOC, both fractions were still extracted with the (I) "POC-before-DOC" method, in order to gain a feeling for the extraction of both fractions from real ice core samples. At least, the POC fraction would give reliable data, if the carbon mass was large enough, and the DO^{14}C value might still be compared to it.
In the second round of sample preparation (B), nine samples from KCI were extracted for DOC and POC. Focusing on the DOC fraction, the ice sample volume was adjusted to ensure that the DOC carbon mass was large enough for ^{14}C analysis, while still keeping the ice volume at a minimum. This adjustment resulted in very low carbon masses for the POC fraction. Still it was hoped for, that a comparison of the ^{14}C fractions for the two carbon fractions might give information about the respective source composition.

Three samples from the KCH core were extracted for DOC and POC to complete the ^{14}C comparison of the three CG deep ice cores.

All samples were selected according to the following criteria:

- the sample was taken from below the firn ice transition, i.e. below pore close-off with a sample density > 0.84 $\frac{g}{cm^3}$, to allow for adequate decontamination.
- the particle concentration, as determined by CFA (Bohleber (2008); Armbruster (2000)), was of an average range to avoid sampling of singular deposition events, that might have an atypical DOC / POC composition.
- there were no strong gradients in the $\delta^{18}O$, particle and conductivity record, which might indicate sudden changes in the environment, leading to exceptional ^{14}C values.

Finally in the third ^{14}C sample charge (C), DOC was extracted from two KCS samples adjacent to KCS-95 and KCS-108. These additional measurements should allow a comparison of the $DO^{14}C$ fraction for the two extraction methods and give $DO^{14}C$ values comparable to the other CG ice cores. Also, DOC was extracted from two ice samples preceding KCI-32 and KCI-74, to test the repeatability of the extraction process.

Note that for two samples, KCI-42 (DOC) and KCI-54 (POC), no ^{14}C value was obtained due to loss of the carbon target after graphitisation.

The POC and DOC samples extracted from the Col du Dôme (CDD) and the Grenzgletscher (GG), have already been discussed in Section 3.4.5. However, they will here be reported and incorporated into the discussion for the sake of completeness. The CDD samples were measured in the first round (A) after the DOC extraction blank was reduced enough for a reliable measurement. For the Grenzgletscher, the POC samples were analysed in round (A), the single DOC sample in round (B) and the other two DOC samples in round (C).

Blank correction

All samples are corrected for the extraction blank according to:

$$m \cdot \ f_m = m_{corr} \cdot \ f_{corr} + m_{blank} \cdot \ f_{blank} \tag{5.1}$$

where m and f are the measured mass and ^{14}C fraction and m_{corr} = (m - m_{blank}). The following blank values were used for correction:

- POC (all except CFA samples): m_{blank} = (5.2 $\pm$ 1.0) μgC; f_{blank} = (0.61 $\pm$ 0.10): as determined in Chapter 3.4.
- POC-CFA: m_{blank} = (7.4 $\pm$ 1.0) μgC; f_{blank} = (0.625 $\pm$ 0.10): the blank value was obtained by one specific CFA blank measurement, the errors have been adopted from the POC blank.
- DOC method (II): m_{blank} = (6.7 $\pm$ 1.0) μgC; f_{blank} = (0.64 $\pm$ 0.07): as determined in Chapter 3.4.

- DOC method (I): m_{blank} = (35.0 $\pm$ 5.0) μgC; f_{blank} = (0.365 $\pm$ 0.07): the blank value was obtained from one specific process blank measurement, the uncertainty of m_{blank} is assumed, Δf_{blank} is adopted from the other DOC blank.

Table 5.1 gives the sample characteristics and the blank corrected ^{14}C values for the CG samples. Table 5.2 contains the ^{14}C results for (1) the Vadret dal Corvatsch VCL ice core samples, (2) the Col du Dôme bomb peak samples and (3) the samples from the Grenzgletscher.

Table 5.1: Characteristics of the ^{14}C samples for the Colle Gnifetti ice core KCI, KCS and KCH. Reported are the ice core number, the depth of the sample, the blank corrected carbon mass, the $\delta^{13}C$ and the blank corrected fraction modern carbon f_{corr}. For the KCS samples, the difference in the sample preparation method is indicated by (I) and (II). The asterisked sample is discarded immediately due to the extremely low carbon mass.

type	**core name and number**	**depth [m w.e.]**	$\mathbf{m}_{corr}$ **[μgC]**	$\Delta\,\mathbf{m}_{corr}$ **[μgC]**	δ^{13}**C [‰]**	$\mathbf{f}_{corr}$	$\Delta\mathbf{f}_{corr}$	
DOC	KCI-32	17.75 ± 0.13	45.1	0.9	-19.6	1.006	0.013	
DOC	KCI-32	17.98 ± 0.11	35.6	1.1	-17.2	1.131	0.022	
POC	KCI-32	17.98 ± 0.11	1.0	1.0	-12.9	1.094	0.739	(*)
DOC	KCI-42	25.44 ± 0.14	28.8	1.1	-	n.a.	n.a.	
POC	KCI-42	25.44 ± 0.14	6.1	1.0	-19.0	0.644	0.090	
DOC	KCI-51	31.98 ± 0.12	16.0	1.0	-7.5	0.947	0.037	
POC	KCI-51	31.98 ± 0.12	2.0	1.0	-14.8	0.916	0.317	
DOC	KCI-54	34.71 ± 0.12	14.3	1.0	-17.7	1.185	0.058	
POC	KCI-54	34.71 ± 0.12	2.2	1.0	-	n.a.	n.a.	
DOC	KCI-63	40.92 ± 0.10	30.5	1.1	-11.6	1.074	0.023	
POC	KCI-63	40.92 ± 0.10	9.4	1.0	-24.0	0.832	0.064	
DOC	KCI-67	43.32 ± 0.13	8.9	1.0	-22.5	1.152	0.073	
POC	KCI-67	43.32 ± 0.13	3.2	1.0	-15.3	0.468	0.177	
DOC	KCI-72	46.39 ± 0.09	17.7	1.0	6.7	0.690	0.030	
POC	KCI-72	46.39 ± 0.09	2.3	1.0	-20.0	0.773	0.250	
DOC	KCI-73	47.46 ± 0.09	31.9	1.1	-20.0	0.870	0.020	
POC	KCI-73	47.46 ± 0.09	2.5	1.0	-18.0	0.664	0.220	
DOC	KCI-74	47.72 ± 0.12	52.2	1.0	-18.7	0.839	0.011	
DOC	KCI-74	47.93 ± 0.09	38.4	1.1	-17.1	0.849	0.017	
POC	KCI-74	47.93 ± 0.09	4.4	1.0	-18.0	0.798	0.135	
POC	KCS-79 (I)	55.19 ± 0.14	4.4	1.0	-3	0.940	0.151	
DOC	KCS-79 (I)	55.19 ± 0.14	5.7	5.0	-32.5	3.080	2.430	
POC	KCS-95 (I)	68.18 ± 0.14	5.2	1.0	-12.1	0.704	0.108	
DOC	KCS-95 (I)	68.18 ± 0.14	31.8	5.1	-26.8	0.551	0.083	
DOC	KCS-95 (II)	68.46 ± 0.14	44.1	1.2	-18.8	1.027	0.018	
DOC	KCS-107 (II)	78.32 ± 0.10	44.1	0.8	-12.2	0.449	0.013	
POC	KCS-108 (I)	78.54 ± 0.12	14.1	1.1	-27.7	0.245	0.047	
DOC	KCS-108 (I)	78.54 ± 0.12	71.4	5.2	-25.1	0.125	0.038	
DOC	KCH-43	22.93 ± 0.09	40.3	1.1	-19.8	1.062	0.019	
POC	KCH-43	22.93 ± 0.09	5.2	1.0	-20.1	0.968	0.130	
DOC	KCH-62	36.42 ± 0.12	79.6	1.4	-20.0	0.680	0.010	
POC	KCH-62	36.42 ± 0.12	13.0	1.0	-21.8	0.969	0.052	
DOC	KCH-70	42.78 ± 0.09	52.1	1.2	-19.7	0.930	0.014	
POC	KCH-70	42.78 ± 0.09	8.0	1.0	-22.6	0.917	0.080	

Table 5.2: Characteristics of ^{14}C samples from the Vadret dal Corvatsch ice core VCL, the three bomb peak samples from the Col du Dôme and five samples from two sampling locations on the Grenzgletscher. Reported are ice core number, the depth of the sample, the blank corrected carbon mass, the δ^{13}C and the blank corrected fraction modern carbon f_{corr}. The asterisked samples are discarded immediately due to the extremely low carbon masses.

type	**core name and number**	**depth [m w.e.]**	$\mathbf{m}_{corr}$ **[μgC]**	$\Delta\,\mathbf{m}_{corr}$ **[μgC]**	δ^{13}**C [‰]**	$\mathbf{f}_{corr}$	$\Delta\mathbf{f}_{corr}$	
CFA	VCL-02	0.44 ± 0.21	4.4	1.0	1.4	0.864	0.180	
CFA	VCL-04	1.27 ± 0.20	1.7	1.0	8	0.969	0.485	(*)
CFA	VCL-7	2.92 ± 0.33	36.8	1.0	-	0.578	0.009	
POC	VCL-07	2.67 ± 0.09	17.6	1.5	-33.6	0.615	0.044	
POC	VLC-09	4.19 ± 0.09	81.6	1.5	-32.4	0.770	0.008	
POC	VCL-14	6.99 ± 0.09	7.1	1.0	-24	0.482	0.037	
POC	VCL-21	10.49 ± 0.11	34.4	1.1	-24.2	0.626	0.007	
CFA	VCL-21/22	10.78 ± 0.40	1.6	1.0	-	0.692	0.466	(*)
DOC	VCL-24/25	12.57 ± 0.17	6.8	1.0	21.0	0.664	0.077	
POC	VCL-27	14.01 ± 0.09	26.6	1.1	-27.4	0.786	0.014	
POC	VCL-30	15.83 ± 0.09	12.6	1.1	-26.3	0.624	0.014	
DOC	VCL-31	16.58 ± 0.18	20	1.0	-28.5	0.591	0.029	
DOC	VCL-34	18.17 ± 0.17	10.5	1.0	7.5	0.627	0.052	
POC	VCL-35	18.65 ± 0.09	52.5	1.2	-29.6	0.977	0.011	
DOC	VCL-37	19.92 ± 0.18	27.1	1.1	-19.1	1.003	0.028	
POC	VCL-38	20.61 ± 0.09	7.8	1.0	-28.7	0.990	0.050	
CFA	VCL-38	20.64 ± 0.31	7.9	1.0	-13.1	0.920	0.102	
POC	VCL-40	21.53 ± 0.09	7.7	1.0	-23.1	0.969	0.048	
POC	VCL-41	22.42 ± 0.09	26	1.1	-23.1	0.931	0.027	
POC	VCL-42	22.86 ± 0.10	21.2	1.1	-32.5	0.935	0.017	
DOC	VCL-40/41	22.12 ± 0.22	95.1	1.6	-17.4	0.875	0.008	
DOC	VCL-42/43	23.13 ± 0.18	86.4	1.5	-15.0	0.848	0.012	
CFA	VCL-44	23.60 ± 0.29	21.6	1.0	-	0.702	0.035	
POC	VCL-45	23.95 ± 0.05	394.8	2.2	-	0.442	0.003	
DOC	CDD-86a	1966 AD	67.3	1.1	-18.3	1.035	0.015	
DOC	CDD-94	1972 AD	89.7	1.2	-15.1	1.224	0.018	
DOC	CDD-105a	1975 AD	37.9	1.0	-21.2	1.303	0.024	
POC	GG_{small}	sample #19	5.6	1.0	4.6	0.419	0.106	
POC	GG_{large}	sample #19	4.7	1.0	4.5	0.792	0.124	
DOC	GG_{small}	sample #19	9.2	1.3	-13.0	1.063	0.077	
DOC	GG_{small}	sample #21	33.3	0.9	-11.0	0.998	0.031	
DOC	GG_{large}	sample #21	52.1	1.0	-20.4	1.117	0.015	

5.1.2 Overview on the Vadret dal Corvatsch ^{14}C data

The carbon concentrations for POC and DOC extracted from the VCL core and corrected for blank contributions (Figure 5.2) show, as expected, overall large POC concentrations with a strong variation. The DOC values on the other hand are relatively low. The increase toward the bedrock is seen in other cores as well, and seems to be a characteristic of basal ice.

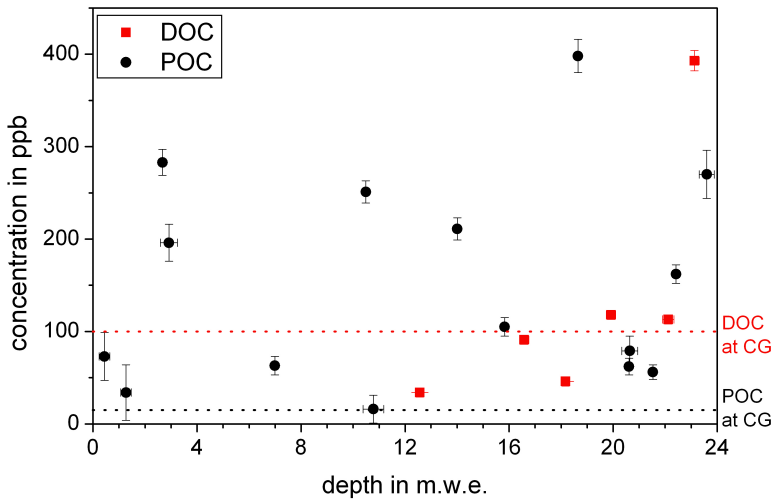

Figure 5.2: DOC and POC concentrations of the extracted ^{14}C samples after blank correction. The dotted lines reflect the typical concentrations of POC and DOC quantified for the ^{14}C samples of the Colle Gnifetti cores.

Figure 5.3 shows the blank corrected ^{14}C values reported in Table 5.2 against depth. The ^{14}C fractions in the upper two thirds of the core show no correlation with depth and are relatively low with a strong variation. It can be concluded that the top part of the core must contain ice from the industrial period indicated by strong contributions from fossil fuel combustion. At about (18.5 ± 0.5) m w.e., the ^{14}C fraction suddenly jumps to nearly modern composition and then declines sharply down to bedrock. At this point, there are no contributions from fossil fuel combustion and the values can be used to date the ice.

Although there are no POC and DOC values for the same samples, the good agreement between PO^{14}C and DO^{14}C in the lower part of the core indicates that both carbon fractions found in the Vadret dal Corvatsch glacier have “young” sources in pre-industrial times with no indication for a reservoir effect, allowing for dating of the ice by both fractions. The CFA POC samples agree well with the other measurements, showing the suitability of this extraction method for PO^{14}C analysis.

5.1.3 Overview on the Colle Gnifetti ^{14}C data

Figure 5.4 shows the extracted, blank corrected DOC and POC concentrations for the three CG cores. The higher concentrations of both DOC and POC in KCH and KCS compared

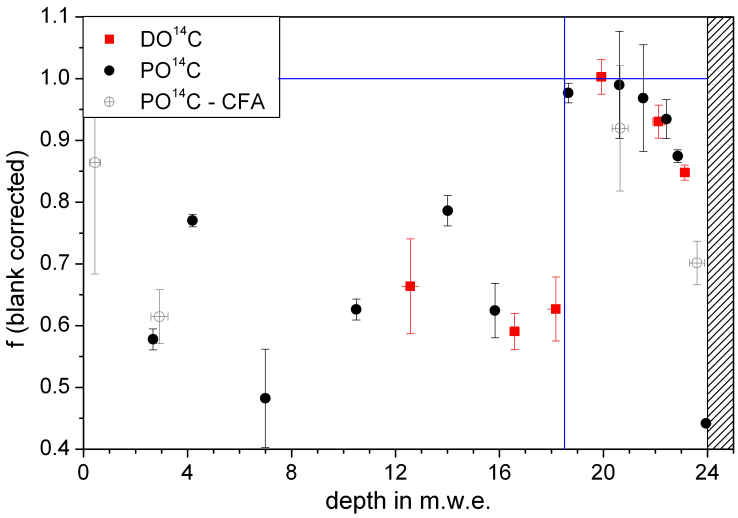

Figure 5.3: ^{14}C values for POC and DOC samples from the Vadret dal Corvatsch ice core corrected for sample preparation blank.

to KCI might indicate a difference in detention of organic aerosol for different accumulation regimes.
The low accumulation of the KCI is in large parts due to the loss of snow blown over the ice cliff. This sink may also be attributed to the aerosol particles being carried in the wind blown snow (Pomeroy and Jones, 1996) and could explain the lower POC concentrations. For DOC the possibility of UV induced oxidation of organic molecules in snow and firn (Hoffmann, 1996) and their subsequent loss to the atmosphere, might be an additional sink for organic compounds and would contribute stronger to a low than to a high accumulation regime. However, these processes should have no effect on the ^{14}C fraction of DOC and POC.
A temporal variation of the organic aerosol source strength could also explain the difference in organic concentrations for the three cores, since the cores themselves as well as the sample selection cover different time intervals.

Regardless of the reasons, due to the lower carbon concentrations and the fact that especially for KCI the ice mass was kept to a minimum, the extracted total carbon masses have been significantly smaller for the KCI samples than for those extracted from KCH and KCS, and are thus stronger influenced by blank contributions. Especially the POC carbon masses are often too low to allow a reliable interpretation of the ^{14}C values.

Before, discussing the ^{14}C results for the Colle Gnifetti ice cores shown in Figure 5.5, the following outliers must be addressed:

(1) For KCH, the second sample (KCH-62) shows a very low DO^{14}C value, which is not in agreement with neither the respective PO^{14}C nor the other DO^{14}C fractions. The preliminary dating of the KCH core also suggests ages younger than 1000 years, i.e. f_m values in the order of 0.9. Also, the DOC concentration as well as the POC concentration of the sample was significantly higher than the other CG samples.
The carbon mass is so high that blank correction has no imminent influence and a large mass

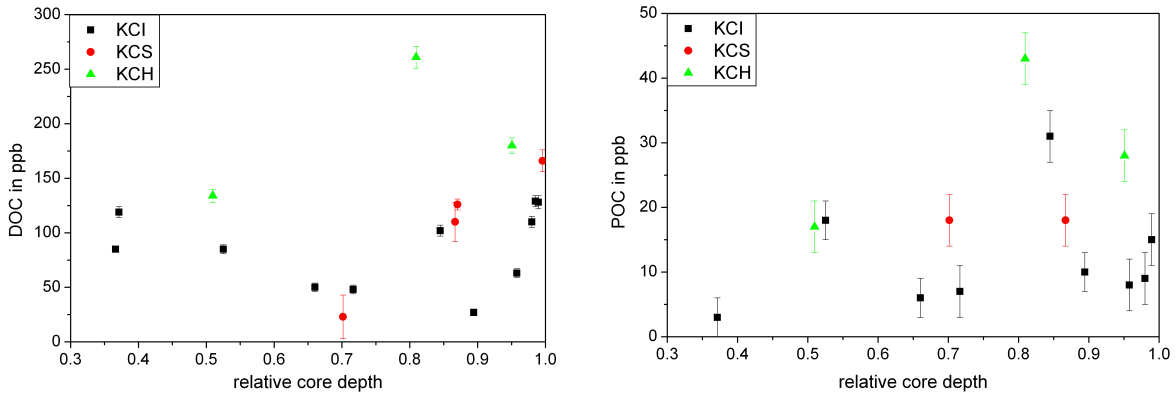

(a) DOC (b) POC

Figure 5.4: Organic carbon concentration for the DOC and POC fraction determined from the extracted carbon mass for the three CG ice cores.

contamination with an exceptional low ^{14}C signature would be needed to increase the f_{corr} value to match the respective PO^{14}C value. However, no problems were encountered during sample preparation, which might explain such an extraordinary high contamination.
The alternative would be a large fraction of "old" organic matter contributing to the DOC fraction in ice. It is expected that any such source contributes in some part also to the POC, which is supported by the increased POC mass, but not by its ^{14}C signature. Without further analysis of the surrounding ice, no final conclusion can be given and the KCH-62 DO^{14}C value is declared as biased by fossil matter, either by contamination or by a "natural" effect. Therefore it is unfit for ^{14}C dating and disregarded in the following investigations.

(2) For KCS, the large blank correction results in an unrealistic DO^{14}C value for the first DOC sample KCS-79 (I). This problem could be solved by reducing the blank mass m_{blank} from 35 μgC to 15 μgC at the same f_{blank}. The newly corrected ^{14}C value would then be f_{corr}(KCS-79 (I)) = (0.967 $\pm$ 0.125). Although this correction is rather arbitrarily, the blank of the (I) "POC-before-DOC" method is not very well constrained, leaving room for speculations. Supporting this blank correction is the fact, that the new blank corrected DOC concentration is also in better agreement with the concentrations encountered in other samples.

(3) Two adjoining samples from core section KCI-32 and KCI-74 respectively were analysed for their DO^{14}C content, in order to show the ability to reproduce the f_m value. The sample preparation was three months apart. The blank corrected DO^{14}C values agreed well for the KCI-74 samples. However, while the DOC concentrations for the two samples from KCI-32 differ only slightly, the ^{14}C fractions disagree significantly by about 10 %. The measurement of two Grenzgletscher samples gave a similar discrepancy, which could there be explained by blank correction. This is not possible for the KCI samples. Reduction of the higher f_{corr} value requires an extremely strong increase of the lower f_{corr} and thus an extremely low f_{blank} value. Since there is no indication for an exceptional contamination during sample preparation, both values are taken as "true" for the moment and possible reasons for the difference will be discussed later.

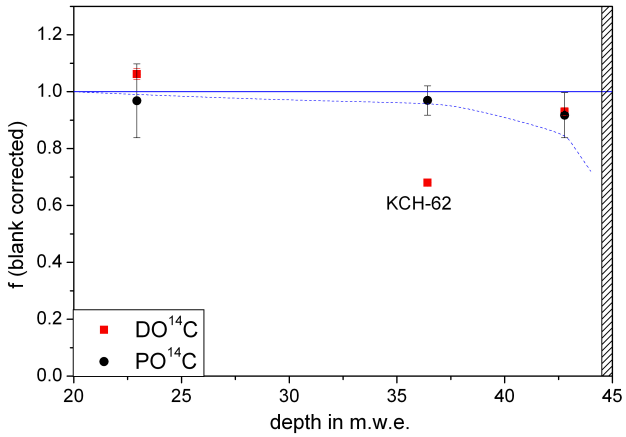

(a) KCH

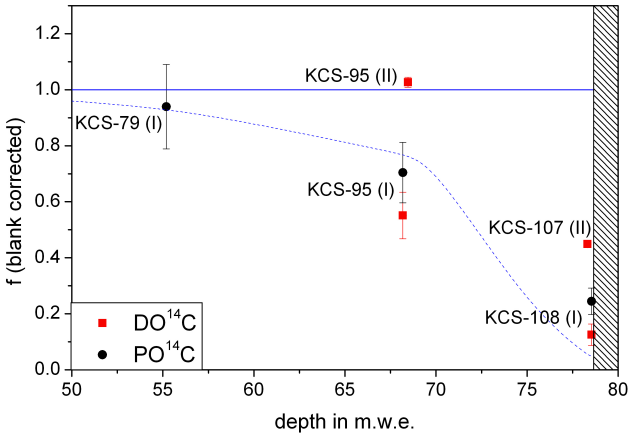

(b) KCS

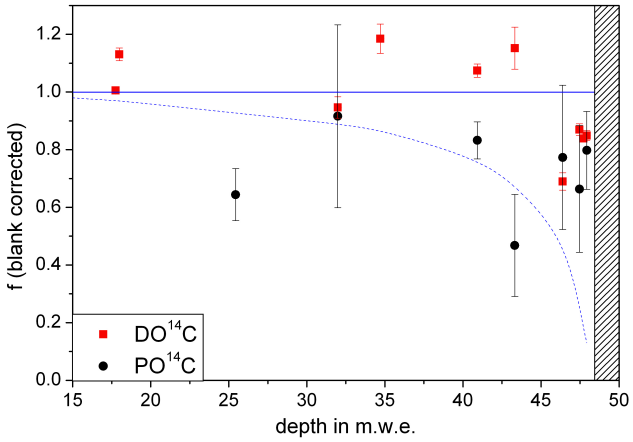

(c) KCI

Figure 5.5: Blank corrected ^{14}C fraction for POC and DOC samples from the Colle Gnifetti ice cores versus core depth. The dashed line indicates the expected ^{14}C values based on the preliminary dating.

Having now a look at the blank corrected ^{14}C values for the different CG cores, several basic problems are encountered, that need to be addressed before any attempt at dating can be made:

- Some of the DO^{14}C values in KCH, KCS and especially KCI are higher than the modern reference level (in the following denoted as "over-modern") and show strong variations without a distinct age-depth relation. Such high values have already been encountered for the Grenzgletscher samples (see Section 3.4.5).
- Comparison of the (I) "POC-before-DOC"and (II) "DOC-before-POC" method for the KCS samples shows a significant difference in the DO^{14}C fraction for the two methods, the second giving significantly higher ^{14}C values, than the first.
- For several ice samples PO^{14}C and DO^{14}C differ significantly.
- For KCI, both PO^{14}C and DO^{14}C increase at the bottom of the core.

The most important and imminent problem is the over-modern DO^{14}C values, encountered mainly for the KCI core, but also for KCH, KCS and the Grenzgletscher samples. Until the reason for these values is not identified, any comparison of PO^{14}C and DO^{14}C is rather futile as well as any attempts at dating.
The main questions to be answered are now:

1. What causes the high ^{14}C values in the DOC fraction?
2. What does this mean for the ability to date ice samples by ^{14}C in DOC?

5.2 Contamination of the ice cores during drilling, storage and sample preparation

The first reason coming to mind for the over-modern ^{14}C values is that the blank correction determined in Section 3.4 does not reflect the true contamination of the ice samples.
Looking at the over-modern ^{14}C values, it is striking that for most samples the uncorrected DO^{14}C fractions are surprisingly high but not over-modern. Only the correction for the extraction blank results in the unreasonable high ^{14}C fractions. Nonetheless, it is unrealistic to assume no blank correction for the extraction process would be necessary for real samples.
Assuming m_{blank} to be smaller would result in less high ^{14}C fractions, but the values would still be relatively large. A reduction of the blank mass was not seen in the blank and standard measurements performed in between the sample extractions and is therefore not supported.
The only other possibility to avoid the over-modern values is an additional contamination of the sample during or before sample preparation. A total correction for the extraction blank and any additional contamination needs a $f_{blank+contamination} > 1$, as all other correction parameters would still lead to ^{14}C values larger than modern.
In the following, the term "blank" is attributed solely to the carbon contributions of the extraction system, while the term "contamination" refers to all other contributions to the sample outside of the DOC extraction system.

5.2.1 Modern ^{14}C contamination of the ice sample

Adsorption of organic compounds onto the ice - Surface contamination

It was shown in Section 3.4.5 that all possible blank contributions during DOC extraction are contained and corrected for in the determined extraction blank. It has also been discussed that any additional surface contamination for real samples before sample processing should be eliminated by the careful decontamination of the ice sample surface. In case of an incomplete decontamination, adsorption of organic compounds onto the sample surface due to the contact with atmosphere between drilling and sample processing would be the most likely source for a significant contamination with high ^{14}C concentration.

Diffusion of organic compounds in ice - Ice bulk contamination

A contamination of the complete ice bulk by the adsorption onto and diffusion into the ice of organic compounds from the air after sampling would not be eliminated by the decontamination process. Moreover, if a continuous exchange of organic molecules between the ice bulk and the surrounding atmosphere could take place, the high ^{14}C concentrations might be the result of a significant amount of present-day organic compounds diffused into the ice matrix.

Soluble organic gases in the atmosphere, like H_2O_2, formaldehyde and methanol, can be absorbed in snow and ice from the air (Wolff and Bales, 1996). The surface uptake of organic gases in ice depends on the solubility and the chemical composition of the ice and has been found to be comparable to the exchange flow between water and air (Wania *et al.*, 1998). However, the diffusion within the ice matrix is for large molecules six orders of magnitudes lower than in water. Whillans and Grootes (1985) calculated the isotopic diffusivity of oxygen in firn at varying densities as well as in ice and reports the temperature dependent diffusivity in firn to be in the order of 10^{-6} to 10^{-8} cm^2 s^{-1}, and 10^{-10} to 10^{-12} cm^2 s^{-1} in ice. This diffusion factor in ice is assumed to be similar for other species, including organic compounds. Thus, although the uptake of organic gases at the ice surface can be significant, the transport inside the ice is far slower and restricts the total amount of carbon diffused into the ice within a few years to negligible concentrations.

The only other way for adsorbed large molecules to reach the inner sample would be microcracks in the ice. These cracks are often not visible, but can provide an easy way into the inner ice. However, they appear randomly, compose a singularity within the ice and transfer of organic molecules would only happen along them. It remains questionable, if the contribution to the total amount of organic carbon would be significant enough to even alter the original ^{14}C signature of the sample and even more, that total equilibrium of the whole ice bulk with the atmosphere could be achieved.

Modern contamination scenarios

Regardless, if a surface or a bulk ice contamination is assumed, the upper limit for $f_{contamination}$ of these contributions is given by the atmospheric $^{14}CO_2$ value since drilling (Table 5.3).

Table 5.3: Atmospheric $^{14}CO_2$ fraction measured at the continental background station Jungfraujoch at the time of ice sampling (Levin and Kromer (2004); Levin *et al.* (2008)) for the different ice samples giving the upper limit of ^{14}C contamination for the respective samples.

name	drilling year	f_m
KCI	2005	1.06
KCS	1995	1.12
KCH	1995	1.12
Grenzgletscher	1992	1.13

The atmospheric $^{14}CO_2$ value for the year 2009, the time of sample preparation, in Heidelberg is f_m = 1.03 (unpublished data, pers. com. I. Levin, 2009). It should be noted, that the f_m value for the atmospheric carbonaceous aerosol fraction during this time can be lower by 10 to 20 % due to anthropogenic activities affecting TOC differently than CO_2, as has been shown for the bomb peak samples from the CDD (see Section 3.4.5) and by different atmospheric aerosol studies (e.g. Szidat *et al.* (2007); May *et al.* (2009)).

For KCI, the upper limit of $f_{contamination}$ = 1.06 is not large enough to reduce or explain the blank corrected ^{14}C values, regardless of $m_{contamination}$. For KCH and KCS (II) the ^{14}C values are lower than the upper atmospheric limit. The same is true for the Grenzgletscher samples. However, in both cases, the near compliance of the blank corrected values with the upper contamination limit would suggest a more or less complete equilibrium with the atmosphere, which is very unlikely.

Overall, the assumption of a contamination through contact with the atmosphere remains unsatisfactory. Surface contamination should be eliminated and diffusion into the ice bulk was found to be negligible. Only the possibility of micro-cracks offering pass ways into the inner ice sample might account for a contamination. However, even if the sample would reach complete equilibrium with the atmosphere, the upper limit of $f_{contamination}$ given by the atmospheric $^{14}CO_2$ is not enough to explain the high ^{14}C values for KCI.

5.2.2 Influence of POC filtration on the DO^{14}C value

A comparison of the two methods was attempted, to deduce if the presence of POC has any influence on the ^{14}C fraction of DOC, which might explain the high ^{14}C values.
After having already processed three ice samples from the KCS core by filtering POC before DOC was extracted, it seemed reasonable to analyse adjoining samples for KCS-95 and KCS-108 respectively by extracting DOC with POC still present in the sample. This approach would also enable a direct comparison of the KCS (II) samples with the other CG ice samples. As indicated in Figure 5.5(b), the PO^{14}C (I) values give similar ages as the preliminary age-depth relationship determined by Armbruster (2000) and can thus be seen as an indicator for the true ^{14}C fraction.

The two DO^{14}C values for the (I) “POC-before-DOC” method are significantly lower, than the one for the (II) “DOC-before-POC”. One might argue, that the difference between KCS-107

and KCS-108 reflects a true age signal. The age is expected to increases rapidly in the basal ice layer, the accumulation during the time of glacier forming can vary strongly and the age of the basal ice must be treated carefully. All this could lead to an exceptionally low $DO^{14}C$ value in the lowermost core section and the large difference to the ^{14}C fraction of KCS-107. However, there is no such explanation for the difference of the KCS-95.

Exchange of organic compounds between DOC and POC

Assuming that the blank correction is adequate and not the reason for the difference in ^{14}C, the presence of POC during DOC UV-irradiation would seem to affect the ^{14}C signature of the extracted DOC sample. ^{14}C values are corrected for fractionation effects and every fractionating process favoring ^{14}C to ^{12}C in one way or another, would also affect the ratio of $^{13}C/^{12}C$, and is thus already eliminated. Therefore, the effect of POC on DOC must be on the total carbon mass and not the isotopic fraction. Following scenarios come to mind:

- part of the POC is cracked by the UV light and contributes to the DOC carbon mass.
- part of the DOC is adsorbed onto the POC and is thus removed from the DOC fraction and added to the POC fraction.

Both scenarios are quite reasonable. However, careful consideration and testing of each point based on the measured values reveals that any possible influence of POC on the extracted DOC carbon mass, is not enough to explain the difference. Even if a scenario could be found, the fact remains that regardless if a “young” carbon fraction is added to the DOC or an “old” fraction removed by the presence of POC, in every case, the higher ^{14}C value would represent the true value for radiocarbon dating.

Blank scenarios

Since the difference in the $DO^{14}C$ fractions can not be explained by an exchange between DOC and POC, the only other possibility is a problem with the blank correction for the two methods. Several facts have to be considered:

- The respective $PO^{14}C$ values for the KCS-95 (I) and KCS-108 (I) are significantly higher than the $DO^{14}C$ ones, hinting that the $DO^{14}C$ signature might be too low.
- The (I) “POC-before-DOC” method has a large blank, which is not very well defined, while the extraction blank for (II) “DOC-before-POC” has been shown to be relatively fix. Thus, it is easier to argue a wrong blank correction for method (I).
- The processing of an Oxalic Acid ^{14}C standard solution using the (I) “POC-before-DOC” method showed that the ^{14}C blank concentration can be quite fossil (see Section 3.4). Assuming a lower ^{14}C blank value is therefore possible.

- KCS-95 (II) has a very high ^{14}C fraction. To reduce this value so far that it agrees with KCS-95 (I), regardless if the PO^{14}C or DO^{14}C value, would require a blank with a very high ^{14}C signature. The possibility of a ^{14}C blank fraction $f_{blank+contamination} > 1$ has been already discussed and was shown to be very arguable.

Surveying this information, a contamination of the KCS-95 (I) and KCS-108 (I) DOC samples with fossil organic matter is the most likely reason for the difference. Matching the respective two DO^{14}C values, would require a ^{14}C blank value of $f_{blank} = 0$, which is as unlikely as a blank value of > 1. However, a blank correction with $f_{blank} = 0.2$ would already result in an adjusting of the DO^{14}C and PO^{14}C values for KCS-95 (I) and KCS-108 (I). If in addition to the change of the blank ^{14}C fraction, the mass blank is increased to $m_{blank} = 45\,\mu$gC as well, the DO^{14}C values for KCS-95 would match up, but not KCS-108 (I) and KCS-107 (II). Figure 5.6 shows the corrected ^{14}C values for the KCS samples for the extraction blank correction and the artificial scenario.

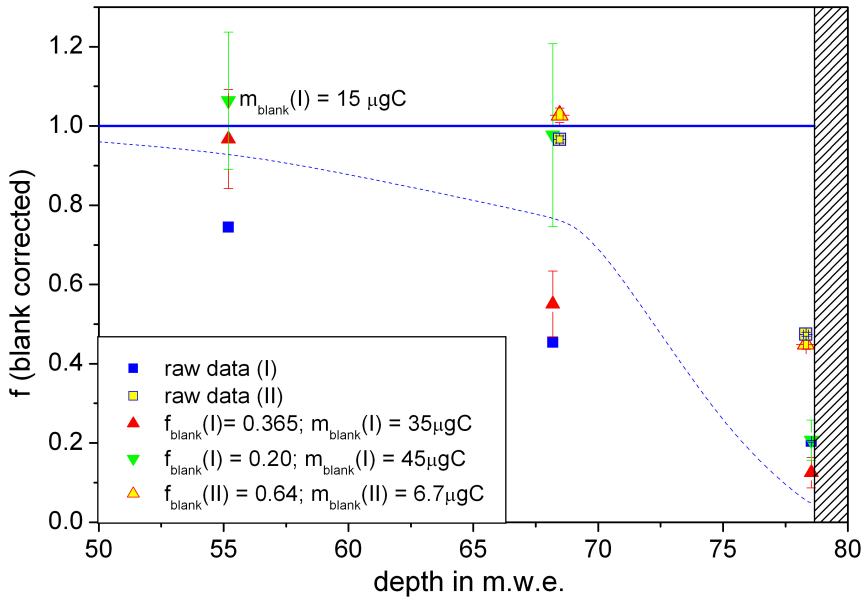

Figure 5.6: Artificial correction of the KCS values in order to match up KCS-95 (I) and KCS-95 (II). Note that for KCS-79 (I) m_{blank} was assumed to be 15 μgC, as discussed above.

The blank for the (I) "POC-before-DOC" method is indeed poorly known, due to the fact that the procedure was discarded as not suitable soon after the KCS measurements. Due to many additional possible blank sources, like filter, filter holder, PFA pot, etc., the blank may vary significantly. Therefore, the above discussed blank correction is not wholly unreasonable and a possible explanation for the difference in DO^{14}C for the KCS-95 samples. For KCS-108 / KCS-107 the new blank correction would not allow a consolidation of the DO^{14}C values, but in this case the difference may be a true age signal. However, the explanation remains unsatisfactory without proof from additional measurements of the (I) "POC-before-DOC" method blank. It should be noted that again the "younger" DO^{14}C value would be considered to be

true, which provides the problem that the value differs significantly from the PO^{14}C and is far higher than would be expected at such a depth.

5.2.3 Conclusion

Concluding, the decontamination procedure was shown to eliminate contamination of the ice sample surface. The diffusion of organic molecules in ice is too small to be of importance to the total organic carbon mass of the ice sample. However, migration along micro-cracks in the ice is a possibility and carries the potential for contamination of the inner part of the ice sample. The exchange of DOC in the ice with the atmosphere along those cracks is probably not significant enough to alter the ^{14}C signal of the sample. While the possibility remains that there is an exchange effect, it is entirely a matter of chance and still does not solve the problem of the high ^{14}C values. After the ^{14}C values of the KCI samples are corrected for the extraction blank, no reasonable contamination source can be identified with a sufficiently high f_m to reduce the ^{14}C signatures to sensible values.

Also, no reason could be found why the presence of POC during DOC extraction should lead to higher ^{14}C fractions. The difference in the DO^{14}C values for method (I) and (II) was ascribed to the contamination of method (I) samples during the extraction process. The contamination of the (I) "POC-before-DOC" method is poorly constrained and seems to vary much. Therefore, any artificial blank scenario is pure speculation and all DOC (I) samples are excluded from the following discussions.

Finally, it is assumed here that the over-modern ^{14}C values are not due to the extraction method and also not due to a contamination of the ice core before ^{14}C sample preparation. The DOC and POC extraction blank applied here has been stable over the time of sample preparation and is warranted for all ^{14}C values derived by method (II) as the only blank contribution.

If contamination can be ruled out as source of the high ^{14}C values, natural ways have to be found to incorporate excess ^{14}C into the ice core.

5.3 Excess ^{14}C in Alpine ice DOC

5.3.1 Incorporation of over-modern organic matter

The only possible source of carbonaceous aerosol with enhanced ^{14}C concentration is organic matter carrying the ^{14}C signature from the bomb peak era. $^{14}CO_2$ fraction in the bomb peak period between 1954 and today range between 1.0 and 2.0.
For all CG cores, the position of the bomb peak was identified with tritium measurements within the firn part of the core, and no samples were taken directly from this period.
However, organic gases can diffuse significantly within snow and firn as long as the pores are not yet closed off from the atmosphere (Whillans and Grootes (1985); Schwander (1996)) and exchange of soluble gases with ice may have an important effect over the time of ice formation (Ravishankara (1996); Hoffmann (2003)). Such exchanges would result in a smoothing of the atmospheric radiocarbon signal (Legrand *et al.*, 2003), and result in an offset and a larger

uncertainty for radiocarbon dates. Thus, the ^{14}C signal of the bomb peak might carry to larger depth than expected.

The bomb peak was identified in the KCI core at 5.75 m w.e. and pore close-off at 17 m w.e. (dated at 250 years BP by Bohleber (2008)). The first KCI ^{14}C sample is at depth 17.98 m w.e. and therefore could see at least part of the bomb peak. However, all deeper KCI samples see nothing of the bomb era, but still have enhanced ^{14}C signatures. Therefore the incorporation of ^{14}C enhanced organic matter from the bomb peak era by diffusion in the firn stage, can not explain the over-modern DOC values.

5.3.2 In situ produced ^{14}C

Having rejected the possibility of ^{14}C enhanced organic matter being deposit onto the glacier, only the direct production of ^{14}C in ice remains as possible solution to the problem.

It has been well known for many years, that ^{14}C is produced in ice by oxygen spallation through cosmogenic radiation (Lal *et al.* (1987); van de Wal *et al.* (1994); Masarik and Reedy (1995)). The main processes for this so called in situ production are ^{16}O(n,n2p)^{14}C and ^{16}O(μ,2p)^{14}C. The recoil energy of the reaction is large enough to disrupt the bonds of molecules and create hot atoms, which then lose their energy within the ice. The atoms will be quickly oxidised and may finally be present within the ice matrix in different chemical species, similar or completely different to the parent compound, e.g. CO, CO_2, CH_4, methanol or formaldehyde (Yankwich *et al.* (1946); Nebeling *et al.* (1985); Petrenko *et al.* (2009)).

Muon induced in situ production is mostly neglected. Having a significantly larger absorption mean free path length than fast neutrons, the contribution to the total production rate at sea level might be significant (van der Kemp *et al.*, 2002), decreases however with altitude and contributes in most cases with less than 7% (Masarik and Reedy, 1995). Therefore only neutron reactions in ice are considered in the following analysis.

The change in ^{14}C concentration in a glacier with time in ^{14}C-atoms per gram ice is given as

$$\frac{dc(t)}{dt} = -\lambda(c_0(t) + c_{insitu}(t)) \tag{5.2}$$

where $\lambda = \frac{ln2}{T_{1/2}}$ is the decay constant of ^{14}C. The time interval, in which in situ production takes place is related to the ice depth z through the accumulation rate A = $\frac{dz}{dt}$. Lal *et al.* (1987) gives the in situ ^{14}C concentration at depth z for a constant accumulation rate as

$$c_{insitu}(z) = \frac{P_0}{\frac{\rho A}{\Lambda} - \lambda}\left(e^{-\frac{\lambda z}{A}} - e^{-\frac{\rho z}{\Lambda}}\right) \tag{5.3}$$

P_0 is the production rate in ice at the surface, depending on latitude, altitude and the ice density ρ and Λ the absorption mean free path expressed in g/cm^2. As can be seen in Figure 5.7 the in situ ^{14}C concentration first increases with depth due to continuous production, which decreases with the scale length Λ/ρ, and finally decreases due to radioactive decay. The maximum concentration of in situ ^{14}C is found at

$$z_{max}(c_{max}) = \frac{A\Lambda}{\rho A - \lambda\Lambda} ln\left(\frac{\rho A}{\lambda\Lambda}\right) \tag{5.4}$$

In most cases, this point lies in the firn region. Below this maximum depth, the total ^{14}C concentration, combining both in situ produced as well as trapped ^{14}C, is then given as:

$$c(z) = (c_0(t) + c_{insitu}(z_{max}))e^{-\lambda t} \tag{5.5}$$

In order to correct any ^{14}C measurement for in situ production, there are several parameters, which must be sufficiently defined. First the production rate P_0 must be determined for the respective latitude and altitude. Lal and Jull (1990) give production rates of 15, 39, 85, 167, 300, 490 $^{14}Cg^{-1}a^{-1}$ for altitudes of 0, 1, 2, 3, 4, 5 km at latitudes > 60° respectively.
For the mean free path length Masarik and Reedy (1995) report values between 157 and 167 g/cm^2. Most papers use a value of Λ = 150 g/cm^2 and an ice density of ρ = 0.9 g/cm^3. Depth and accumulation rates are then given as meter ice equivalent.

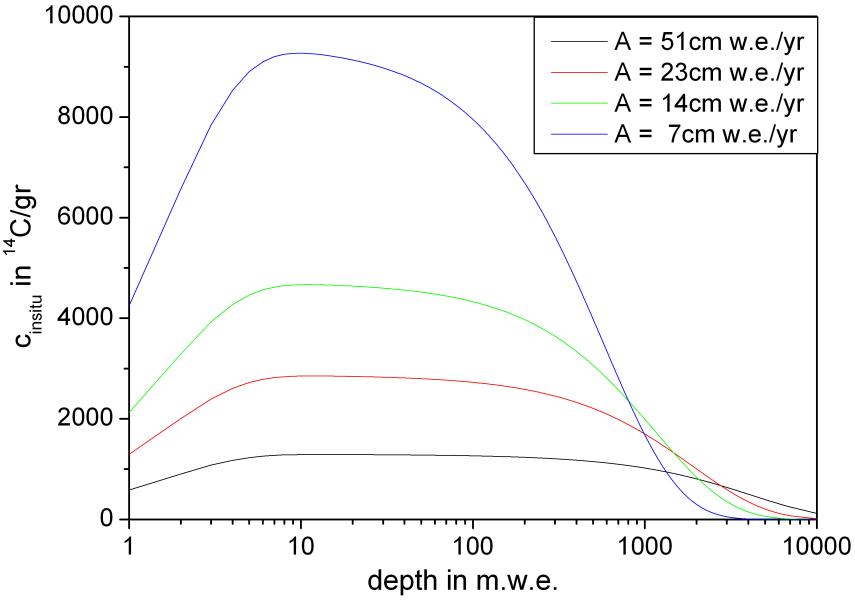

Figure 5.7: Concentration of the in situ produced ^{14}C with increasing depth for different accumulation rates. Production becomes negligible in all cases at a depth of ≈ 10 m w.e.

The question remains how well the produced in situ ^{14}C is retained in the firn in its different molecular form, or if there is a significant loss to the atmosphere by diffusion. The fact that in situ ^{14}C is found in the deeper parts of the ice cores at estimated rates along with other findings leads to the conclusion that the in situ ^{14}C is well retained in the ice matrix (Jull *et al.* (1994); Lal *et al.* (1997); Smith *et al.* (2000)).

In the past, only in situ ^{14}C in the form of CO and CO_2 have been measured, finding that about 60% is present as CO and 40% as CO_2 (Rowland and Libby (1953); Lal *et al.* (1990)). However, Yankwich *et al.* (1946) found for neutron irradiation of nitrogeneous substances, that methanol and formic acid appeared in the presence of water.

For the here presented measurements of ^{14}C in DOC the contribution of in situ production is difficult to determine. In situ ^{14}C in form of CO_2 is eliminated from the melt water during the

IC degassing step of the sample preparation. CO is also extracted during this step to a certain extent. To assess the amount of CO lost during CO_2 degassing, their transfer velocities k = $\frac{D}{z}$ (see Section 3.2.1) are compared. Assuming that the layer thickness z is equal for both gases the diffusion coefficients show, that k_{CO} is 1.07 k_{CO_2}, i.e. the transfer velocity of CO is as fast as CO_2, if not faster. Chemical enhancement for CO_2 is not considered, because due to the reduced pH value it is in the gaseous phase. The presence of bubbles during degassing enhance the transfer for both gases, by directly transporting the gas and creating turbulence. Therefore, most likely all CO is degassed at the time CO_2 is completely extracted.

Finally there is the unknown fraction of in situ produced ^{14}C in organic molecules to consider. No information is available for any in situ ^{14}C incorporated in organic molecules. As already stated Yankwich *et al.* (1946) found significant in situ ^{14}C in methanol and formic acid in the presence of water during irradiation of nitrogenous solutions. Additionally, Woon (2002) reports the formation of methanol and formaldehyde via

$$\begin{aligned} H + CO &\overset{cat}{\rightarrow} HCO \\ H + HCO &\overset{cat}{\rightarrow} HCOH \\ H + H_2CO &\overset{cat}{\rightarrow} H_3CO \\ H + H_3CO &\overset{cat}{\rightarrow} H_3COH \end{aligned}$$

During ^{14}C in situ production the H_2O molecule can be disrupt by the high recoil energy, resulting in the required free H atoms. The ice can function as catalyst. H atoms might also be produced near the surface through disintegration of H_2O by solar UV radiation (λ = 185 nm) (Bar-Nun and Hartman, 1993).
Thus a significant part of in situ ^{14}C may be present as formaldehyde and methanol. However, as there is no information on the fraction ϵ present in organic molecules, three scenarios are investigated, (1) 10%, (2) 20% and (3) 30% of the produced in situ ^{14}C is contained in the extracted DOC sample.
In order to correct the blank corrected f value for in situ ^{14}C, the age of the sample must be known.

$$^{14}C_{corr} - c_{insitu} \cdot m_{ice} \cdot \epsilon \cdot e^{-\lambda t} = {}^{14}C_0 \cdot e^{-\lambda t} \quad (5.6)$$

$$f_{insitucorr} = f_0 \cdot e^{-\lambda t} \quad (5.7)$$

$^{14}C_{corr}$ gives the measured number of ^{14}C atoms, m_{ice} the extracted ice sample mass and ϵ is the fraction of in situ produced ^{14}C oxidised to organic molecules. The left hand side of the equation gives the input value for the OxCal program to calculate the most likely age span for the respective value. Therefore, the correction of ^{14}C for in situ production requires an iterative process: (1) calculating an age (1 σ probability), (2) correcting the number of in situ producted ^{14}C atoms for the radioactive decay, (3) correcting the blank corrected f value for the decay corrected in situ ^{14}C, (4) = (1) calculating an age with the new value. This is done, until the in situ corrected value does not change anymore.

Figure 5.7 shows the blank and in situ corrected ^{14}C fractions for the three scenarios together with the blank corrected value for the KCI samples.

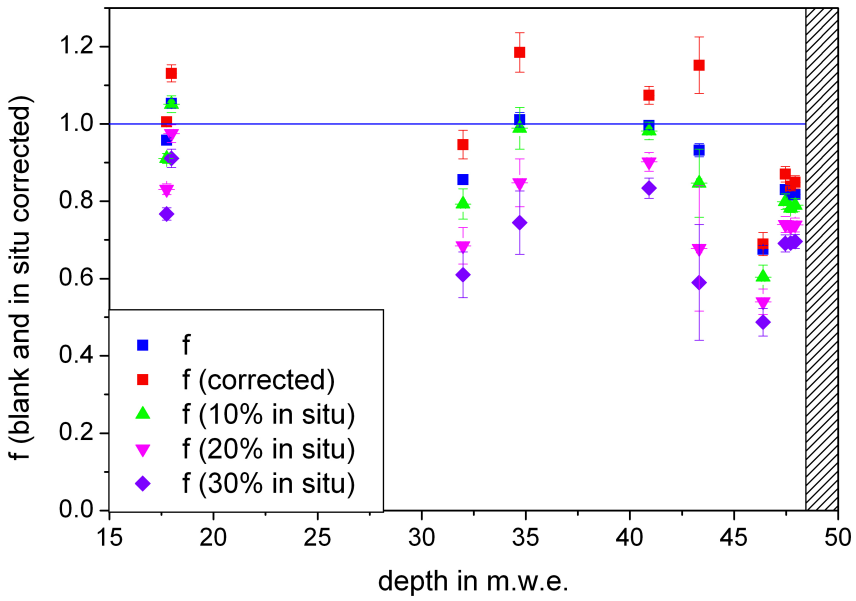

Figure 5.8: ^{14}C values for the KCI samples versus core depth for different in situ scenarios. All values have been corrected for the extraction blank before an additional in situ correction as described in the text was executed.

As can be seen, already 10 % of in situ ^{14}C in organic form is sufficient to correct the over-modern value in the KCI core. For 20 % the KCI DO^{14}C values become reasonable for the respective ice core depth. Applying the same correction scenarios to KCH, KCS and CDD, shows less effect due to the larger accumulation rates and the higher carbon concentrations, but the over-modern values are eliminated. However, the VCL values are also reduced and show now a discrepancy to the POC values. The Grenzgletscher samples are a different problem, as they have been taken from an ablation area, where additional production of in situ ^{14}C takes place during the rise of the ice to the surface. An estimation suggests a production of in situ ^{14}C for over 150 years to reduce the measured ^{14}C values significantly enough. However, without detailed information about the flow dynamics and the accumulation area of the measured ice, the Grenzgletscher ^{14}C values can not be corrected for in situ production.

5.3.3 Conclusion

The incorporation of ^{14}C enhanced organic compounds into the ice samples from the bomb peak era by diffusion in the firn can not explain the high ^{14}C values found in the deeper core sections of KCI.

Therefore only direct production of ^{14}C in ice remains as explanation of the enhanced ^{14}C concentrations. The production of ^{14}C in ice by cosmic radiation is a well known fact and has already been investigated in CO and CO_2 and was recently observed in CH_4. The incorporation of in situ ^{14}C into organic molecules has not been specifically investigated, but neutron irradiation experiments with nitrate solutions showed that in the presence of water

simple organic molecules are formed incorporating the hot carbon atom. In combination with UV-induced chemistry in snow and ice, the assumption of a significant contribution of in situ ^{14}C to the organic carbon fractions in ice is not unreasonable. Therefore, in situ produced ^{14}C becoming incorporated in DOC may be a sensible explanation for the over-modern values found in the KCI, KCH and KCS cores and will here be assessed to correct the measured DO^{14}C values.

The presence of in situ ^{14}C however, brings now the problem, of three additional parameters influencing the ^{14}C concentration:

1. accumulation rate A: the accumulation rate is expected to vary with time and the larger the accumulation rate, the smaller is the amount of in situ produced ^{14}C
2. in situ organic carbon fraction ϵ: the ^{14}C fraction of in situ produced ^{14}C, that is bound in organic molecules is virtually unknown and may depend on the solar UV radiation and the chemical composition of the ice.
3. production rate P_0: the production rate is modulated by the solar activity, and varies only by some percent over decades (Usoskin, 2008)

These differing parameters may explain the outliers, variation and disagreement with PO^{14}C of the DO^{14}C record and strongly disturb the time signal.

Having now investigated the reasons for enhanced DO^{14}C in ice, the remaining questions to be answered are:

1. What does it mean for the ability to date ice with DO^{14}C?
2. What information can be gained from PO^{14}C and DO^{14}C?

6 Assessment and implications for ^{14}C dating of Alpine glaciers

Having decided that the extraction blank correction is as far as can be determined sensible for real samples and that an additional correction for in situ produced ^{14}C is necessary for the DOC fraction, an attempt is made to determine, if the blank and in situ corrected ^{14}C data for DOC and POC can still be used for dating and what additional information may be gained. For both the VCL and the Colle Gnifetti cores, the ^{14}C ages will be compared to other dating techniques and the age-depth relationship (re)evaluated.

6.1 Vadret dal Corvatsch - ^{14}C age constrain for a low level glacier

6.1.1 Dating with DO^{14}C?

In order to correct the DO^{14}C values from the Vadret dal Corvatsch ice core for in situ ^{14}C, a production rate P_0 of 208 ^{14}C g^{-1} a^{-1} was calculated for an altitude of 3 400 m a.s.l. based on the rates given by Lal *et al.* (1987) for latitudes > 60 °. Since the neutron production rate in the atmosphere is smaller at lower latitudes, this value may be regarded as an upper limit. Nonetheless, P_0 is relative stable and only small variations in the order of a few percent can be expected on time scales of a few decades.
For the accumulation rate, an average value of 16 cm w.e./a was determined between the 1901/1902 Saharan dust event, identified at a depth of 10.5 m w.e. and the tritium peak at 1963, that is supposed to be at 0.4 m w.e. However, the accumulation probably changes significantly (Rau, 2008) and even periods of ablation may have occurred, making this parameter highly variable in case of the Vadret dal Corvatsch.
The rate ϵ of in situ ^{14}C incorporated in the organic molecules is the largest uncertainty. Since no information is given on the oxidation rate of hot ^{14}C atoms to organic compounds or the factors influencing these reactions, any value can be chosen for ϵ and it might even vary strongly with time.

Investigating the influence of different scenarios of in situ ^{14}C contribution to the measured DO^{14}C values, Table 6.1 shows a variation of the three DO^{14}C values in the pre-industrial core section of 1 - 9 %, when assuming accumulation changes between 16 and 30 m w.e. and

ϵ between 0 and 20 %. For the samples from the industrial period, the values change even by up to 34 %.

Table 6.1: Blank corrected DO^{14}C fraction f_{corr} and two scenarios for an additional correction of in situ contribution for the 6 DOC samples extracted from the Vadret dal Corvatsch core. For both scenarios a production rate P_0 = 208 ^{14}C g^{-1} a^{-1} was used.

name	depth	f_{corr}	$f_{corr,insitu}(\epsilon = 0.2)$	
	[m w.e.]	-	A = 30 cm w.e./a	A = 16 cm w.e./a
VCL-24/25	12.57 $\pm$ 0.17	0.664 $\pm$ 0.077	0.546 $\pm$ 0.079	0.444 $\pm$ 0.084
VCL-31	16.58 $\pm$ 0.18	0.591 $\pm$ 0.029	0.537 $\pm$ 0.030	0.491 $\pm$ 0.030
VCL-34	18.17 $\pm$ 0.17	0.627 $\pm$ 0.052	0.527 $\pm$ 0.053	0.440 $\pm$ 0.056
VCL-37	19.92 $\pm$ 0.18	1.003 $\pm$ 0.028	0.963 $\pm$ 0.028	0.931 $\pm$ 0.028
VCL-40/41	22.12 $\pm$ 0.22	0.931 $\pm$ 0.027	0.884 $\pm$ 0.027	0.846 $\pm$ 0.027
VCL-42/43	23.13 $\pm$ 0.18	0.848 $\pm$ 0.012	0.837 $\pm$ 0.012	0.828 $\pm$ 0.012

While the influence from in situ ^{14}C to the pre-industrial DO^{14}C values is relative moderate and might at first be regarded as tolerable, it is at the same time a highly uncertain contribution. In case of the Vadret dal Corvatsch glacier, not only the unknown production rate and the unknown ϵ cause problems for the dating, but the glacier itself is a highly inhomogeneous, complex system with changing accumulation and ablation rates. Even if P_0 and ϵ would be determined for the present-day conditions by dedicated experiments, their temporal variation and especially the glaciological changes of accumulation and ablation would be difficult to estimate. Therefore, DOC should not be used to date such extremely complex ice bodies.

While the in situ correction hinders the ^{14}C dating with DOC, it might provide a tool for identifying periods of ablation and changes in the accumulation rates. Reduction in accumulation or ablation of ice results in a higher in situ ^{14}C concentrations due to longer production times. If an age-depth relationship is established for an ice core and the parameters of in situ ^{14}C in organic molecules of Alpine ice cores are more constrained by experiments, the deviation of DO^{14}C from the expected ^{14}C concentration at the respective time might even allow a quantification of accumulation as described in Section 6.2.3 and as previously applied to in situ $^{14}CO_2$ and ^{14}CO (Lal *et al.* (1987); Lal *et al.* (1997)).

6.1.2 Comparing DO^{14}C and PO^{14}C - Information on the organic source mix

Figure 6.1 presents the blank corrected PO^{14}C values together with the blank and in situ corrected DO^{14}C fractions from Table 6.1.

As already stated, the ^{14}C values for both DOC and POC show in the upper two thirds of the core no correlation with depth and relative low values, suggesting most likely ice from the industrial period with significant fossil contribution. Only the lower core section reflects the decrease in ^{14}C indicating increasing age of ice.

The sudden leap from strongly fossil influenced ^{14}C values to nearly modern concentration

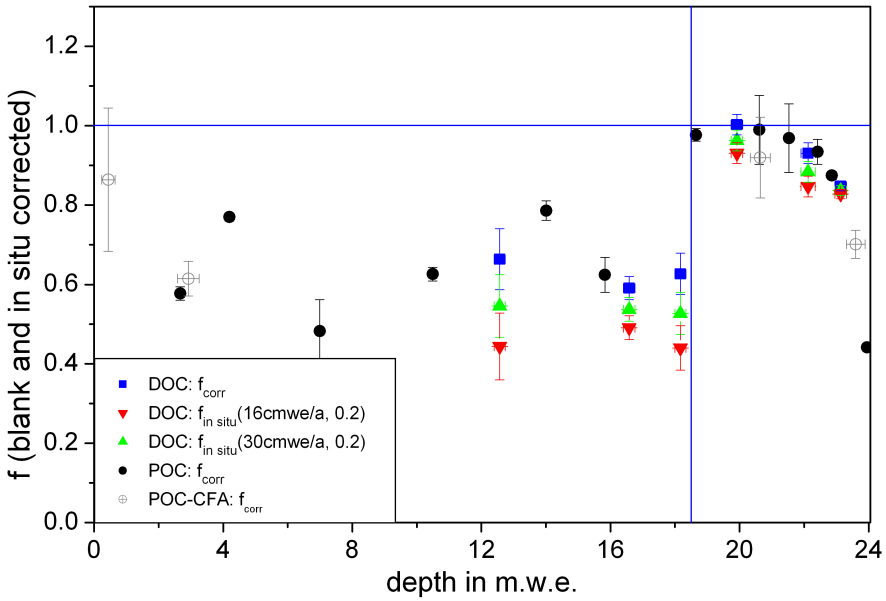

Figure 6.1: PO^{14}C and DO^{14}C: POC (black) and DOC (blue) have been corrected for the blank. DOC has also been corrected for a 20 % in situ ^{14}C fraction in the organic compounds with green: A = 16 cm w.e./a, red: A = 30 cm w.e./a

is not expected. Combustion of fossil fuel, like coal and petroleum, started sometime around 1850 AD and increased steadily but slowly. With begin of the industrialisation in the second half of the 19th century, the atmospheric concentration of carbonaceous compounds from fossil sources increased more rapidly especially after 1950 (IPCC, 2007). It would therefore be expected to see a slow rise in the ^{14}C concentration with increasing depth instead of the sudden leap encountered at 18.5 m w.e. Most likely this rapid change is due to a discontinuity in the ice core. It might be, that at some point after 1850, part of the Vadret dal Corvatsch glacier melted, just like it has been observed between 2001 and 2007, loosing several tens of years. There is however nothing out of the ordinary seen in the particle concentration, conductivity or density record, that would indicate a strong melting.

Although, no VCL sample was extracted for both POC and DOC, the inter-comparison of the values can still give information about source contributions to the respective fraction. The average of the blank corrected ^{14}C values for POC and DOC are equal for the industrial period. Including the in situ correction (ϵ = 0.2), the DOC value can be up to 30 % smaller than the POC values, which would indicate that fossil fuel combustion, quite unexpectedly, contributes equal or even more to the DOC, than to the POC fraction.

In the pre-industrial core section, the PO^{14}C and DO^{14}C agree surprisingly well, with and without the variation in DOC due to the in situ correction, and reflect a surprisingly smooth decline with depth, considering the expectation of strongly variable conditions. This agreement of POC with the DOC fraction, which is supposed to origin purely from biogenic sources carrying the atmospheric ^{14}C signal, leads to the conclusion that POC is a good dating tool for the pre-industrial ice in the Vadret dal Corvatsch glacier.

6.1.3 Establishing an age-depth relationship based on ^{14}C

After having discussed the ^{14}C values for DOC and POC and their ability to use for dating, an age-depth relationship for the VCL core is established.
For the blank corrected ^{14}C values below 18.5 m w.e. Oxcal 4.1. returns the following calibrated radiocarbon ages in years before 1950 (BP) (Figure 6.2).

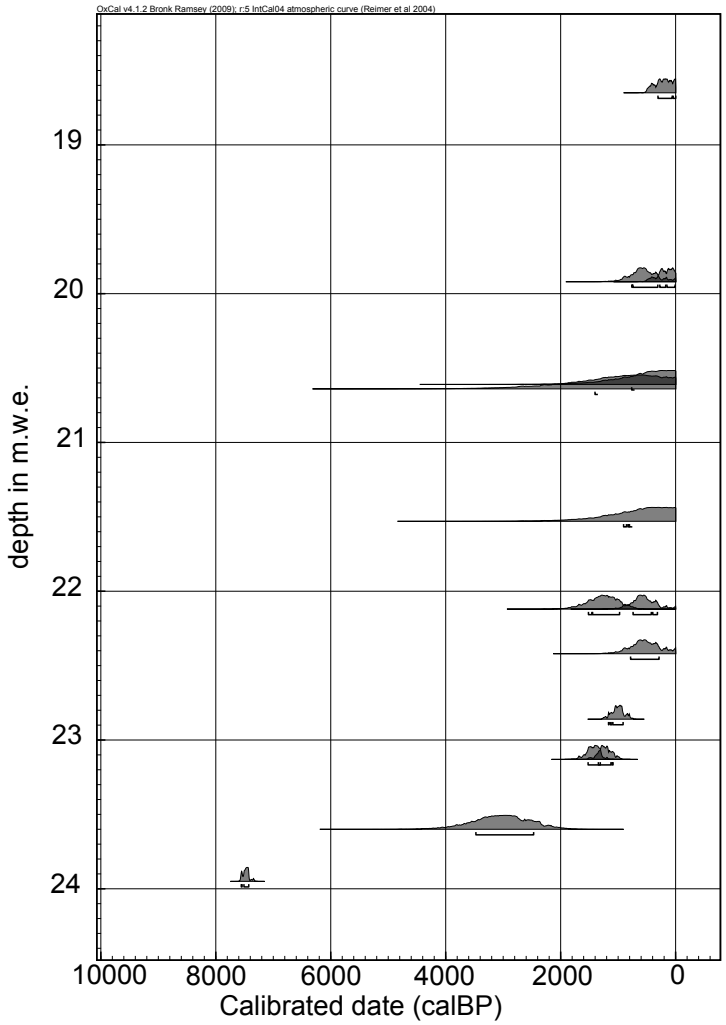

Figure 6.2: Probability distributions of the calibrated radiocarbon ages given by OxCal 4.1 for the DO^{14}C and PO^{14}C samples of VCL. Shown are the age probability distributions for each sample (gray area) and the 1 σ age interval (line) versus the depth of the sample.

Figure 6.3 gives the ages, this time in years before 2000 AD, distinguishing between POC, POC-CFA and DOC samples. For DOC the ages for the different in situ correction scenarios are given to illustrated the age uncertainty. A cubic spline[1] is used to illustrate the increase in

[1] $x_i(t) = 1/6\,[(-t^3+3t^2-3t+1)x_{i-1}+(3t^3-6t^2+4)x_i+(-3t^3+3t^2+3t+1)x_{i+1}+t^3x_{i+2}]$ and analog

age with depth.

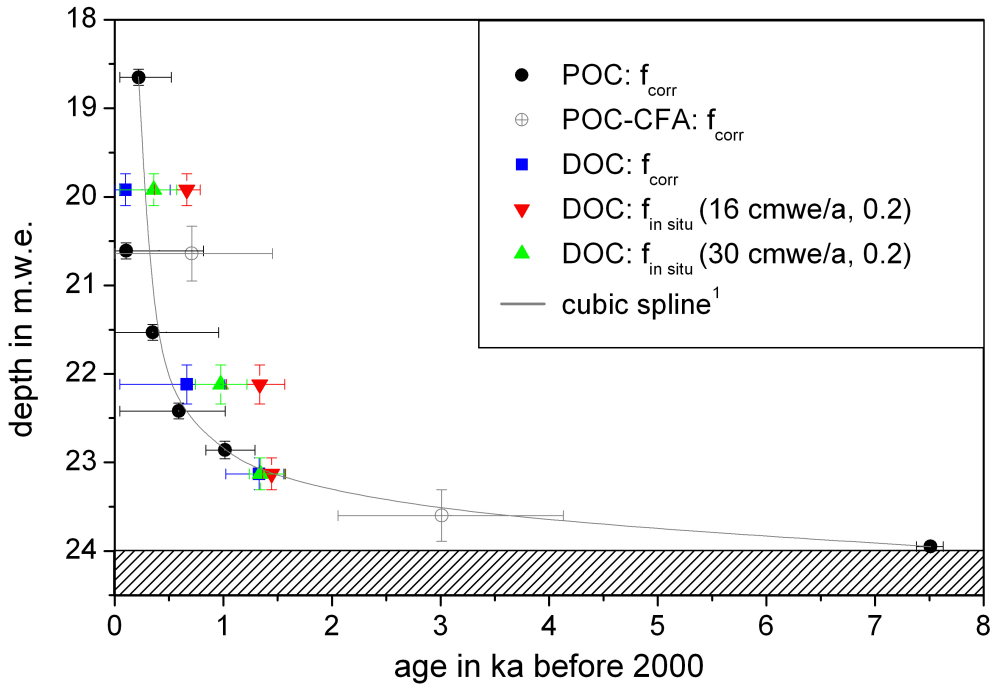

Figure 6.3: ^{14}C dating of the lower core section of the Vadret dal Corvatsch deep core. The radiocarbon ages are given with the 1 σ interval, i.e. the probability of the age lying in the given interval is 68.2%

Overall the age increases relative steadily with depth, but the DO^{14}C values indicate that the accumulation rate and / or ϵ was probably not constant over time and may have changed by up to a factor of 2.
The oldest sample of the Vadret dal Corvatsch ice core dates at an age of (7500 $\pm$ 100) a. This age gives an upper age limit and indicates, that the glacier grew and persisted after this time, which falls together with the period of the Holocene Climate Optimum between 5000 and 10 000 BP, where temperatures were about 1 to 2 °C higher than today (IPCC (2007); Saltzman (2002)). The special position of the basal layer within an ice core will be discussed in more detail in Section 6.3.

Having now a first inkling for the age of the glacier, different traditional dating techniques have been applied, in order to verify the ^{14}C ages by the extension of the age-depth relationship into the upper core section.

Identification of absolute time horizons

Three absolute time horizons within the last 100 years were identified. Tritium measurements revealed that the 1963 maximum due to atmospheric bomb tests can not be found in the ice

[1] for $y_i(t)$.

core anymore. The largest values, which are significantly higher than present day natural values, were measured at the ice surface (0.4 m w.e.) by Rau (2008), suggesting a calender age of the glacier surface at drilling position of (1962 $\pm$ 2) AD . Furthermore, two prominent Saharan dust events of the 20th century could be identified: (1) 1947 AD: 4.2 m w.e. and (2) 1900/1901 AD: 10.5 m w.e.

Radiometric dating with ^{210}Pb

Stempel (2009) measured the ^{210}Pb activity for samples from 8 different depth (see Table 6.2). The sample with the lowest concentration (VCL-41), lying in the lower core section and thus expected to have no ^{210}Pb, was used for blank correction. The lowest sample VCL-44 is disregarded on the assumption of either being influenced by an uncertain blank contribution or disturbed by the bedrock.

Table 6.2: ^{210}Pb analysis of 8 samples from the Vadret dal Corvatsch deep core VCL analysed by Stempel (2009). Dating was achieved relative to VCL-09 (4.01 m w.e.), which was appointed the age of the 1947 AD dust event at 4.2 m w.e.

name	depth [m w.e.]	^{210}Pb [dpm/kg]	age [a before 2000]
VCL-9	4.01	4.6 $\pm$ 1.1	52 $\pm$ 10
VCL-9	4.01	4.3 $\pm$ 1.0	54 $\pm$ 9
VCL-16	8.10	3.4 $\pm$ 0.8	62 $\pm$ 10
VCL-16	8.10	3.8 $\pm$ 0.9	58 $\pm$ 10
VCL-22	11.14	0.88 $\pm$ 0.17	106 $\pm$ 8
VCL-27	13.90	0.37 $\pm$ 0.11	136 $\pm$ 12
VCL-34	17.90	0.81 $\pm$ 0.13	109 $\pm$ 8
VCL-40	21.81	0.13 $\pm$ 0.03	176 $\pm$ 12
VCL-41	22.64	0.03 $\pm$ 0.02	-
VCL-44	23.32	1.7 $\pm$ 0.3	84 $\pm$ 8

^{210}Pb is a radioactive isotope and decays with a half life of $T_{1/2}$ = 22.3 a according to $A = A_0\ e^{-\lambda t}$. The initial activity A_0 is determined by setting the boundary condition, that VCL-09 at a depth of 4.01 m w.e. has the same age as the 1947 AD dust horizon at 4.2 m w.e. From this condition, a tentative initial activity is calculated of (22.9 $\pm$ 4.0) dpm/kg for the corresponding year 2000 AD. Based on this reference, all other dates have been calculated. Below 10 m w.e. the age varies significantly. However, the initial activity deposit onto the glacier is not constant and changes significantly with time, thus resulting in the strong age variation.

Annual layer counting

The particle concentration and the conductivity record have been used for annual layer counting, as proposed by Bohleber (2008), using the absolute time horizons for calibration.

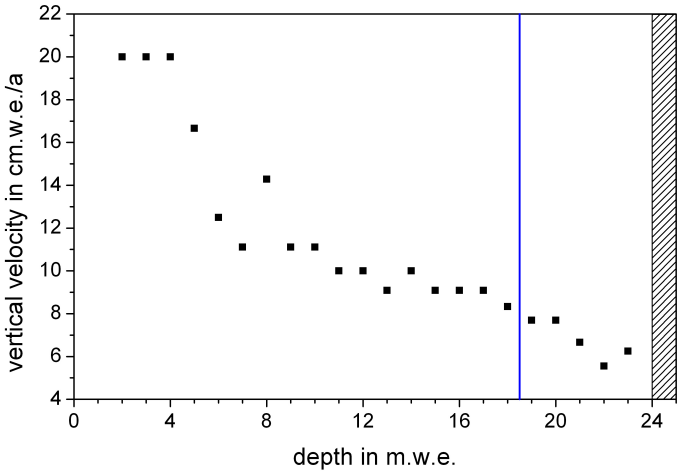

Figure 6.4: Vertical velocity versus depth derived from annual layer counting of the particle concentration and conductivity signal.

The vertical velocity derived from annual layer counting shows a relative smooth, linear decrease with depth, but does not approach zero at the bedrock as expected. This is a clear sign that the seasonal signal can no longer be distinguished in the bottom of the core due to the strong layer thinning and multi-year layers are counted. There is no indication at which point the seasonal signal vanishes, but keeping in mind, that a loss of years is suspected around 18.5 m w.e. the dating by annual layer counting should be applied only down to this depth. Also, the large annual layer thickness in the upper core section carries the possibility of counting inter-seasonal variations instead of annual layers, which causes large uncertainties.

Figure 6.5 summarises the results from all dating techniques. The different dating methods present together a consistent picture. The absolute time horizons, the annual layer counting and the ^{210}Pb dates are consistent in the upper core section down to about 18 m w.e. This consistency is only partly due to the fact, that the ^{210}Pb values as well as the annual layer counting have been calibrated using the absolute horizons. The two lowest ^{210}Pb values differ significantly from the other dating techniques. However, the ^{210}Pb measurement blank is not very well constrained and the initial activity can vary strongly with time. Therefore the two ^{210}Pb ages may be discarded. Surprisingly, there is no indication for a hiatus between annual layer counting ages and ^{14}C ages at depth 18 m w.e. However, taking the uncertainties of both methods into account, the agreement between the two methods is precarious anyway.

Modeling of the age-depth relationship is due to the geometry of the glacier and the complex bedrock topography difficult and was previously attempted by Wagner (1996) with finite element modeling. In the asymmetric 2D model (see Section 4.2.2, the ice flow was assumed to be orthogonal to the ice crest and the steep slope acted as accumulation area. However, the contour lines indicate a strong flow component parallel to the crest (see Figure 6.6). In this case the accumulation regime for the ice core lies up-stream of the bore hole position close to the ice crest.

A simple model approach for a glacier with an inclined bedrock is the ice slap model described

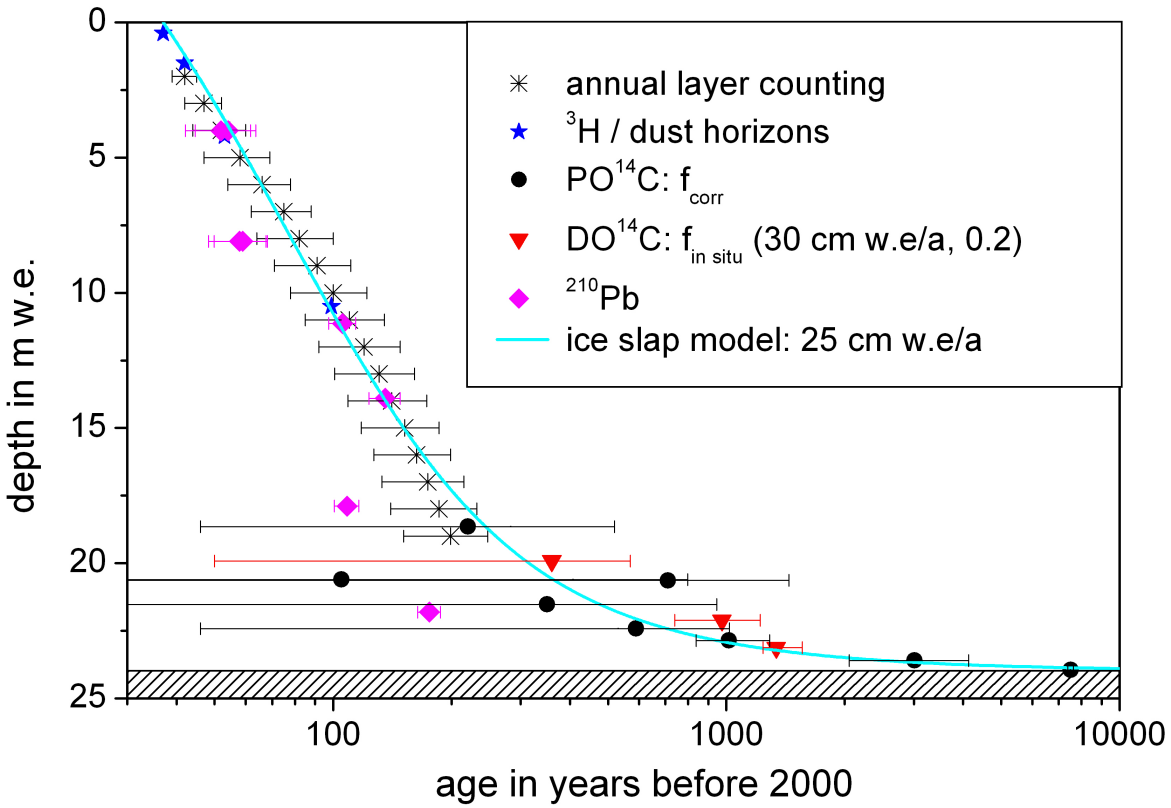

Figure 6.5: Annual layer counting, ^{210}Pb and ^{14}C dating as well as an ice slap model with 25 m w.e./a for the VCL ice core.

in Section 2.3.4. It assumes that the glacier is frozen to the bedrock, in steady state and has a temporal and spatial constant accumulation. The horizontal and vertical velocities are given as:

$$
\begin{aligned}
v_x(x,z) &= \frac{5}{4}\frac{A}{H}\cdot x\left(1-\left(\frac{z}{H}\right)^4\right) \\
v_z(z) &= A\left(1-\frac{5}{4}\left(\frac{z}{H}\right)+\frac{1}{4}\left(\frac{z}{H}\right)^5\right)
\end{aligned}
$$

A being the accumulation rate and H the glacier thickness. Despite the fact that the Corvatsch glacier has most certainly not constant accumulation nor is it in steady state, this model describes the measurement based age-depth relationship of the VCL core surprisingly well, giving an average accumulation rate of 25 cm w.e./a. Nonetheless, the modeled ages can only be seen as a first approach. In the future, a three dimensional finite element model must be developed and a variable glacier geometry applied, to gain a better understanding of the system.

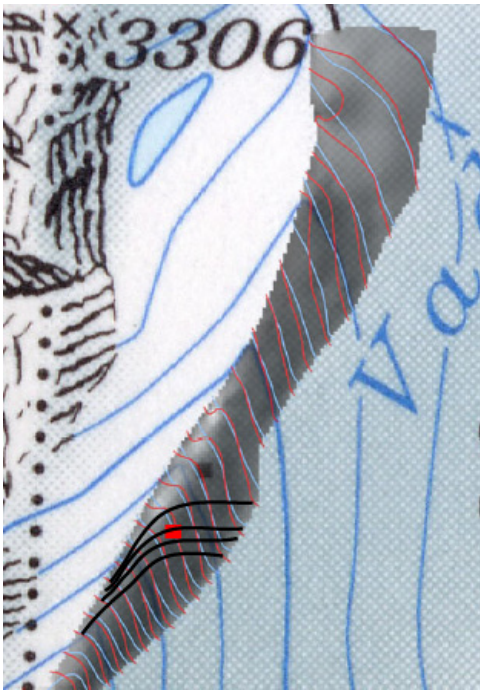

Figure 6.6: Illustration of the ice flow close to the borehole region: red: contour lines 2000, blue: contour lines 2007, black: illustration of the flow lines for the 2000 topography.

6.1.4 Summary on the Vadret dal Corvatsch chronology

Overall, the Vadret dal Corvatsch ice core is less than 7 500 years old and is made up by ice from the industrial period in the upper 3/4 of the core. The sudden leap from the anthropogenic influenced ^{14}C values in the industrial period to the nearly recent ^{14}C concentrations at 18.5 m w.e. suggests a discontinuity in the ice stratigraphy due to mass loss in the second half of the 18th century. However no disturbance can be found in the particle concentration, conductivity and δ^{18}O records.
Different dating techniques show consistent ages and a surprisingly smooth age-depth relationship. It has to be considered that annual layer counting can not account for periods of glacier melting and ^{210}Pb dating is heavily dependent on the unknown and varying initial activity of ^{210}Pb. The DO^{14}C values suggest varying in situ contribution which could be attributed to changes in the accumulation rate by a factor of 2, while the PO^{14}C ages increase smoothly with depth.
Crudely estimating the age depth relationship with a 2D ice slap model assuming steady state and constant accumulation fits surprisingly well with the measured ages and suggests an average accumulation rate of 25 cm w.e./a. However, this model should only be regarded as a first approach and a more sophisticated 3D model with a varying glacier geometry should be attempted in the future.

Without any idea about the age contained in the Corvatsch ice cap, ^{14}C measured on POC has proved to be a reliable dating tool for the complex glacieret and has helped to establish a

first age-depth relation, which now allows further interpretation of the various tracer records, like δ^{18}O. Suspecting a contribution of in situ produced ^{14}C to the DO^{14}C fraction without knowing its significance to the surprisingly low DOC concentrations, DO^{14}C could not be used for dating. However, the comparison with PO^{14}C ages suggested not only a "young" biogenic source for both fractions, but indicated also a variation in accumulation rate and / or the organic in situ ^{14}C fraction ϵ. Furthermore it put forward the surprising possibility, that anthropogenic fossil fuel combustion might contributed equally or even stronger to the DOC fraction, than to the POC fraction found in Alpine ice. The question remains, if this is a true source signal or is due to the different transport behaviour of soot particles compared to gaseous precursors to higher altitudes.

6.2 Colle Gnifetti - Interpreting ^{14}C ages in a high Alpine glacier

6.2.1 Information gained from DO^{14}C and PO^{14}C

For the Colle Gnifetti ice cores, the in situ production rate at an altitude of 4 500 m a.s.l. is calculated at 380 ^{14}C g^{-1} a^{-1} based on Lal *et al.* (1987). Similar to the Vadret dal Corvatsch, this value should be regarded as an upper limit, being derived from production rates for latitudes > 60°. The accumulation rate for the three cores has been given in Table 4.1. Assuming ϵ = 0.2, Figure 6.7 shows the blank and in situ corrected DO^{14}C results together with the blank corrected PO^{14}C.

The least affected by this in situ correction scenario are the KCS samples changing by 1-5 %, followed by KCH with 6-8 %. In both cases the assumed accumulation rate and the determined DOC concentrations are large enough to reduce the in situ influence. For the KCI, however, the combination of low carbon concentration and low accumulation rates, renders DO^{14}C strongly affected by in situ ^{14}C (< 39 %) and thus useless for dating, as long as the in situ ^{14}C contribution to organic molecules ϵ is not constrained. Even after gaining a better understanding of the possible contribution of in situ ^{14}C to the organic compounds in ice at present, changes in ϵ and the accumulation rate in the past, would still prevent DO^{14}C to be a relibale dating technique on its own.

With the DO^{14}C fraction being so wholly uncertain, comparison of PO^{14}C and DOC^{14}C can reveal no information on the sources of the two carbon fractions. Only for the two KCH samples DO^{14}C and PO^{14}C agree within their uncertainties, indicating that both fractions may have similar source compositions. For KCS and KCI, however, no consens can be found between the two fractions, being a result of the small carbon masses for POC and the strong influence of in situ ^{14}C on DOC, which is most obviously not as constant as assumed for the present correction scenario. However, assuming strong variation of the in situ component, would explain the difference in the adjoining DO^{14}C samples in the KCI at about 18 m w.e. (KCI-32) as well as the large difference in PO^{14}C and DO^{14}C for the KCS at 68.5 m.w.e (KCS-95).

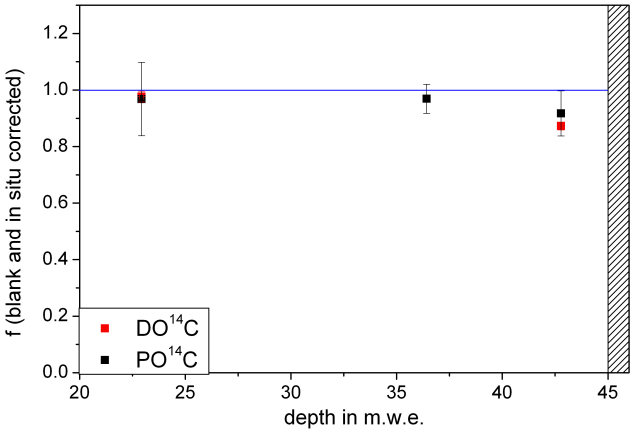

(a) KCH

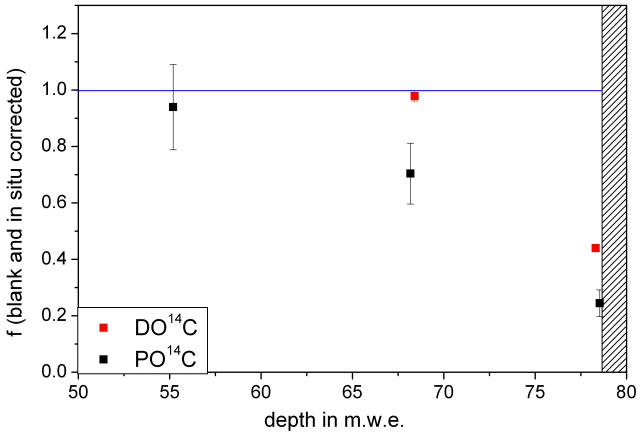

(b) KCS

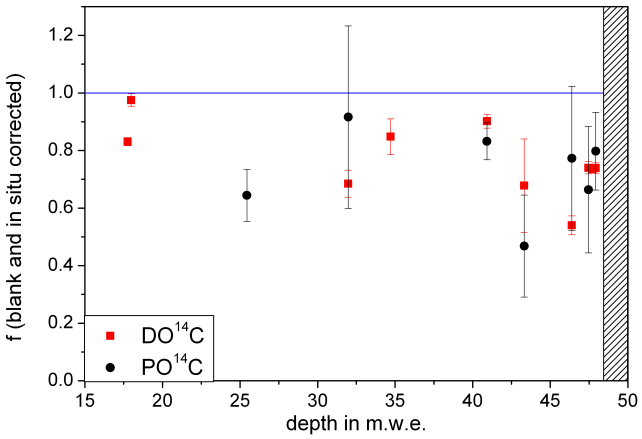

(c) KCI

Figure 6.7: Blank corrected PO^{14}C as well as the blank and in situ corrected DO^{14}C values versus depth.

Concluding, for the presented KCH samples, both $DO^{14}C$ and $PO^{14}C$ might cautiously be used for dating. For KCS, the small effect of the in situ correction scenario suggests, that $DO^{14}C$ might here also be usable for dating, but the strong difference between $DO^{14}C$ and $PO^{14}C$ indicates a problem, that must be investigated first. Nonetheless, the $PO^{14}C$ values as well as the KCS-107 $DO^{14}C$ value, which is due to the large carbon concentration not sensitive to the presented in situ correction, will be able to restrain the total age of the ice. For KCI, unfortunately neither the $PO^{14}C$ nor the $DO^{14}C$ values obtained in this study can give reliable dates.

Perusing the Colle Gnifetti samples, it is apparent, that in most cases further ^{14}C measurements on DOC and POC are required to support the various conjectures made, before any definite information can be gained, which allows to constrain the previous dating of the Colle Gnifetti. Nonetheless, a comparison of the ^{14}C ages with the preliminary dating of the different cores will be attempted, hoping to get an additional perspective on the derived ^{14}C values.

6.2.2 Comparing calibrated ^{14}C ages with previous dating scenarios

The ages for the ^{14}C values presented above have been calculated with OxCal 4.1 and are reported here in years before 2000 AD. The given period represents the 68.2 % propability time frame.

For KCH and KCS, the ^{14}C ages seem to agree with the previous dating (except for the KCS-95 DOC sample). For the KCI POC ages, a decline with depth is observed for all but three values. Two ^{14}C ages seem strongly biased toward older ages and the lowest sample indicates an age inversion. Since the POC samples are very sensitive to the blank contribution, these ages may be simply attributed to contamination and are therefore ignored. For the DOC ages, overall an increase of age with depth can be made out, but there are several samples deviating from the main relation. Especially, the age inversion in the lowest core section, seen also in the POC ages, is curious. However, contrary to POC, these $DO^{14}C$ values are very stable and have been reproduced for three samples.

KCH

The radiocarbon ages for both fractions agree within their errors with the previous age-depth relationship by Armbruster (2000). The older ages of the first sample origin probably from anthropogenic fossil fuel contributions, as the sample covers the beginning of the industrial period. The lower samples however support and further consolidate the previous dating, but suggest slightly younger ages in the lower core. Since the preliminary dating fails especially at the bottom of the core, the ^{14}C ages constrain the total age of the ice core (Figure 6.9).

However, although the extracted carbon masses have been larger than for the KCI core, the age uncertainties are still significant and additional measurements are required to fix the age at the bottom of the core. The disagreement between the POC and DOC age of the lowest sample, is most likely due to the uncertainty pertaining from the in situ correction of $DO^{14}C$

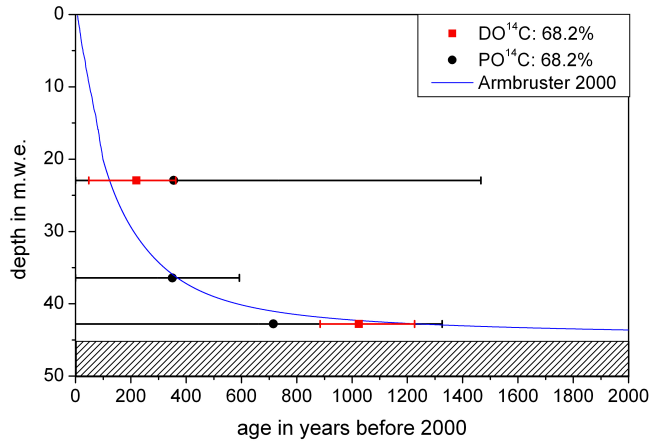

(a) KCH

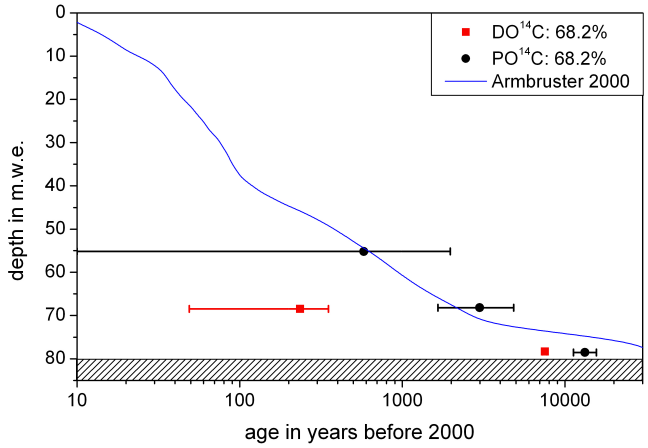

(b) KCS

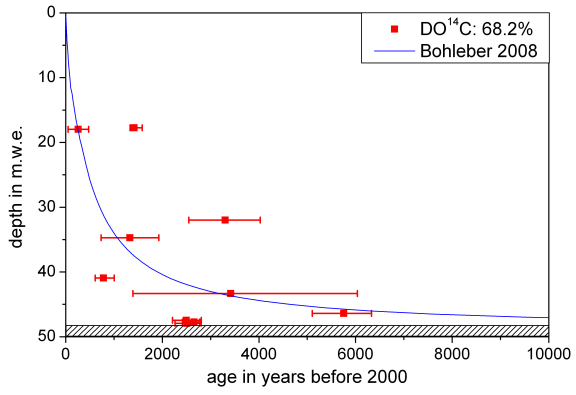

(c) KCI: DOC

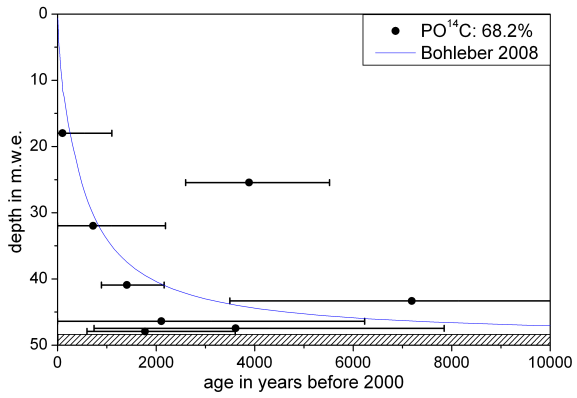

(d) KCI: POC

Figure 6.8: DO^{14}C and PO^{14}C ages for the three Colle Gnifetti deep cores and the respective preliminary age-depth relationship from Armbruster (2000) and Bohleber (2008).

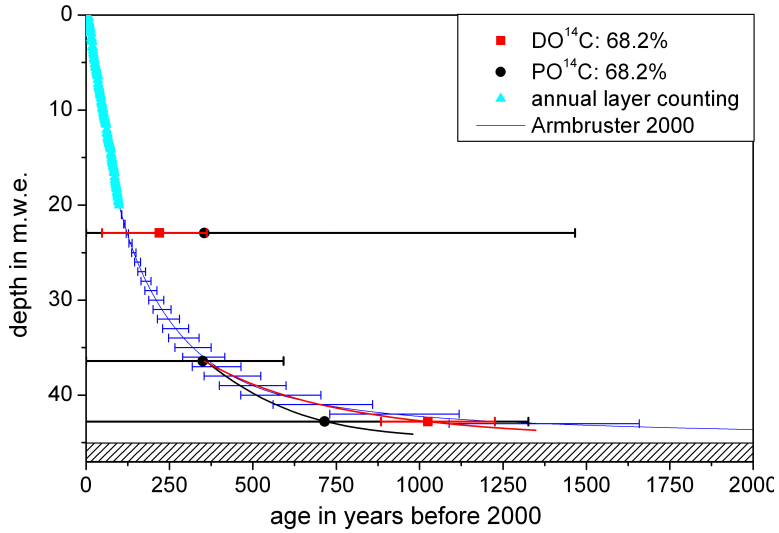

Figure 6.9: Dating of the KCH core: given are the annual layer counting (light blue) and the resulting age-depth relationship by Armbruster (2000) (blue line) compared to the DO^{14}C (black) and PO^{14}C (red) ages. The red and the black line illustrate the age-depth relationship based on the respective ^{14}C results.

and thus the PO^{14}C gives the best age guess for the moment.

KCS

Overall, the three PO^{14}C values give believable ages for the respective depths compared to the preliminary dating and can be used to correct and restrain the previous age-depth relationship for the bottom of the KCS core. The large carbon concentration of the KCS-107 sample makes the DO^{14}C fraction more insensitive to the in situ ^{14}C contribution and it may be suitable for dating.

The ^{14}C based age-depth relationship shown in Figure 6.10 agrees very well with the preliminary one down to about 70 m w.e. Below this depth, the ^{14}C age constrains the age-depth relationship to smaller ages than the preliminary dating. Only after reaching the basal layer does the ice age suddenly explode within 40 cm w.e. from about (7.5 ± 0.2) ka to (13.2 ± 2.2) ka. This near bedrock feature agrees with recent findings by Jenk *et al.* (2009) for the Colle Gnifetti CG03 ice core drilled not far from the KCS position (see Figure 6.11(a)). Similar to the presented results, the CG03 core has a POC radiocarbon age of > 15.2 ka for the lowest core section and (8.4 ± 0.75) ka for the sample directly above this. However, the decline of the CG03 core is relative smooth (Figure 6.11(b)) compared to the KCS.

The uneven age-depth relationship of the KCS supports the assumption of changes in accumulation rate. Based on the fact that changes in accumulation are to be expected due to the up-stream effect as well as due to temporal accumulation changes and that the KCS and the CG03 exhibit many similar features e.g. in their δ^{18}O record, the smooth age-depth relation of the CG03 core seems a little suspicious. The different accumulation rate would explain the

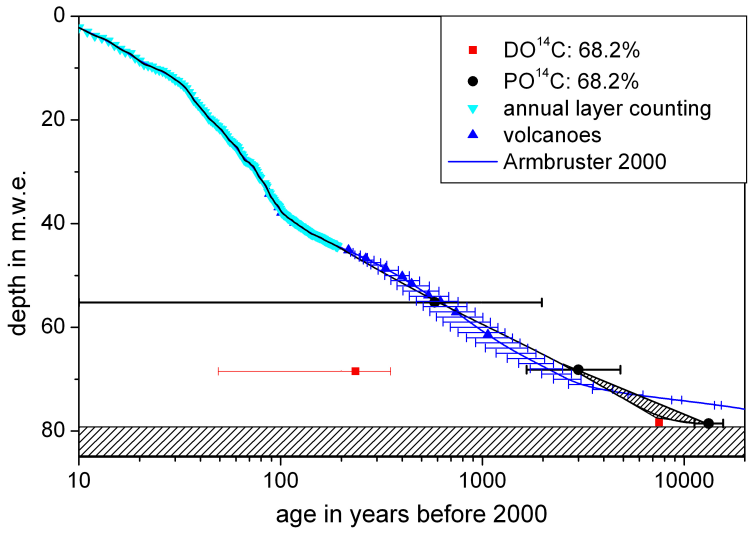

Figure 6.10: Dating of the KCS core: given are the annual layer counting (light blue), postulated volanic eruption horizons (blue) and the resulting age-depth relationship by Armbruster (2000) (blue line) compared to the DO^{14}C (red) and PO^{14}C (black) ages. The black line illustrate the age-depth relationship based on the respective ^{14}C results. The lined area indicates the region of uncertainty given by the use or neglect of the DO^{14}C age of KCS-107.

strong aberration of DO^{14}C and PO^{14}C at 68.5 m w.e. If the accumulation was significantly smaller than today, the in situ correction would be far stronger, resulting in an increase of the DO^{14}C age.

KCI

For the KCI samples, POC and DOC are regarded separately. The PO^{14}C gives overall, even with the large uncertainties, younger ages than proposed by Bohleber (2008) with a maximum dated age at 47.5 m w.e. (98 % core depth) of (3.6 $\pm$ 3.5) ka.

However, due to the large uncertainties, an adaption of the previous age-depth relationship to the ^{14}C ages as show in Figure 6.12 would be presumptuous.

The DO^{14}C ages, after being corrected for in situ with ϵ = 0.2 and A = 14 cm w.e./a, support partially the Bohleber (2008) age-depth relationship. However, the information gained from this agreement, is rather that the in situ correction with ϵ = 0.2 is valid, than an affirmation of the core dating. The divergence of DOC ages from the dating scenario, are again suspected to be due to variations in the in situ contribution indicating possible changes in the accumulation rate.

Having now stated on several occasions, that changes in the in situ fraction are the reason for the variations in DO^{14}C, it should be investigated if the required accumulation rate changes are even reasonable.

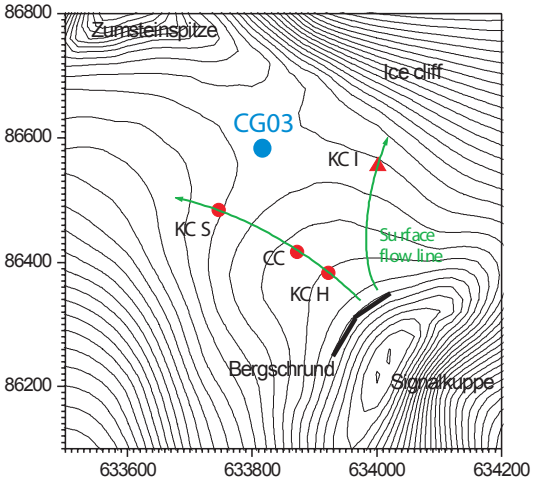

(a) Map of the Colle Gnifetti deep core positions including an estimated core position for the CG03 core.

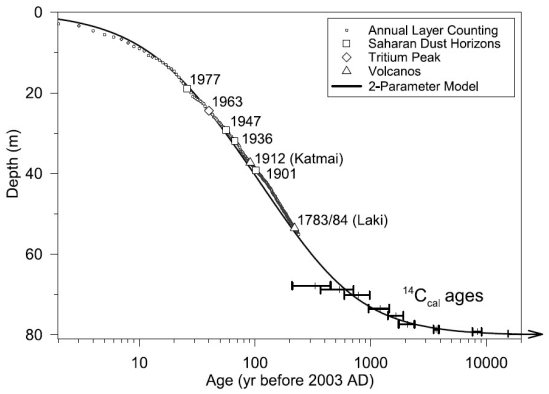

(b) Age-depth relation for the CG03 core, based on PO^{14}C ages and absolute time horizons (Jenk *et al.*, 2009).

Figure 6.11: Position and dating of the CG03 ice core drilled in 2003 and analysed at the Paul Scherer Institute (PSI), Switzerland.

6.2.3 Accumulation rate changes and in situ ^{14}C

Although, the contribution of in situ produced ^{14}C to organic compounds in ice, is at this time only an assumption, and the parameters governing the production and contribution to the organic carbon in Alpine glacier ice is completely unknown, an investigation of the possibility to determine accumulation changes offered by this unexpected parameter will be explored.

Since the amount of in situ produced ^{14}C atoms in ice depends on the accumulation rate A, the measurement of the ^{14}C content at a certain depth with a known ice age, could allow the reconstruction of the surface accumulation rate around that time (see Section 5.3.2):

$$\begin{aligned} {}^{14}C_{insitu} &= \frac{P_0 \cdot \epsilon \cdot m_{ice}}{\frac{\rho A}{\Lambda} - \lambda} \cdot e^{-\lambda t} \\ \Rightarrow A &= \frac{P_0 \cdot \epsilon \cdot m_{ice} \cdot \Lambda}{\rho \cdot ({}^{14}C_{meas} - {}^{14}C_{expected})} \cdot e^{-\lambda t} + \frac{\lambda \cdot \Lambda}{\rho} \end{aligned} \tag{6.1}$$

Of course, to actually quantify accumulation rates, the production rate P_0 and especially the ratio ϵ of in situ rate in organic molecules must be well constrained. Natural changes of P_0 are in the order of a few percent. ϵ has been assumed to be 0.2, since this value gives the most sensible DO^{14}C fraction for the KCI core, but the true value as well as its temporal variation are unknown. Assuming both factors to be constant in time, Table 6.3 gives the accumulation rates required to match the measured DO^{14}C values with the ages determined by Bohleber (2008) and Armbruster (2000). For the samples at the bottom of the cores, a minimum age was estimated rather than using the theoretical ages.

For the KCH core, the accumulation rates required to match the previous dating are in the

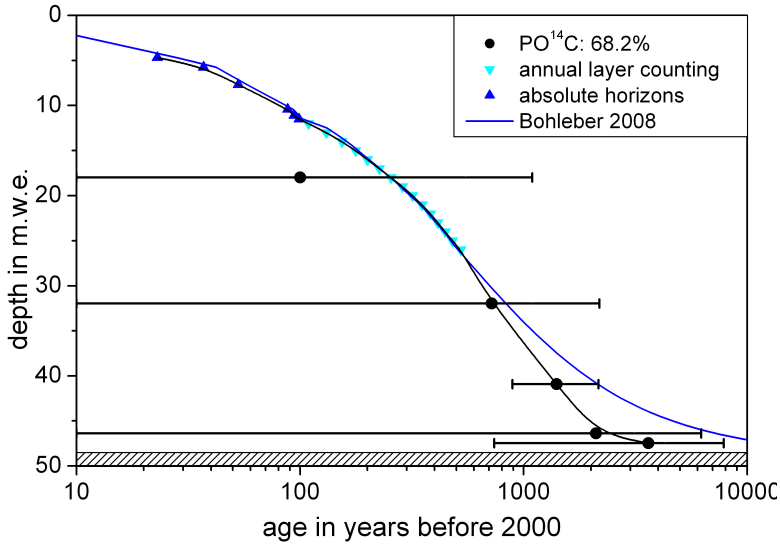

Figure 6.12: Dating of the KCI core: given are the annual layer counting (light blue), absolute time horizons (blue) and the resulting age-depth relationship by Bohleber (2008) (blue line) compared to the PO^{14}C (black) ages. The black line illustrates the age-depth relationship based on the ^{14}C results.

order of the assumed accumulation rate and could therefore very easily explain the deviance from the previous dating. However, to consolidate the DO^{14}C value with the POC age, the accumulation would have to be 108 cm w.e./a.

The accumulation for the KCS-95 sample of 7 cm w.e./a is equal to the accumulation rate determined for the KCI at the same age. Such a low accumulation is possible, especially considering, that 2 500 years ago an ongoing cooling trend since 5 ka reached a minimum(IPCC (2007); Saltzman (2002)), resulting maybe in a lower precipitation rate and a stronger loss of light snow by wind. The slop of the age-depth relation for KCS indicates a reduction of the accumulation rate anyhow. On the other hand the accumulation for the bottom of the KCS core is difficult to interpret. Since the supposed age suggests already ice from the last glacial, such low accumulation rates would be quite possible. This possibility, however, makes the determined DO^{14}C age less reliable s previously assumed.

The determined accumulation for the KCI seems to alternate between the present-day determined value of about 14 cm w.e./a and periods of lower accumulation of about 7 cm w.e./a. However, two extreme events would be necessary to explain the KCI-32 and KCI-51 DO^{14}C. Bohleber (2008) dates the KCI-51 sample at around 800 BP, which is generally known as the Medieval Climate Optimum (MCO) characterised by higher temperatures and especially high solar activity. The larger temperatures could cause such an enhanced accumulation rate as seen in Table 6.3. For the KCI-32 samples, the explanation is more difficult. First off, there is no well known climate signal, that indicates the cause for such a high accumulation rate at 250 BP. Even more problematic is the fact, that the adjoining sample suggests a normal 14 cm w.e./a accumulation, resulting in an abrupt change in precipitation sampling over the course of 10 years. The only remaining explanation is that different factors may contribute to

Table 6.3: Surface accumulation rates determined from ^{14}C concentration measured in DOC and based on the assumption of an in situ ^{14}C contribution. The expected ages are taken from the dating scenario of Armbruster (2000) and Bohleber (2008), the expected ^{14}C values have then been estimated by backwards calculation given by Equation 6.1. For the values marked with an (*), the expected ages were chosen as a minimum.

sample name	**depth [m w.e.]**	**exp. age [a before 2000]**	**$f_{expected}$ [dim.less]**	**f_{corr} [dim.less]**	**A [cm w.e./a]**
KCH-43	22.93	123 ± 5	0.99 ± 0.0001	1.062 ± 0.019	28 ± 7
KCH-70	42.78	1240 ± 50	0.855 ± 0.005	0.930 ± 0.014	17 ± 3
KCS-95 (II)	68.46	2225 ± 100	0.762 ± 0.01	1.027 ± 0.018	7.3 ± 0.6
KCS-107 (II)	78.32	$> 10000 \pm 1500$ (*)	0.10 ± 0.10	0.449 ± 0.013	$< 3.6 \pm 2$
KCI-32	17.75	247 ± 7	0.9730 ± 0.0001	1.006 ± 0.013	86 ± 34
KCI-32	17.98	254 ± 7	0.9728 ± 0.0001	1.131 ± 0.022	14 ± 2
KCI-51	31.98	835 ± 70	0.900 ± 0.01	0.947 ± 0.037	107 ± 88
KCI-54	34.71	1070 ± 80	0.873 ± 0.01	1.185 ± 0.051	16 ± 3
KCI-63	40.92	2150 ± 150	0.769 ± 0.01	1.074 ± 0.023	6.8 ± 0.6
KCI-67	43.32	3175 ± 250	0.693 ± 0.02	1.152 ± 0.073	15 ± 3
KCI-72	46.39	7320 ± 500	0.451 ± 0.03	0.690 ± 0.030	7.3 ± 1.4
KCI-73	47.46	$> 8000 \pm 1000$ (*)	0.33 ± 0.13	0.870 ± 0.020	$< 2.1 \pm 0.4$
KCI-74	47.72	$> 9000 \pm 1300$ (*)	0.18 ± 0.16	0.839 ± 0.011	$< 1.5 \pm 0.3$
KCI-74	47.93	$> 10000 \pm 1500$ (*)	0.10 ± 0.10	0.849 ± 0.017	$< 1.3 \pm 0.3$

alter the ^{14}C signal. A combination of a slight decrease in the ^{14}C production signal, a reduction of the fraction of in situ ^{14}C in DOC together with a change in the accumulation and a possible contribution of old matter might all add up to result in the 10 % difference of the two adjoining samples.

Comparison of the in situ accumulation rates with the vertical velocities, derived by Bohleber (2008) from particle concentration and the density profiles (Figure 6.13), shows no conclusive evidence in the vertical velocities for an increase in accumulation rate at core depth 17.75 m w.e. (KCI-32). However, at 32 m w.e. (KCI-51) a step is found in the density derived velocity, indicating a strong increase in accumulation. On the other hand, at core depth 42 m w.e. and 46.4 m w.e. the vertical velocity suggests a decrease of accumulation which is in agreement with the ^{14}C derived accumulation changes. Annual layer counting thus supports the in situ derived accumulation changes.

Concluding, the in situ derived accumulation changes are mostly within a reasonable range, can be partially explained by known changes in past climatic conditions and are generally supported by annual layer counting derived vertical velocities. Only the strong change in accumulation for the KCI-32 samples can not be explained or supported by other data. The difference in DO^{14}C for the KCI-32 samples therefore shows not the accumulation signal, but another influence on ^{14}C concentration.

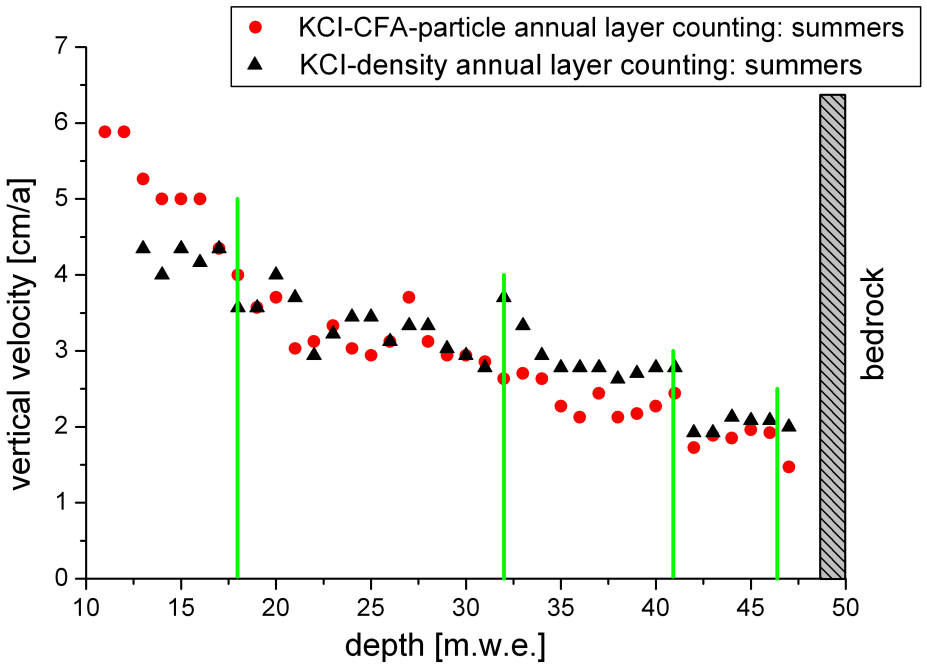

Figure 6.13: Vertical velocity derived by annual layer counting of the particle concentration and density profile (data from Bohleber (2008)).

6.2.4 Summary on the Colle Gnifetti results

Overall, the DO^{14}C values from the Colle Gnifetti core can not be used for dating and no information can be given for the sources of the two carbon fractions. Nonetheless, the PO^{14}C ages support the general preliminary age depth relationship for KCH, but suggest slightly younger ages in the lower core.

For KCS the PO^{14}C ages agree well with the pre-liminary dating of Armbruster (2000) down to 70 m w.e. The PO^{14}C age of the basal ice gives an upper age limit of < 13 000 years. Assuming no strong effect of in situ for the KCS-107 DOC sample, the age would increase within 40 cm w.e. from 7 500 years to < 13 000 years. This sudden age increase has also been found by Jenk *et al.* (2009) in another ice core CG03 in the saddle point area close to the KCS. However, assuming a far lower accumulation rate during the last glacial, would result in a stronger in situ ^{14}C component in the KCS-107 sample and a possibly higher DO^{14}C age closer to basal ice age.

The PO^{14}C values return smaller ages than the preliminary dating with a maximum age of 3 500 years at 98 % core depth. However the uncertainties are too large to establish a new age-depth relationship. DO^{14}C could not be used for dating, but may be deployed for infering past accumulation changes as it broadly shows agreement with vertical velosity features and past historic climate conditions.

Concluding, no immediately useful ^{14}C based dating could be established for the Colle Gnifetti ice cores. In all cores, the influence of in situ ^{14}C to the DO^{14}C fraction was to unpredictable

to allow reliable dating. For PO^{14}C the sample masses were still too low and the uncertainties therefore too large to give well constrained ages. Nonetheless, the PO^{14}C ages indicate for all cores lower ages in the lower core sections than predicted from modeling.

6.3 The problem of bottom ice core ages

The bottom of an ice core is always a sensitive region and the area of major unknown. For the ice cores studied in this work, only two, KCS and VCL, reached the basal ice layer indicated by a yellow silt, while the other two are not drilled down to very bedrock.

Determination of minimal glacier extension from the VCL

For cold glaciers, that are close to pressure melting point, like the Vadret dal Corvatsch, the basal layer reflects an upper age limit. The age indicates the time, when climatic conditions where favorable for persistent ice growth. The determined age would thus give advice on the minimal glacier extension. However, in addition to the influence of the bedrock on the basal age, it is possible that before that date only a small ice patch existed alternately growing and ablating for a long time before the glacier started to grow steadily to significant proportions.

For the Vadret dal Corvatsch a maximum ice age of (7.5 ± 0.1) ka was determined, which falls into the period of the Holocene Climate Optimum (5 000-10 0000 BP), with grand average temperatures being about 1 to 2 °C higher than today (IPCC (2007); Saltzman (2002)). It is reasonable that any ice at the location of the Corvatsch glacier being present during the ice age was melted during the first part of the Holocene optimum, before growing again during the cooler periods. Other investigations on minimal glacier extensions in the Alps, e.g. by Baroni and Orombelli (1996) or Joerin *et al.* (2008), gave similar results.
If the rapid increase in ice age is due to layer thinning or because the glacier did not grow steadily in the beginning, can not be decided. However the fact, that temperatures were still high after 7.5 ka BP and that the second lowest PO^{14}C age is well after the climate optimum, indicates that the glacier did very likely not grow steadily in the beginning, but alternated between growing and ablating. A DOC ^{14}C sample might give information on this.

Indication of Pleistocene ice in the KCS

For high Alpine cold glaciers, like the CG, where temperature and precipitation conditions kept the ice temperature always far below 0 °C, the majority of age information is contained in the bottom part of the core and any determined radiocarbon age would represent an average age over sample depth. Incorporation of bedrock material and disturbance of the glacier flow through the uneven ground may disturb this age distribution as well. Therefore the age determined from a basal layer ice sample has to be regarded carefully and may not necessarily reflect the age of the local glacier ice.

For KCS, the ^{14}C ages show a very strong increase in ice age in the basal layer. While the ice directly above the basal layer was dated by DO^{14}C at (7.5 ± 0.2) ka, the last 25 cm w.e.

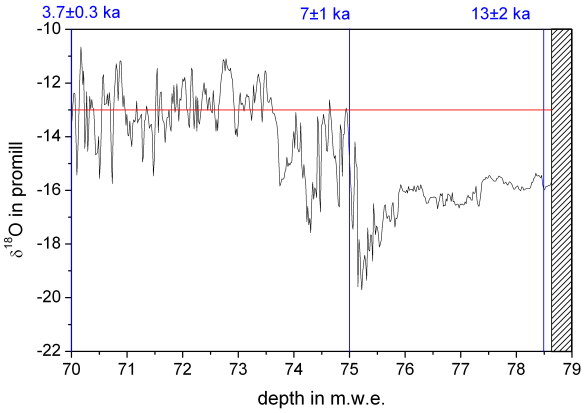

(a) ... KCS. The given age intervals are taken from the new ^{14}C based dating scenario shown in Figure 6.10.

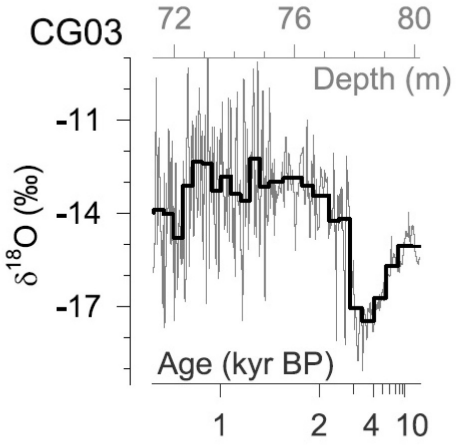

(b) ... CG03. Plot taken from (Jenk *et al.*, 2009).

Figure 6.14: δ^{18}O signal at the bottom of...

of the KCS core, being completely from the basal layer, give a PO^{14}C age of (13.2 $\pm$ 2.2) ka. It should be noted, that the DO^{14}C age is not wholly reliable, since a longtime change in accumulation could increase the age of the sample to cover the Pleistocene. However, the same behaviour has been reported by Jenk *et al.* (2009) for the CG03 core, which exhibits also a similar δ^{18}O signal.

The ^{14}C dates suggest that, although Pleistocene ice may be present in the basal ice, the strong dip in the δ^{18}O in the bottom core section is not due to the glacial-interglacial transition.

The age inversion in the KCI core

For the KCI, the ^{14}C values of DOC and POC show an apparent age inversion in the bottom core section. This anomaly has been reproduced for three independent DOC samples and one POC sample. Relative large carbon masses make the values robust to blank correction and the standard in situ correction with ϵ = 0.2 and A = 14 cm w.e./a has little influence. There are two possibilities:

1. enhanced in situ production through reduced accumulation

2. source region anomaly

(1) To make this observation a natural phenomenon, the accumulation rate needs to be maintained at 1-2 cm w.e./a (see Table 6.3) for several tens of years. Such a low accumulation rate however is very unlikely for a high Alpine glacier in the early Holocene. Reducing accumulation down to less then 1 cm w.e./a would result in DO^{14}C ages lying in the last glacial. The average δ^{18}O value for the respective interval of the samples is -15.3 ‰, which normally does not indicate glacial ice through being significant lower than the late Holocene mean. However

compared to the δ^{18}O values for Pleistocene ice in KCS and CG03, it may be possible for the ice of the three over-modern samples to origin in the last glacial.

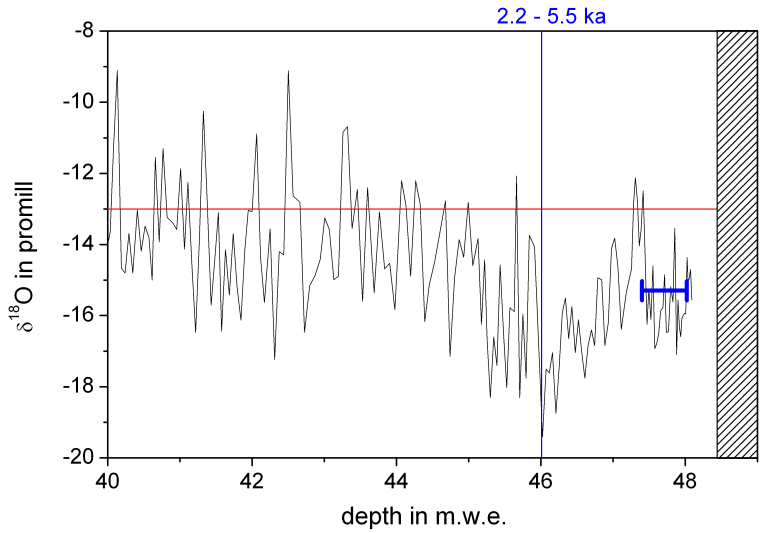

Figure 6.15: δ^{18}O in the bottom of the KCI core. The thin blue line marks the oldest age given by PO^{14}C and DO^{14}C. The thick blue line indicates the interval of the measured age inversion.

The fact that the high DO^{14}C values are measured over a depth of 1 m w.e., not accounting for the missing ice down to bedrock, indicates that the low accumulation rate needs to be maintained for several hundreds of years. There is no cold period in the Holocene long enough to allow such behaviour.
The fact remains that, although with a large uncertainty, the lowest PO^{14}C value supports the high DO^{14}C fraction and the age inversion. This context means, that either POC interacts and exchanges with DOC on long time scales or in situ ^{14}C and changes in accumulation are not the reason for the age inversion.

(2) For all CG cores the accumulation area is at the north-west slope of the Signalkuppe. In this region lies the so called Bergschrund, a crevass between the flowing and stagnant part of the glacier.
This crevass is constantly filled with present-day precipitation or young firn flowing in from the steep slope upwards of the Bergschrund. This matter would then be incorporated into the lower parts of the glacier and be transported down stream (see Figure 6.16) (Keck, 2001). The ice added to the bottom of the glacier by such a process is not only younger than typical for the respective ice depth, but due to the contribution from the steep slope, were the accumulation rate is extremely low and the concentration of in situ produced ^{14}C very high, the ice would be strongly enriched in ^{14}C. Ice from the Bergschrund could therefore produce the apparent inversion of age encountered in the lower KCI core. However, it is arguable, if a mass contribution from the Bergschrund would take up more than 1 m w.e. at the bottom of the glacier. Also, if the Bergschrund has such a large influence, why is there no indication for it seen in

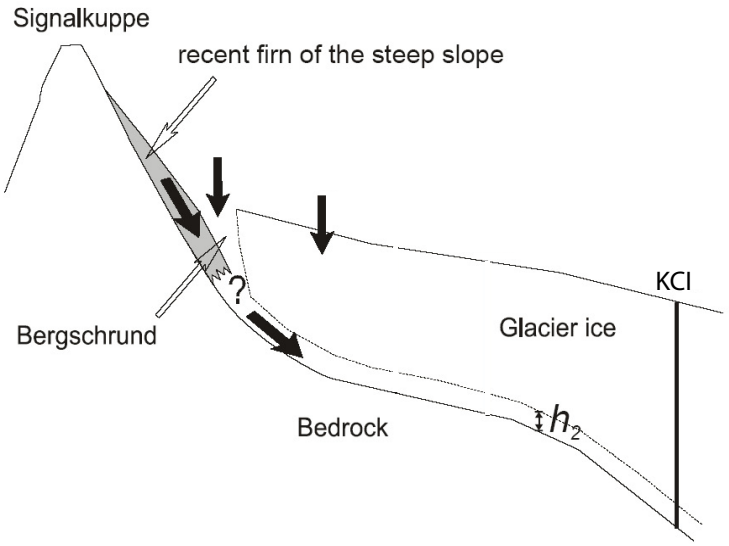

Figure 6.16: Illustration of incorporation of snow into the lower section of the glacier at the Bergschrund.

the KCS and KCH core?

A reason for the age inversion in the lower part of the KCI can not be given conclusively. However, while the addition of ice from the Bergschrund is possible, it is hard to believe, that it would take up more than 1 m w.e. of the bottom of the core. Also, if such a strong recent contribution from the source region is feasible, than one would expect an effect in the KCS and KCH core as well.

A change in accumulation rate and an increase in in situ production, would only be an option, if the ice origins in the last glacial. Only then are almost zero accumulation rates for a long period of time possible. δ^{18}O comparison with Pleistocene dated ice from KCS and CG03 suggest, that the three age inversion samples might contain glacial ice.

7 Conclusion and outlook

The eventual aim of this work was the dating of Alpine ice bodies through ^{14}C microanalysis on dissolved organic carbon. It was envisioned, that the DOC fraction, being present in ice in larger quantities than particulate organic carbon and not expecting any reservoir effects for this fraction, would provide correct ages for smaller ice volumes. The methodical adaption held many difficulties and had to be finally defined sufficient enough although the blank contribution remains significant. The extraction system allows handling of up to 700 g ice samples and allows for getting reliable ^{14}C results for carbon masses of > 30 μgC.

The unexpected identification of an additional ^{14}C source, which could not be explained by blank and was considered actually as in situ ^{14}C production in ice contributing to the dissolved organic carbon fraction, prevents the use of DOC for dating. Especially for low and strongly variable accumulation regimes, DOC can not give reliable ages. At present, the contribution of in situ ^{14}C is not known and dedicated experiments are necessary to determine if and how strongly in situ ^{14}C contributes to organic carbon in Alpine glacier ice. At first, further measurements are needed to ascertain that the enhanced ^{14}C concentration in DOC is indeed due to in situ production and not imposed through a not yet identified, external contamination. If contamination continuous to be ruled out, the determination of the production rate and more importantly the conversion efficiency of the hot ^{14}C atoms in ice into organic compounds need to be quantified. Information is needed on the oxidation processes, its dependence on the ice structure, impurities in the ice and intensity of UV radiation. However, even if these parameters and their temporal changes may be determined sufficiently to allow a correction of DO^{14}C values, the problem of varying accumulation rates still prevents the use for dating. However, similar to the use of in situ $^{14}CO_2$ in polar ice sheets, a well defined in situ ^{14}C fraction may be used to infer past changes in accumulation for a well dated Alpine glacier.
Concluding, it seems at present, that DO^{14}C must be discarded as dating tool, holds however the chance of identifying accumulation changes. On a side note, DOC may still hold the possibility for dating exotic ice, like cave ice, where in situ production does not contribute.

Having also extracted the particulate organic carbon fraction from the ice, although often getting too low carbon masses compared to the blank contribution, POC proved to be a better ^{14}C age carrier, not showing as expected any significant reservoir effects. Although the ice volume required for PO^{14}C analysis should be by a factor of 2 larger, the benefits of dating the lowest core section as shown for the CG KCS core and dating of small glacier caps, like the Vadret dal Corvatsch, is significant. The most work here must be put into the reduction of the filtration blank.

Despite the many problems with in situ ^{14}C and small carbon samples, dating of the Vadret dal

Corvatsch glacier cap was successful and a first age-depth relationship could be established. The maximum age of the basal ice of (7.5 ± 0.2) ka gives an upper limit for the time of minimal glacier extension in the Alpes and interpretation of the δ^{18}O signal can now be attempted.

For the basal layer of the CG cores, it was determined that the strong δ^{18}O signal is not due to the glacial-interglacial transition, although Pleistocene ice is found in the basal ice of KCS. For KCI, there is evidence that the lowest m w.e. of the core may also contain Pleistocene ice.

Although expectation for DO^{14}C dating could not be met, a possible indicator of accumulation changes was found. The focus of ^{14}C dating must now rest on the POC fraction.

Bibliography

[Alean *et al.* 1983] ALEAN, J. ; HAEBERLI, W. ; SCHÄDLER, B.: Snow accumulation, firn temperature and solar radiation in the area of the Colle Gnifetti core drilling site (Monte Rosa, Swiss Alps): distribution patterns and interrelationships. *Zeitschrift für Gletscherkunde und Glazialgeologie* 12. 1983

[Armbruster 2000] ARMBRUSTER, M.: *Stratigraphische Datierung hochalpiner Eisbohrkerne über die letzten 1000 Jahre*, Institut für Umweltphysik, Universität Heidelberg, master thesis, 2000

[Arnold and Libby 1949] ARNOLD, J.R. ; LIBBY, W.F.: Age determinations by radiocarbon content: Checks with samples of known age. *Science* 110. p. 678. 1949

[Bar-Nun and Hartman 1993] BAR-NUN, A. ; HARTMAN, H.: Synthesis of organic compounds from carbon monoxide and water by UV photolysis. *Origins of Life* 9. p. 93–101. 1993

[Bard *et al.* 2004] BARD, E. ; BRONK RAMSEY, C. ; DAVIS, O.K. ; DRUFFEL, E.R.M. ; GROOTES, P. ; KUZMIN, Y. ; LEAVITT, S.W. ; NAKAMURA, T. ; MCNICHOL, A.P. ; POVINEC, P. ; SCHIFFER, M.B. ; SCOTT, E.M. ; SPARKS, R. ; PLICHT, J. van der ; VOGEL, J.S. ; ZHOU, W.: IntCal04: Calibration Issue. *Radiocarbon* 46. 2004

[Baroni and Orombelli 1996] BARONI, C. ; OROMBELLI, G.: The Alpine “Iceman” and Holocene Climatic Change. *Quaternary Research* 46. p. 78–83. 1996

[Bengel 2005] BENGEL, I.: *Spurenstoffglaziologische Pilotuntersuchungen an einer kalten Miniatureiskappe*, Institut für Umweltphysik, Universität Heidelberg, master thesis, 2005

[Benner and Hedges 1993] BENNER, R. ; HEDGES, J.I.: A test of the accuracy of freshwater DOC measurements by high-temperature catalytic oxidation and UV-promoted persulfate oxidation. *Marine Chemistry* 41. 1993

[Beukens 1992] BEUKENS, R.B.: *Radiocarbon mass spectrometry: background, precision and accuracy*. In: Radiocarbon after four decades, Springer Verlag, New York. 1992

[Biegalski *et al.* 1998] BIEGALSKI, S.R. ; CURRIE, L.A. ; FLETCHER, R.A. ; KLOUDA, G.A. ; WEISSENBÖK, R.: AMS and microprobe analysis of combusted particles in ice and snow. *Radiocarbon* 40. 1998

[Biosciences 2002] BIOSCIENCES, LI-COR: *Li-820 Instruction Manual*. LI-COR Inc., Nebraska. 2002. – URL `http://www.licor.com/env/Products/GasAnalyzers/li820/820.jsp`

[Boehlert 2005] BOEHLERT, R., Geographisches Institut der Universität Zürich, master thesis, 2005

[Bohleber 2008] BOHLEBER, P.: *Age distribution and δ ^{18}O variability in a low accumulation Alpine ice core: perspective for paleoclimate studies*, Institut für Umweltphysik, Universität Heidelberg, master thesis, 2008

[Broecker and Peng 1974] BROECKER, W.S. ; PENG, T.-H.: Gas exchange rate between air and sea. *Tellus - Series B* 26. 1974

[Bronk Ramsey 2009] BRONK RAMSEY, C.: Bayesian analysis of radiocarbon dates. *Radiocarbon* 51. p. 337–360. 2009

[Busarello 2002] BUSARELLO, C.: *Sondierung des Gletscherbetts am Vadret dal Corvatsch mittels Georadar*, Geographisches Institut, Universität Zürich, master thesis, 2002

[Cecil *et al.* 2004] CECIL, L.D. (ed.) ; GREEN, J.R. (ed.) ; THOMPSON, L.G. (ed.): *Earth paleoenvironments: Records preserved in mid- and low-latitude glaciers*. Bd. 9. Kluwer Academic, Dortrecht, Netherlands. 2004

[Cherkinsky 1996] CHERKINSKY, A.E.: ^{14}C dating soil organic matter dynamics in arctic and sub arctic ecosystems. *Radiocarbon* 38. p. 241–245. 1996

[Chýlek *et al.* 1995] CHÝLEK, P. ; JOHNSON, B. ; DAMIANO, P.A. ; TAYLOR, K.C. ; CLEMENT, P.: Biomass burning record and black carbon in the GISP2 ice core. *Geophysical Research Letters* 22. 1995

[Clark and Fritz 1997] CLARK, I.D. (ed.) ; FRITZ, P. (ed.): *Environmental isotopes in hydrogeology*. CrC. 1997

[Collins and Williams 1977] COLLINS, K.J. ; WILLIAMS, P.J. le B.: An automated photochemical method for the determination of the dissolved organic carbon in sea and estuarine waters. *Marine Chemistry* 5. 1977

[Dansgaard 1964] DANSGAARD: Stable isotopes in preciptiation. *Tellus* 16. p. 436–468. 1964

[Deevey *et al.* 1954] DEEVEY, E.S. ; GROSS, M.S. ; HUTCHINSON, G.E. ; KRAYBILL, H.L.: The natural ^{14}C contents of materials from hard-water lakes. *Proceedings of the National Academy of Science* 40. p. 285–288. 1954

[EPICA 2004] EPICA: Eight glacial cycles from an Antarctic ice core. *Nature* 429. p. 623–628. 2004

[Friedrich 2003] FRIEDRICH, R.: *Helium in polaren Eisschilden*, Institut für Umweltphysik, Universität Heidelberg, master thesis, 2003

[Gelencsér 2005] GELENCSÉR, A. (ed.): *Carbonaceous aerosol*. Springer. 2005

[Gelencsér *et al.* 2007] GELENCSÉR, A. ; MAY, B. ; SIMPSON, D. ; SÁNCHEZ-OCHOA, A. ; CASEIRO, A.: Source apportionment of PM2.5 organic aerosol over Europe: primary/secondary, natural/anthropogenic, fossil/biogenic origin. *Journal of Geophysical Research* 112. 2007

[Gershey *et al.* 1977] GERSHEY, R.M. ; MACKINNON, M.D. ; WILLIAMS, P.J. le B. ; MOORE, R.M.: Comparison of the three oxidation methods used for the analysis of the dissolved organic carbon in seawater. *Marine Chemistry* 7. 1977

[Gäggeler *et al.* 1983] GÄGGELER, H. ; CRUTZEN, H.R. von ; RÖSSLER, E. ; OESCHGER, H. ; SCHOTTERER, U.: ^{210}Pb-dating of cold Alpine firn/ice cores from Colle Gnifetti, Switzerland. *Journal of Glaciology* 29. p. 165–177. 1983

[Grasshoff *et al.* 1999] GRASSHOFF, K. (ed.) ; KREMLING, K. (ed.) ; EHRHARDT, M. (ed.): *Methods of Seawater Analysis*. Bd. 3. Wiley-VCH Verlag GmbH. 1999

[Greilich 1998] GREILICH, S.: *Messung des organischen Kohlenstoffgehalts alpiner Eisproben*, Institut für Umweltphysik, Universität Heidelberg, master thesis, 1998

[Haeberli and Alean 1985] HAEBERLI, W. ; ALEAN, J.: Temperature and accumulation of high altitude firn in the Alpes. *Annals of Glaciology* 6. 1985

[Haeberli *et al.* 2004] HAEBERLI, W. ; FRAUENFELDER, R. ; KÄÄB, A. ; WAGNER, S.: Characteristics and potential climatic significance of “miniature ice caps” (crest and cornice type low-altitude ice archives). *Journal of Glaciology* 50. 2004

[Hager 2002] HAGER, P.: *Glaziologische Untersuchungen am Gipfelgrat des Vadret dal Corvatsch: Thermik und Oberflächenprozesse*, Geographisches Institut der Universität Zürich, master thesis, 2002

[Hoffmann 1996] HOFFMANN, M.R.: *Possible chemical transformations in snow and ice solar (UV photons) and cosmic irradiation (muons)*. In: Chemical exchange between the atmosphere and polar snow, p. 353–378, Springer Verlag. 1996

[Hoffmann 2003] HOFFMANN, M.R.: Sensitivity of hydrogen peroxide (H2O2) and formaldehyde (HCHO) preservation in snow to changing environmental conditions: Implications for ice core records. *Journal of Geophysical Research* 108. 2003

[IPCC 2007] IPCC ; SOLOMON, S. (ed.) ; QUIN, D. (ed.) ; MANNING, M. (ed.) ; CHEN, Z. (ed.) ; MARQUIS, M. (ed.) ; AVERYT, K.B. (ed.) ; TIGNOR, M. (ed.) ; MILLER, H.L. (ed.): *Climate Change 2007: The physical sience basis*. Bd. 1. Cambridge University Press, Cambridge, United Kingdom and New York, USA. 2007

[Jaenicke 1987] JAENICKE, Ruprecht (ed.): *Atmosphärische Spurenstoffe*. VCH. 1987

[Jenk *et al.* 2009] JENK, T.M. ; SZIDAT, S. ; BOLIUS, D. ; SIGL, M. ; GÄGGELER, H.W. ; WACKER, L. ; RUFF, M. ; BARBANTE, C. ; BOUTRON, C.F ; SCHWIKOWSKI, M.: A novel radiocarbon dating technique applied to an ice core from the Alps indicating late Pleistocene ages. *Journal of Geophysical Research* 114. 2009

[Jenk *et al.* 2006] JENK, T.M. ; SZIDAT, S. ; SCHWIKOWSKI, M. ; GÄGGELER, H.W. ; BRÜTSCH, S. ; WACKER, L. ; SYNAL, H.-A. ; SAURER, M.: Radiocarbon analysis in an Alpine ice core: record of anthropogenic and biogenic contributions to carbonaceous aerosols in the past (1650-1940). *Atmospheric Chemistry and Physics* 6. p. 5905–5931. 2006

[Jenk *et al.* 2007] JENK, T.M. ; SZIDAT, S. ; SCHWIKOWSKI, M. ; GÄGGLER, H.W. ; WACKER, L. ; SYNAL, H.-A. ; SAURER, M.: Microgram level radiocarbon (^{14}C) determination on carbonaceous particles in ice. *Nuclear Instruments and Methods in Physics Research B* 259. p. 518–525. 2007

[Joerin *et al.* 2008] JOERIN, U.E. ; NICOLUSSI, K. ; FISCHER, A. ; STOCKER, T.F. ; SCHLÜCHTER, C.: Holocene optimum events inferred from subglacial sediments at Tschierva glacier, Eastern Swiss Alps. *Quaternary Science Reviews* 27. p. 337–350. 2008

[Jull *et al.* 1994] JULL, A.J.T. ; LAL, D. ; DONAHUE, D.J. ; MAYEWSKI, P. ; LORIUS, C. ; RAYNAUD, D. ; PETIT, J.R.: Measurements of cosmic-ray-produced ^{14}C in firn and ice from Antarctica. *Nuclear Instruments and Methodsin Physics Research B* 92. p. 326–330. 1994

[Junge 1963] JUNGE, C. E.: *International Geophysics Series*. Bd. 4: *Air Chemistry and radioactivity*. Academic Press New York and London. 1963

[Keck 2001] KECK, L.: *Climate significance of stable isotope records from Alpine ice cores*, Insitut für Umweltphysik, Universität Heidelberg, phd thesis, 2001

[van der Kemp *et al.* 2002] KEMP, W.J.M. van der ; ALDERLIESTEN, C. ; BORG, K. van der ; JONG, A.F.M. de ; LAMERS, R.A.N. ; OERLEMANS, J. ; THOMASSEN, M. ; WAL, R.S.W. van de: In situ produced ^{14}C by cosmic ray muons in ablating Antarctic ice. *Tellus - Series B* 54. p. 186–192. 2002

[Kromer *et al.* 1987] KROMER, B. ; PFLEIDERER, C. ; SCHLOSSER, P. ; LEVIN, I. ; MÜNNISCH, K.O. ; BONANI, G. ; SUTER, S. ; WÖLFLI, W.: AMS ^{14}C measurements of small volume oceanic water samples: expermintal procedure and comparison with low-level counting technique. *Nuclear Instruments and Methodsin Physics Research B* 29. p. 302–305. 1987

[Lal and Jull 1990] LAL, D. ; JULL, A.J.T.: On determining ice accumulation rates in the past 40,000 years using in situ cosmogenic ^{14}C. *Geophysical Research Letters* 17. p. 1303–1306. 1990

[Lal *et al.* 1997] LAL, D. ; JULL, A.J.T. ; BURR, G.S. ; DONAHUE, D.J.: Measurements of in situ ^{14}C concentrations in Greenland Ice Sheet Project 2 ice covering a 17-kyr time span: Implications to ice flow dynamics. *Journal of Geophysical Research* 102. p. 26505–26510. 1997

[Lal *et al.* 1990] LAL, D. ; JULL, A.J.T. ; DONAHUE, D.J. ; BURTNER, D. ; NISHIIZUMI, K.: Polar ablation rates measured using in situ cosmogenic ^{14}C. *Letters to Nature* 346. p. 350–352. 1990

[Lal *et al.* 1987] LAL, D. ; NISHIIZUMI, K. ; ARNOLD, J.R.: In situ cosmogenic ^{3}H, ^{14}C and ^{10}Be for determining the net accumulation and ablation rates of ice sheets. *Journal of Geophysical Research* 92. p. 4947–4952. 1987

[Lal and Peters 1967] LAL, D. ; PETERS, B.: *Cosmic ray produced radioactivity on the Earth*. In: Handbuch der Physik XLVI (2), p. Springer, New York, 1967

[Legrand *et al.* 2007] LEGRAND, M. ; PREUNKERT, S. ; SCHOCK, M. ; CERQUEIRA, M. ; KASPER-GIEBL, A.: Major 20th century changes of organic carbonaceous aerosol components (EC, WinOC, DOC, HULIS, carboxylic acids, and cellulose) derived from Alpine ice cores. *Journal of Geophysical Research* 112. 2007

[Legrand *et al.* 2003] LEGRAND, M. ; PREUNKERT, S. ; WAGENBACH, D. ; CACHIER, H. ; PUXBAUM, H.: A historical record of formate and acetate from a highelevation Alpine glacier: Implications for their natural versus anthropogenic budgets at the European scale. *Journal of Geophysical Research* 108. 2003

[Levin *et al.* 2008] LEVIN, I. ; HAMMER, S. ; KROMER, B. ; MEINHARDT, F.: Radiocarbon observations in atmospheric CO_2: Determining fossil fuel CO_2 over Europe using Jungfraujoch observations as background. *Science of the total environment* 391. p. 211–216. 2008

[Levin and Kromer 2004] LEVIN, I. ; KROMER, B.: The tropospheric $^{14}CO_2$ level in midlatitudes of the Northern Hemisphere (1959-2003). *Radiocarbon* 46. 2004

[Levin *et al.* 1985] LEVIN, I. ; KROMER, B. ; SCHOCH-FISCHER, H. ; BRUNS, M. ; MÜNNICH, M. ; BERDAU, D. ; VOGEL, J.C. ; MÜNNICH, K.O.: 25 years of tropospheric ^{14}C observations in central Europe. *Radiocarbon* 27. 1985

[Libby 1946] LIBBY, W.F.: Atmospheric Helium three and Radiocarbon from Cosmic Radiation. *Physical Review* 69. p. 671. 1946

[MacKinnon 1978] MACKINNON, M.D.: A dry oxidation method for the analysis of T.O.C. in seawater. *Marine Chemistry* 7. 1978

[Masarik and Beer 1999] MASARIK, J. ; BEER, J.: Simulation of particle fluxes and cosmogenic nuclide production in the Earth's atmosphere. *Journal of Geophysical Research* 104. p. 12099. 1999

[Masarik and Reedy 1995] MASARIK, J. ; REEDY, R.C.: Terrestrial cosmogenic-nuclide production systematics calculated from numerical simulations. *Earth and Planetary Science Letters* 136. p. 381–395. 1995

[Maupetit *et al.* 1995] MAUPETIT, F. ; WAGENBACH, D. ; WEDDEKING, P. ; DELMAS, R.J.: Seasonal fluxes of major ions to a high altitude Alpine glacier. *Atmospheric Environment* 29. p. 1–9. 1995

[May *et al.* 2009] MAY, B. ; WAGENBACH, D. ; HAMMER, S. ; STEIER, P. ; PUXBAUM, H. ; PIO, C.: The anthropogenic influence on carbonaceous aerosol in the European background. *Tellus - Series B* 61. 2009

[Menzel and Vaccaro 1964] MENZEL, D.W. ; VACCARO, R.F.: The measurement of dissolved and particulate carbon in seawater. *Limnology and Oceanography* 9. 1964

[Middelton 1984] MIDDELTON, R.: A review of ion sources for accelerator mass spectrometry. *Nuclear Instruments and Methods in Physics Research B* 5. p. 192. 1984

[Mommert 2007] MOMMERT, M.: *Extraktion von gelöstem organischem Kohlenstoff aus Wasser*. Practical report, Institut für Umweltphysik, Universität Heidelberg. 2007

[Mook 2000] MOOK, W. G.: *Environmental isotopes in the hydrological cycle. Principles and Applications*. International Atomic Energy Agency (IAEA), Vienna, Austria. 2000. – http://www.iaea.org/programmes/ripc/ih/volumes/volume1.htm

[Naegler 2005] NAEGLER, Tobias: *Simulating Bomb Radiocarbon: Implications for the Global Carbon Cycle*, Dissertation, IUP Universität Heidelberg, phd thesis, 2005

[Nave 2005] NAVE, C.R.: *Hyper Physics - Carbon dating*. 2005. – http://hyperphysics.phy-astr.gsu.edu/hbase/nuclear/cardat.html

[Nebeling *et al.* 1985] NEBELING, B. ; RÖSSLER, K. ; STÖCKLIN, G.: Reaction of recoiling carbon atoms with water vapour. *Radiochimica Acta* 38. p. 15–20. 1985

[NGRIP 2004] NGRIP: High-resolution record of Northern Hemisphere climate extending into the last interglacial period. *Nature* 431. p. 147–151. 2004

[Oeschger and Langway 1989] OESCHGER, H. (ed.) ; LANGWAY, L.L. (ed.): *The environmental record in glaciers and ice sheets*. John Wiley & Sons. 1989

[Oppenländer and Gliese 2000] OPPENLÄNDER, T. ; GLIESE, S.: Mineralization of organic micropollutants (homologous alcohols and phenols) in water by vacuum-UV-oxidation (H_2O-VUV) with an incoherent xenon-excimer lamp at 172 nm. *Chemosphere* 40. 2000

[Paterson 1994] PATERSON, W.S.B. (ed.): *The physics of glaciers*. 3. Pergamon Press. 1994

[Pessenda *et al.* 2000] PESSENDA, L.C.R. ; GOUVEIA, S.E.M. ; ARAVENA, R. ; GOMES, B.M. ; BOULET, R. ; RIBEIRO, A.S.: ^{14}C dating and stable carbon isotopes of soil organic matter in forest-savanna boundary areas in the southern brazilian amazon region. *Radiocarbon* 40. p. 1013–1022. 2000

[Petit *et al.* 2000] PETIT, J.R. ; JOUZEL, J. ; RAYNAUD, D. ; BARKOV, N.I. ; BARNOLA, J.-M. ; BASILE, I. ; BENDER, M. ; CHAPPELLAZ, J. ; DAVISK, M. ; DELAYGUE, G. ; DELMOTTE, M. ; KOTLYAKOV, V.M. ; LEGRAND, M. ; LIPENKOV, V.Y. ; LORIUS, C. ; PÉPIN, L. ; RITZ, C. ; SALTZMANK, E. ; STIEVENARD, M.: Climate and atmospheric history of the past 420,000 years from the Vostok ice core, Antarctica. *Chemosphere* 40. 2000

[Petrenko *et al.* 2009] PETRENKO, V.V. ; SMITH, A.M. ; BROOK, E.J. ; LOWE, D. ; RIEDEL, K. ; BRAILSFORD, G. ; HUA, Q. ; SCHAEFER, H. ; REEH, N. ; WEISS, R.F. ; ETHERIDGE, D. ; SEVERINGHAUS, J.P.: $^{14}CH_4$ measurements in Greenland ice: Investigating last glacial termination CH_4 sources. *Science* 324. 2009

[Pichlmayer *et al.* 1998] PICHLMAYER, F ; SCHÖNER, W. ; SEIBERT, P. ; STICHLER, W. ; WAGENBACH, D.: Stable isotope analysis for characterization of pollutants at high elevation Alpine sites. *Atmospheric Environment* 32. p. 4075–4085. 1998

[Pomeroy and Jones 1996] POMEROY, J.W. ; JONES, H.G.: *Wind-blown snow: sublimation, transport and changes to polar snow*. In: Chemical exchange between the atmosphere and polar snow, p. 453–490, Springer Verlag. 1996

[Pringle *et al.* 1955] PRINGLE, R.W. ; TURCHINETZ, W. ; FLUNT, B.L.: Liquid scintillation techniques for radiocarbon dating. *Review of Scientific Instruments B* 35. p. 284. 1955

[Rau 2008] RAU, S.: *Stratigraphische Untersuchungen an einem tiefen Eisbohrkern der alpinen Miniatureiskappe Vadret dal Corvatsch*, Institut für Umweltphysik, Universität Heidelberg, master thesis, 2008

[Ravishankara 1996] RAVISHANKARA, A.R.: *Processes at ice surfaces: physical uptake and reaction*. In: Chemical exchange between the atmosphere and polar snow, p. 339–352, Springer Verlag. 1996

[Rowland and Libby 1953] ROWLAND, F.S. ; LIBBY, W.F.: Hot atoms recoil from $^{12}C(\gamma,n)^{11}C*$. *Journal of Chemical Physics* 21. p. 1493–1494. 1953

[Ruff 2008] RUFF, M.: *Radiocarbon Measurement of Micro-Scale Samples - A carbon dioxide inlet system for AMS*, Department für Chemie und Biochemie, Universität Bern, phd thesis, 2008

[Saltzman 2002] SALTZMAN, B.: *Dynamical Paleoclimatology - Generalized theory of global climate change*. Academic Press. 2002

[Sander 1996] SANDER, R.: *Compilation of Henry's Law Constants for Inorganic and Organic Species of Potential Importance in Environmental Chemistry*. Max-Planck-Institut of Chemistry, Mainz. 1996. – URL `http://www.mpch-mainz.mpg.de/ sander/res/henry.html`

[Schock 2001] SCHOCK, M.: *Optimierung eines UV-induzierten Oxidationsverfahrens zur Untersuchung der Gehalte an gelösten, organischen Kohlenstoffverbindungen in hochalpinen Eisbohrkernen*, Institut für Umweltphysik, Universität Heidelberg, master thesis, 2001

[Schwander 1996] SCHWANDER, J.: *Gas diffusion on firn*. In: Chemical exchange between the atmosphere and polar snow, p. 527–540, Springer Verlag. 1996

[Sharp *et al.* 1995] SHARP, J.H. ; BENNER, R. ; BENNETT, L. ; CARLSON, C.A. ; FITZWATER, S.E. ; PELTZER, E.T. ; TUPAS, L.M.: Analyses of dissolved organic carbon in seawater: the JGOFS EqPac methods comparison. *Marine Chemistry* 48. 1995

[Sharp *et al.* 2002] SHARP, J.H. ; CARLSON, C.A. ; PELTZER, E.T. ; CASTLE-WARD, D.M. ; SAVIDGE, K.B. ; RINKER, K.R.: Final dissolved organic carbon broad community intercalibration and preliminary use of DOC reference materials. *Marine Chemistry* 77. 2002

[Smith *et al.* 2000] SMITH, A.M. ; LEVCHENKO, V.A. ; ETHERIDGE, D.M. ; LOWE, D.C. ; HUA, Q. ; TRUDINGER, C.M. ; ZOPPI, U. ; ELCHEIKH, A.: In search of in-situ radiocarbon in Law Dome ice and firn. *Nuclear Instruments and Methods in Physics Research B* 172. p. 610–622. 2000

[Steier *et al.* 2006] STEIER, P. ; DROSG, R. ; FEDI, M. ; KUTSCHERA, W. ; SCHOCK, M. ; WAGENBACH, D. ; WILD, E.M.: Radiocarbon determination of particulate organic carbon in non-temperated, Alpine glacier ice. *Radiocarbon* 48. 2006

[Stempel 2009] STEMPEL, R.: *Einsatz von ^{210}Pb zur Abschätzung der Altersstruktur kalter Firngebiete*. Staatsexamensarbeit, Institut für Umweltphysik, Universität Heidelberg. 2009

[Stricker 2008] STRICKER, P.: *Umbau und Charakterisierung einer Apparatur zur DOC-Analyse des organischen Kohlenstoffgehalts von Gletschereis*, Institut für Umweltphysik, Universität Heidelberg, master thesis, 2008

[Stuiver and Polach 1977] STUIVER, M. ; POLACH, A.: Reporting of ^{14}C data. *Radiocarbon* 19. Nr. 3. p. 355–363. 1977

[Stuiver and Quay 1981] STUIVER, M. ; QUAY, P.D.: Reporting of ^{14}C data. *Earth and Planetary Science Letters* 53. p. 349–362. 1981

[Sugimura and Suzuki 1988] SUGIMURA, Y. ; SUZUKI, Y.: A High-Temperature Catalytic Oxidation Method for the Determination of Non-Volatile Dissolved Organic Carbon in Seawater by Direct Injection of a Liquid Sample. *Marine Chemistry* 24. 1988

[Suter *et al.* 1981] SUTER, S. ; BALZER, R. ; BONANI, G. ; WÖLFLI, W. ; BEER, J. ; OESCHGER, H. ; STAUFFER, B.: Radioisotope Dating using an EN-Tandem Accelerator. *IEEE Transactions on Nuclear Science* 28. p. 1475. 1981

[Suter *et al.* 2001] SUTER, S. ; LATERNSER, M. ; HAEBERLI, W. ; FRAUENFELDER, R. ; HOELZLE, M.: Cold firn and ice of high-altitude glaciers in the Alps: measurements and distribution modelling. *Journal of Glaciology* 47. p. 85–96. 2001

[Szidat *et al.* 2004] SZIDAT, S. ; JENK, T. M. ; GÄGGELER, H. W. ; SYNAL, H.-A. ; FISSEHA, R. ; BALTENSPERGER, U. ; KALBERER, K. ; SAMBUROVA, V. ; REIMANN, S. ; KASPER-GIEBL, A. ; HAJDAS, I.: Radiocarbon-deduced biogenic and anthropogenic contributions to organic carbon (OC) of urban aerosols from Zürich, Switzerland. *Atmospheric Environment* 38. p. 4035–4044. 2004

[Szidat *et al.* 2007] SZIDAT, S. ; S. H. PRÉVÔT, A.S.H. ; SANDRADEWI, J. ; RAMI ALFARRA, M. ; SYNAL, H.-A. ; WACKER, L. ; BALTENSPERGER, U.: Dominant impact of residential wood burning on particulate matter in Alpine valleys during winter. *Geophysical Research Letters* 34. 2007

[Tegen and Dörr 1996] TEGEN, I. ; DÖRR, H.: ^{14}C measurements of soil organic matter, soil CO_2 ans dissolved organic carbon (1987-1992). *Radiocarbon* 38. p. 247–251. 1996

[Thompson *et al.* 1995] THOMPSON, L.G. ; MOSLEY-THOMPSON, E. ; DANSGAARD, W. ; GROOTES, P.M.: The “Little Ice Age” as recorded in the stratigraphy of the tropical Quelccaya ice cap. *Science* 234. p. 361–364. 1995

[Usoskin 2008] USOSKIN, I.G.: A history of solar activity over millennia. *Living Reviews in Solar Physics* 5. 2008

[Wagenbach 2001] WAGENBACH, D.: *Environmental and climatic records from high elevation Alpine glaciers (ALPCLIM) - Final Report*. EC - contract: ENV4-CT-0693. 2001

[Wagenbach and Geiss 1989] WAGENBACH, D. ; GEISS, K.: *The mineral dust record in a high altitude Alpine glacier (Colle Gnifetti, Swiss Alps)*. In: Paleoclimatology and paleometeorology: modern and past patterns of global atmospheric transport, p. 543–564, Kluwer Academic Publishers. 1989

[Wagenbach *et al.* 1992] WAGENBACH, D. ; HAEBERLI (ED.), W. ; STAUFFER (ED.), B.: Special problems of mid-latitude gacier ice-core research. *In: Greenhouse Gases, Isotopes and Trace Elements in Glaciers as Climatic Evidence of the Holocene* Versuchsanstalt für Wasserbau, Hydrologie und Glaziologie der Eisgenössischen Technischen Hochschule Zürich. 1992

[Wagner 2005] WAGNER, G.A.: *Altersbestimmung von jungen Gesteine und Artefakten*. Enke-Verlag, Stuttgart. 2005

[Wagner 1996] WAGNER, S.: *Dreidimensionale Modellierung zweier Gletscher und Deformationsanalyse von eisreichem Permafrost*. VAW, ETH-Zürich. 1996

[van de Wal *et al.* 1994] WAL, R.S.W. van de ; ROIJEN, J.J. van ; RAYNAUD, D. ; BORG, K. van der ; JONG, A.F.M. de ; OERLEMANS, J. ; LIPENKOV, V. ; HUYBRECHTS, P.: From $^{14}C/^{12}C$ measurements towards radiocarbon dating of ice. *Tellus - Series B* 46. p. 94–102. 1994

[Wania *et al.* 1998] WANIA, F. ; HOFF, J.T. ; JIN, C.Q. ; MACKAY, D.: The effects of snow and ice on the environmental behaviour of hydrophobic organic chemicals. *Environmental Pollution* 102. p. 25–41. 1998

[Weissenbök *et al.* 1998] WEISSENBÖK, R. ; BIEGALSKI, S. R. ; CURRIE, L. A. ; KLINEDINST, D. B. ; GOLSER, R. ; KLOUDA, G. A. ; KUTSCHERA, W. ; PRILLER, A. ; ROM, W. ; STEIER, P. ; WILD, E.: ^{14} measurement of sub-milligram carbon samples from aerosols. *Radiocarbon* 40. 1998

[Weissenbök *et al.* 2000] WEISSENBÖK, R. ; CURRIE, L.A. ; GRÖLLER, C. ; KUTSCHERA, W. ; MAROLF, J. ; PRILLER, A. ; PUXBAUM, H. ; ROM, W. ; STEIER, P.: Accelerator mass spectrometry analyses of non-soluble carbon in aerosol particle from high Alpine snow (Mt. Sonnblick, Austria). *Radiocarbon* 42. 2000

[Whillans and Grootes 1985] WHILLANS, I.M. ; GROOTES, P.M.: Isotopic diffusion in cloud snow and firn. *Journal of Geophysical Research* 90. p. 3910–3918. 1985

[Wolff and Bales 1996] WOLFF, E.W. (ed.) ; BALES, R.C. (ed.): *Chemical exchange between the atmosphere and polar snow*. Springer Verlag. 1996

[Woon 2002] WOON, D.E.: Modeling gas-grain chemistry with quantum chemical cluster calculations I. Heterogeneous hydrogenation of CO and H_2CO on icy grain mantles. *The Astrophysical Journal* 569. p. 541–548. 2002

[Yankwich *et al.* 1946] YANKWICH, P.E. ; ROLLEFSON, G.K. ; NORRIS, T.H.: Chemical forms assumed by ^{14}C produced by neutron irradiation of nitrogenous substances. *The Journal of Chemical Physics* 14. p. 131–140. 1946

List of Figures

List of Tables

APPENDIX

A ^{14}C definition

The ^{13}C and ^{14}C ratio

^{13}C concentrations are given as the ratio of the number of ^{13}C atoms relative to the number of ^{12}C atoms:

$$^{13}R = \frac{^{13}N}{^{12}N} \tag{A.1}$$

The concentration of ^{14}C is given as the ratio of the number of ^{14}C atoms to the total number of carbon atoms in a sample

$$^{14}R = \frac{^{14}N}{^{12}N + {}^{13}N} \tag{A.2}$$

Note, that the contribution of radiocarbon atoms to the total number of carbon is neglected.

Carbon isotope ratios are reported in the δ-notation, denoting the relative deviation of the isotope ratio from a standard in ‰:

$$\delta^i C_{sample} = (\frac{^iR_{sample}}{^iR_{standard}} - 1) \cdot \ 1000 \ (i = 13, 14) \tag{A.3}$$

The international used standard for ^{13}C is the PDB (Pee-Dee Belemnite). The standard for ^{14}C is the NBS OxAI (Oxalic Acid) (Stuiver and Polach, 1977). $^iR_{sample}$ is always directly determined relative to the standard and neither $^{13}R_{standard}$ nor $^{14}R_{standard}$ is explicitly measured.

Definition of the fractionation

In general the three carbon isotopes and ^{12}C behave differently in various processes due to their different masses. This leads to the so called fractionation effect and changes the sample's isotopic signature. Thus the measured isotopic ratio deviates from the atmospheric value. Fractionation processes occur naturally during exchange between two reservoirs (e.g. transfer of CO_2 from air to biomass during photosynthesis) or during sample processing and measurement in the laboratory.

The isotopic fractionation factor α for the transition from one compound A into another compound B is defined as the isotope ratio ^{i}R (i = 13, 14) of compound B divided by the ratio of

compound A (Mook, 2000):

$$\begin{aligned} {}^{i}\alpha_{A\to B} &= \frac{{}^{i}R_B}{{}^{i}R_A} \\ &= \frac{{}^{i}\delta_B + 1}{{}^{i}\delta_A + 1} \end{aligned} \tag{A.4}$$

Note that δ is not given in ‰, but as its absolute small value.
The isotopic fractionation ϵ = α - 1 can then be determined by:

$$\begin{aligned} {}^{i}\epsilon_{A\to B} &= \frac{{}^{i}\delta_B + 1}{{}^{i}\delta_A + 1} - 1 \\ &\approx {}^{i}\delta_B - {}^{i}\delta_A \end{aligned} \tag{A.5}$$

The fractionation of ^{13}C and ^{14}C is correlated (Mook, 2000):

$${}^{14}\alpha_{A\to B} \approx ({}^{13}\alpha_{A\to B})^2 \tag{A.6}$$

δ^{13}C normalisation and the definition of Δ^{14}C

To allow direct comparison of radiocarbon concentrations from different origin and differently processed samples, a normalisation for fractionation processes is necessary. Assuming a carbon sample with the measured ratio ${}^{14}R_{meas}$ and the ^{13}C signature $\delta^{13}C_{meas}$, it is possible to calculate the normalised ratio ${}^{14}R_{norm}$, using the relationships derived above.

$$\begin{aligned} {}^{13}\epsilon_{meas\to norm} &= \delta^{13}C_{norm} - \delta^{13}C_{meas} \\ \Rightarrow {}^{13}\alpha_{meas\to norm} &= \delta^{13}C_{norm} - \delta^{13}C_{meas} + 1 \end{aligned} \tag{A.7}$$

$$\begin{aligned} {}^{14}R_{norm} &= {}^{14}R_{meas} \cdot {}^{14}\alpha_{meas\to norm} \\ &= {}^{14}R_{meas} \cdot ({}^{13}\alpha_{meas\to norm})^2 \\ &= {}^{14}R_{meas} \cdot ((\delta^{13}C_{norm} - \delta^{13}C_{meas}) + 1)^2 \\ &\approx {}^{14}R_{meas} \cdot (1 - 2 \cdot (\delta^{13}C_{meas} - \delta^{13}C_{norm})) \end{aligned}$$

Note, that in the calculations above the δ values are again given as absolute values.
For δ^{13}C in ‰, ${}^{14}R_{norm}$ is described as follows:

$${}^{14}R_{norm} = {}^{14}R_{meas} \cdot (1 - 2 \cdot \frac{\delta^{13}C_{meas} - \delta^{13}C_{norm}}{1000}) \tag{A.8}$$

With this correction, it is possible to define a new scale for reporting ^{14}C concentration: the Δ-notation of a sample describes the relative deviation of the sample ratio from a standard ratio, corrected for fractionation, in ‰ (Stuiver and Polach, 1977). This notation is the international used form for reporting ^{14}C concentrations.

$$\Delta^{14}C_{sample} = (\frac{{}^{14}R_{sample,norm}}{{}^{14}R_{standard,absolute}} - 1) \cdot 1000 \tag{A.9}$$

The ^{14}C absolute standard material is wood grown in 1890, age corrected for the reference year 1950. The nowadays used Oxalic Acid standard $^{14}R_{Ox}$ can be calculated back to the absolute standard by:

$$^{14}R_{standard,absolute} = 0.95 \cdot \ ^{14}R_{Ox} \cdot (1 - 2 \cdot \frac{\delta^{13}C + 19}{1000}) \cdot e^{\lambda(t-1950)} \tag{A.10}$$

The Oxalic Acid standard is in this connection conventionally normalised to δ^{13}C = -19‰. λ is the decay constant for radiocarbon and t the year of measurement.
$^{14}R_{sample,norm}$ is conventionally normalised to $\delta^{13}C_{norm}$ = -25‰:

$$^{14}R_{sample,norm} = \ ^{14}R_{meas} \cdot (1 - 2 \cdot \frac{\delta^{13}C_{meas} + 25}{1000}) \tag{A.11}$$

Another form for reporting ^{14}C concentrations is the pmC scale (**p**ercent **m**odern **C**arbon), which gives the normalised ^{14}C ratio relative to the absolute standard ratio for 1950 in percent (Stuiver and Polach, 1977).

$$pmC_{norm} = \frac{^{14}R_{sample,norm}}{^{14}R_{standard,absolute}} \cdot 100\ \% \tag{A.12}$$

The pmC value is correlated with the Δ-notation:

$$pmC_{norm} = \frac{\Delta\ ^{14}C}{10} + 100\ \% \tag{A.13}$$

Correcting and reporting ^{14}C-signatures in pmC

Concluding, this means, that for a carbon sample with a measured radiocarbon ratio $^{14}R_{meas}$ and a ^{13}C signature $\delta^{13}C_{meas}$ the following corrections have to be done:

1. The measured ^{14}C ratio has to be corrected for the measurement blank, which is determined independently.
$$^{14}R_{corr} = \ ^{14}R_{meas} - \ ^{14}R_{blank} \tag{A.14}$$

2. The correction for the fractionation is done using
$$^{14}R_{sample,norm} = \ ^{14}R_{corr} \cdot (1 - 2 \cdot \frac{\delta^{13}C_{meas} + 25}{1000}) \tag{A.15}$$
for the sample and
$$^{14}R_{standard,absolute} = 0.95 \cdot \ ^{14}R_{Ox} \cdot (1 - 2 \cdot \frac{\delta^{13}C + 19}{1000}) \tag{A.16}$$
for the standard.

3. This work reports its ^{14}C concentrations as f_m = pmC/100, which is calculated according to
$$pmC_{norm} = \frac{^{14}R_{sample,norm}}{^{14}R_{standard,norm}} \cdot 100\ \% \tag{A.17}$$

B DOC analysis systems

B.1 The DOCster

A detailed description about the DOCster DOC measurement system is given in Stricker (2008).

The Phoenix 8000 is a commercial system for the quantification of TOC and TIC in liquid samples from the Firma Teledyne Tekmar. The DOC is converted to CO_2 by UV-induced oxidation and degassed by purging the sample with clean synthetic air. The CO_2 is measured by leading the gas stream through a non-dispersive infrared detector (NDIR).

Table B.1: Specification of the Phoenix 8000 system given by Teledyne Tekmar.

method	UV induced photo-chemical oxidation with persulfat
detector	non-dispersive infrared detector (NDIR)
measurement parameter	TOC (NPOC), TC-IC, TC, IC, (POC optional)
analysis	detection limit: 0.5 ppb
maximal concentration	10 000 ppm (depending on sample volume and dilution)
accuracy	2% RSD or CV, $\pm$ 1 ppb or $\pm$ 0.02 μgC depending on the purity of cleaning water, reagent and purging gas cleanliness of sample bin as well as the sample matrix
sample volume	500 μl to 20 ml
time of analysis	4 to 8 minutes
data processing	real time display of measurement curve

Figure B.1 illustrates the main component of the Phoenix 8000 system for DOC analysis.

Stricker (2008) adapted the measurement principle to allow DOC analysis of small ice samples and renamed the system **fig:DOCster**. The standard measurement procedure after the adaption can be summarised as follows:

- charging the IC- and UV-reactor with 4 ml clean water and 0.5 ml acid respectively
- determination of the base line signal from the IC-reactor
- exhaustion of the IC-reactor

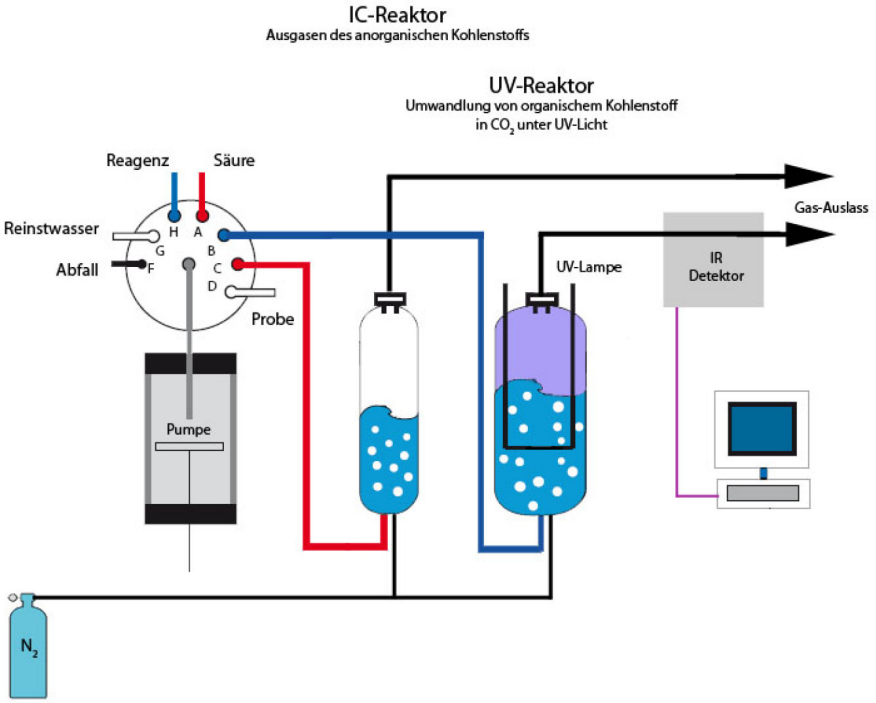

Figure B.1: Illustration of the DOC measurement system Phoenix 8000. Figure taken from Stricker (2008).

- charging the IC-reactor with 4 ml sample volume and 0.5 ml acid
- purging with clean synthetic air and waiting for complete IC degassing
- determination of the base line signal from the UV-reactor
- transfer of the sample from the IC- into the UV-reactor
- purging with clean synthetic air and waiting for complete UV-oxidation and CO_2 degassing

During the whole procedure, the UV lamp is on, the sample and acid volume can be adjusted and the total time of analysis is now 15-20 min. Measurements of artificial and real samples gave a detection limit of 5 ppb, a relative measurement error of 12 - 4 % for typical Alpine ice DOC concentrations and a oxidation efficiency of over 80 %.

B.2 The WALTER

For a more detailed description on the WALTER DOC quantification system see Schock (2001) and Greilich (1998).

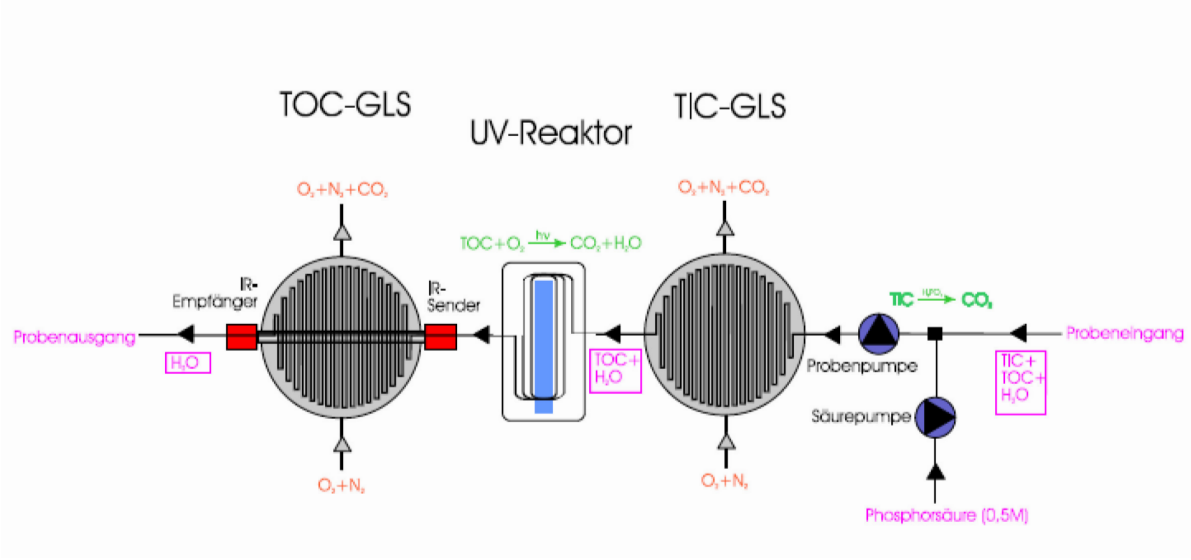

Figure B.2: Illustration of the DOC quantification system WALTER. Figure taken from Schock (2001).

The UltraTOC system, measures DOC in a water stream by UV-induced wet-chemical oxidation and degassing through semi-permeable membrane. The system was originally intended as a continuous flow system, but to reduce the necessary sample mass, a sample loop was installed and the system renamed WALTER.
In this flow-through system, the acid and persulfate is added to a liquid sample stream before it enters a gas-liquid separator. This separator consists of an stainless steel housing with a meandering circuit bordering at one side on a hydrophob, semipermeable membrane. The CO_2 diffuses due to the concentration gradient through the membrane into a clean gas stream. After thus removing IC, the stream passes a UV-lamp before entering a second gas-liquid separator. The extracted CO_2 is then quantified by leading the carrier gas stream through a NDIR CO_2 detector.

The efficiency of the WALTER is about 100 % for simple organic molecules, like oxalate, phtalate and saccharose. For humic acid the efficiency is only 40 to 50 %. The detection limit was smaller than 10 ppb and the total time of analysis around 10-15 min.

B.3 Schema of the extraction system

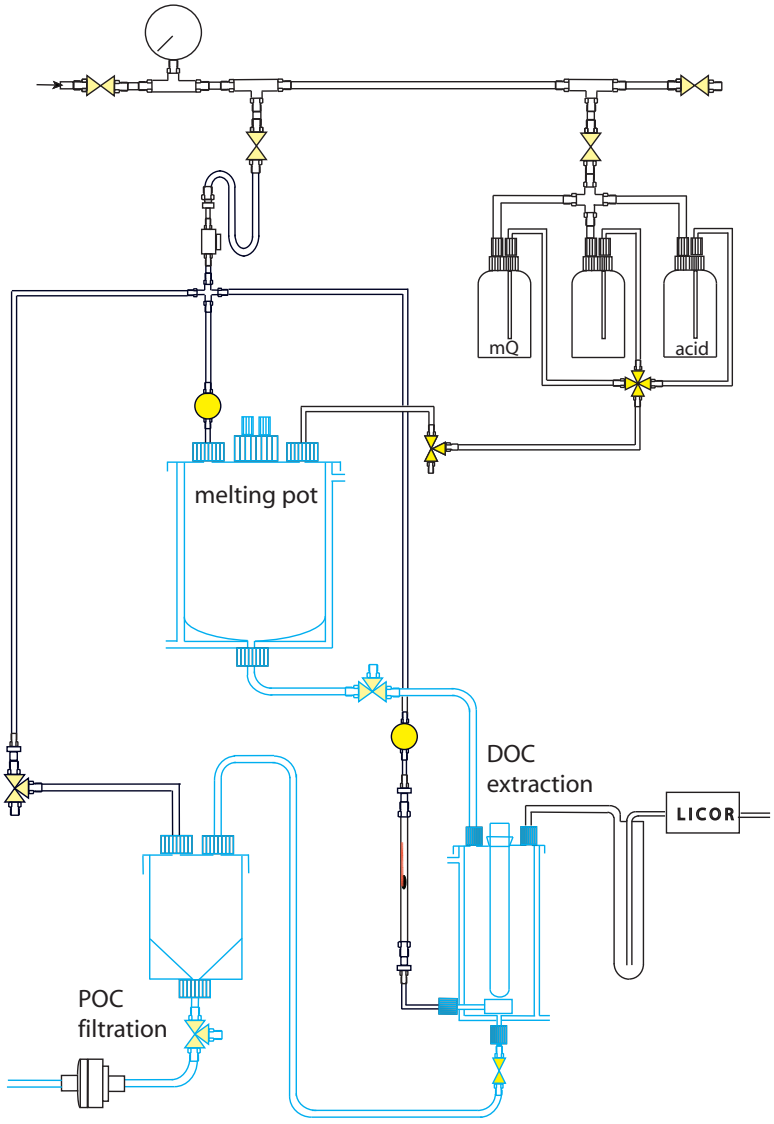

Figure B.3: Illustration of the complete DOC / POC extraction system.

C Efficiency of POC filtration

Filtration of clean water resulted in an increase of particle concentration for both filter types, probably due to dust on the filter or in the surrounding air and, in case of the quartz filter, due to quartz fibers. These background values were subtracted from the granite solution measurement. Surprisingly, for both filter mediums a filtration efficiency of only 80% was found. This proofs the poor particle extraction efficiency already stated above and gives no advantage for one medium.

Table C.1: Filtration efficiency for mQ water and a granite solution.

	quartz filter			silver filter		
	c [$\frac{part}{ml}$]	V [ml]	v [$\frac{ml}{min}$]	c [$\frac{part}{ml}$]	V [ml]	v [$\frac{ml}{min}$]
mQ before	140 ± 80	650	-	100 ± 20	650	-
mQ after	1300 ± 250	650	325	360 ± 100	350	17.5
granite before	42500 ± 1800	650	-	28000 ± 1500	650	-
granite after	9200 ± 650	300	15	5500 ± 600	150	7.5

D Tables of measured sample data

Table D.1: Parameter of KCI samples (mass and ^{14}C values are uncorrected).

core number	sample name DOC	sample name POC	preparation date	extracted volume [ml]	VERA number	graphitisation date	m_{VERA} [μgC]	Δm_{VERA} [μgC]	$\delta^{13}C$ [‰]	f_{meas}	Δf_{meas}	depth [m w.e.]	
KCI-32	**171**		29.06.09	500	**V50300**	Aug. 09	51.8	0.6	-19.6	0.958	0.006	17.75	0.13
KCI-32	**143**		07.04.09	300	**V50214**	06.05.09	42.3	0.5	-17.2	1.053	0.012	17.98	0.11
KCI-32		**042**	07.04.09	300	**V50245**	17.05.09	6.2	0.1	-12.9	0.688	0.013	17.98	0.11
KCI-42	**144**		08.04.09	340	**V50215**	07.05.09	35.5	0.4	70.0	0.434	0.032	25.44	0.14
KCI-42		**043**	08.04.09	340	**V50246**	17.05.09	11.3	0.2	-19.0	0.629	0.007	25.44	0.14
KCI-51	**145**		09.04.09	320	**V50216**	05.05.09	22.7	0.3	-7.5	0.856	0.013	31.98	0.12
KCI-51		**044**	09.04.09	320	**V50247**	17.05.09	7.2	0.1	-14.8	0.695	0.014	31.98	0.12
KCI-54	**148**		15.04.09	295	**V50217**	05.05.09	21.0	0.3	-17.7	1.011	0.019	34.71	0.12
KCI-54		**045**	15.04.09	295	**V50248**	20.05.09	7.4	0.2	82.0	0.553	0.025	34.71	0.12
KCI-63	**149**		16.04.09	300	**V50218**	06.05.09	37.2	0.4	-11.6	0.996	0.011	40.92	0.10
KCI-63		**046**	16.04.09	300	**V50249**	20.05.09	14.6	0.2	-24.0	0.753	0.008	40.92	0.10
KCI-67	**150**		17.04.09	330	**V50219**	05.05.09	15.6	0.2	-22.5	0.932	0.017	43.32	0.13
KCI-67		**047**	17.04.09	330	**V50250**	20.05.09	8.4	0.2	-15.3	0.556	0.008	43.32	0.13
KCI-72	**151**		20.04.09	280	**V50220**	06.05.09	24.4	0.3	6.7	0.676	0.010	46.39	0.09
KCI-72		**048**	20.04.09	280	**V50251**	21.05.09	7.5	0.2	-20.0	0.660	0.013	46.39	0.09
KCI-73	**153**		21.04.09	290	**V50221**	07.05.09	38.6	0.4	-20.0	0.830	0.010	47.46	0.09
KCI-73		**049**	21.04.09	290	**V50252**	21.05.09	7.7	0.2	-18.0	0.627	0.010	47.46	0.09
KCI-74	**168**		02.07.09	400	**V50305**	Aug. 09	58.9	0.7	-18.7	0.816	0.005	47.72	0.12
KCI-74	**154**		22.04.09	300	**V50222**	07.05.09	45.1	0.5	-17.1	0.818	0.009	47.93	0.09
KCI-74		**050**	22.04.09	300	**V50253**	21.05.09	9.6	0.2	-18.0	0.696	0.015	47.93	0.09

Table D.2: Parameter of KCS and KCH samples (mass and ^{14}C values are uncorrected).

core number	**sample name**		**preparation date**	**extracted volume [ml]**	**VERA number**	**graphitisation date**	$\mathbf{m}_{VERA}$ **[μgC]**	$\Delta\mathbf{m}_{VERA}$ **[μgC]**	δ^{13}**C [‰]**	$\mathbf{f}_{meas}$	$\Delta\mathbf{f}_{meas}$	**depth [m w.e.]**	
	DOC	**POC**											
KCS-79 (I)		**x**	21.01.09	250	**V50162**	04.02.09	9.6	0.2	-3	0.761	0.019	55.19	0.14
KCS-79 (I)	**x**		21.01.09	250	**V50163**	31.01.09	40.7	0.5	-32.5	0.745	0.007	55.19	0.14
KCS-95 (I)		**x**	22.01.09	290	**V50164**	04.02.09	10.4	0.2	-12.1	0.657	0.010	68.18	0.14
KCS-95 (I)	**x**		22.01.09	290	**V50165**	31.01.09	66.8	0.8	-26.8	0.454	0.005	68.18	0.14
KCS-95 (II)	**167**		25.06.09	350	**V50303**	Aug. 09	43.0	0.6	-18.8	0.966	0.009	68.46	0.14
KCS-107 (II)	**166**		24.06.09	200	**V50301**	Aug. 09	50.8	0.3	-12.2	0.474	0.005	78.32	0.10
KCS-108 (I)		**x**	23.01.09	145	**V50166**	04.02.09	19.3	0.3	-27.7	0.343	0.006	78.54	0.12
KCS-108 (I)	**x**		23.01.09	145	**V50167**	31.01.09	106.4	1.3	-25.1	0.204	0.002	78.54	0.12
KCH-43	**157**		24.04.09	300	**V50223**	12.05.09	47.0	0.5	-19.8	1.002	0.011	22.93	0.09
KCH-43		**53**	24.04.09	300	**V50254**	22.05.09	10.4	0.2	-20.1	0.789	0.016	22.93	0.09
KCH-62	**158**		25.04.09	305	**V50224**	12.05.09	86.3	1.0	-20.0	0.677	0.007	36.42	0.12
KCH-62		**54**	25.04.09	305	**V50255**	22.05.09	18.2	0.2	-21.8	0.866	0.008	36.42	0.12
KCH-70	**159**		27.04.09	290	**V50225**	12.05.09	58.8	0.7	-19.7	0.897	0.009	42.78	0.09
KCH-70		**55**	27.04.09	290	**V50256**	22.05.09	13.2	0.2	-22.6	0.796	0.008	42.78	0.09

Table D.3: Parameter of VCL samples (mass and ^{14}C values are uncorrected).

core number	sample name DOC	sample name POC	preparation date	extracted volume [ml]	VERA number	graphitisation date	m_{VERA} [μgC]	Δm_{VERA} [μgC]	$\delta^{13}C$ [‰]	f_{meas}	Δf_{meas}	depth [m w.e.]	
VCL-02		**CFA**	Jan. 09	60	**V50192**	09.02.09	11.8	0.2	1.4	0.714	0.013	0.44	0.21
VCL-04		**CFA**	Jan. 09	50	**V50193**	11.02.09	9.1	0.2	8	0.689	0.011	1.27	0.20
VCL-07		**x**	08.01.09	130	**V50168**	05.02.09	42.0	0.5	-33.6	0.582	0.007	2.67	0.09
VCL-7		**CFA**	Nov. 08	90	**V50150**	Nov. 08	25.0	0.3	-	0.618	0.008	2.92	0.33
VLC-09		**x**	09.01.09	126	**V50169**	05.02.09	86.8	1.1	-32.4	0.761	0.007	4.19	0.09
VCL-14		**x**	10.01.09	112	**V50170**	05.02.09	12.3	0.2	-24	0.536	0.007	6.99	0.09
VCL-21		**x**	13.01.09	137	**V50171**	30.01.09	39.6	0.5	-24.2	0.624	0.006	10.49	0.11
VCL-21/22		**CFA**	Nov. 08	100	**V50151**	Nov. 08	9.0	0.2	-	0.637	0.007	10.78	0.40
VCL-24/25	**135**		31.03.09	200	**V50226**	10.05.09	13.5	0.2	21.0	0.652	0.017	12.57	0.17
VCL-27		**x**	13.01.09	126	**V50172**	30.01.09	31.8	0.4	-27.4	0.757	0.010	14.01	0.09
VCL-30		**x**	14.01.09	120	**V50173**	01.02.09	17.8	0.3	-26.3	0.620	0.007	15.83	0.09
VCL-31	**136**		01.04.09	220	**V50227**	10.05.09	26.7	0.3	-28.5	0.603	0.013	16.58	0.18
VCL-34	**137**		02.04.09	230	**V50228**	10.05.09	17.2	0.2	7.5	0.632	0.016	18.17	0.17
VCL-35		**x**	15.01.09	132	**V50174**	30.01.09	57.7	0.7	-29.6	0.944	0.009	18.65	0.09
VCL-37	**139**		03.04.09	230	**V50229**	11.05.09	33.8	0.4	-19.1	0.931	0.014	19.92	0.18
VCL-38		**x**	15.01.09	125	**V50175**	09.02.09	13.0	0.2	-28.7	0.838	0.009	20.61	0.09
VCL-38		**CFA**	Jan. 09	100	**V50194**	01.02.09	15.3	0.2	-13.1	0.777	0.007	20.64	0.31
VCL-40		**x**	16.01.09	138	**V50176**	06.02.09	12.9	0.2	-23.1	0.824	0.009	21.53	0.09
VCL-40/41	**140**		03.04.09	230	**V50230**	11.05.09	32.7	0.4	-17.4	0.871	0.013	22.12	0.22
VCL-41		**x**	16.01.09	131	**V50177**	01.02.09	26.4	0.3	-23.1	0.871	0.008	22.42	0.09
VCL-42		**x**	17.01.09	122	**V50178**	06.02.09	100.3	1.2	-32.5	0.861	0.008	22.86	0.10
VCL-42/43	**141**		04.04.09	220	**V50231**	11.05.09	93.1	1.1	-15.0	0.833	0.010	23.13	0.18
VCL-44		**CFA**	Nov. 08	80	**V50152**	Nov. 08	29.0	0.3	-	0.682	0.006	23.60	0.29
VCL-45		**x**	Nov. 07	-	**V50117**	21.01.08	400.0	2.0	-28.2	0.444	0.003	23.95	0.05

Table D.4: Parameter of different ice samples from Col du Dôme (CDD and CDK), Grenzgletscher and Gornergrat (ice wedge) (mass and ^{14}C values are uncorrected).

core number	sample name DOC	sample name POC	preparation date	extracted volume [ml]	VERA number	graphitisation date	m_{VERA} [μgC]	Δm_{VERA} [μgC]	$\delta^{13}C$ [‰]	f_{meas}	Δf_{meas}
CDD 86a	**131**		26.03.09	365	**V50232**	08.05.09	74.0	0.5	-18.3	0.999	0.011
CDD 94	**132**		27.03.09	380	**V50233**	08.05.09	96.4	0.7	-15.1	1.183	0.015
CDD 105a	**133**		28.03.09	180	**V50234**	08.05.09	44.6	0.3	-21.2	1.203	0.014
Grenzgletscher		**small**	Nov. 08	100	**V50199**	02.02.09	10.8	0.2	4.6	0.511	0.013
Grenzgletscher		**large**	Nov. 08	500	**V50200**	02.02.09	9.9	0.2	4.5	0.697	0.009
Grenzgletscher	**127**		16.03.09	315			15.9	0.8	-13.0	0.885	0.026
Grenzgletscher	**169**		30.06.09	300	**V50298**	Aug. 09	40.0	0.5	-11.0	0.938	0.023
Grenzgletscher	**170**		01.07.09	600	**V50299**	Aug. 09	58.8	0.7	-20.4	1.063	0.009
CDK-183	**156**		23.04.09	100	**V50257**	15.05.09	56.4	0.7	-21.2	0.717	0.005
CDK-183		**52**	23.04.09	100	**V50258**	24.05.09	22.5	0.3	-22.1	0.617	0.005
Gornergrat-A		**x**	Nov. 08	-	**V50185**	29.01.09	10	0.2	-25.9	0.588	0.008
Gornergrat-B		**x**	Nov. 08	390	**V50186**	29.01.09	15.5	0.2	-25.8	0.319	0.005
Gornergrat-C		**x**	Nov. 08	-	**V50187**	29.01.09	11.5	0.2	-25.6	0.668	0.011
Gornergrat-B	**128**		17.03.09	300	**V50278**	11.05.09	106.0	1.0	-28.5	0.900	0.005
Gornergrat-B		**39**	17.03.09	300	**V50279**	11.05.09	46.0	0.5	-26.2	0.723	0.005

Danksagung

Ich möchte mich an dieser Stelle bei einigen Menschen bedanken, ohne deren Unterstützung diese Arbeit nicht möglich gewesen wäre:

Vor allem danke ich meinem Betreuter und Chef Dietmar Wagenbach für das Ermöglichen dieser Arbeit, für die kontinuierliche Unterstützung, die guten Ratschläge (auch wenn sie nicht immer befolgt wurden) und die unermüdliche Ausrichtung, wenn ich mal wieder vom Kurs abgekommen bin... frei nach dem Motto “Wer seinen Hafen nicht kennt, dem sind keine Winde günstig!”. Ich habe viel gelernt und bin um so manche Erfahrung und Lebensweisheit reicher geworden. Vor allem möchte ich mich für die moralische Unterstützung in den letzten Wochen dieser Arbeit bedanken, ohne die ich zeitweise wohl verzweifelt wäre.

Ich danke meinem “offiziellen” Doktorvater Prof. Dr. Werner Aeschbach-Hertig, für seine Bereitschaft dieses Amt zu übernehmen und meine Arbeit zu begutachten. Ebenso danke ich Prof. Dr. Augusto Mangini, dass er als mein Zweitgutachter diese Arbeit mit soviel Elan gelesen hat.

Weiterhin danke ich den Kollegen am VERA-Labor des Institut für Isotopenforschung und Kernphysik in Wien, besonders Dr. Peter Steier für das grundlegende Wissen zum Thema POC-Extraktion, die Einführung in die Graphitisierung und AMS Messung, sowie für ein stets offene Ohr für meine zahlreichen Fragen, wenn mein Wissen zum Thema ^{14}C erschöpft war.
Jakob Liebl und Roswitha Drosg danke ich für die Aufbereitung und Messung meiner Proben und für die unentbehrliche Unterstützung und Hilfestellung im Labor bei meinen diversen Besuchen in Wien.
Der Werkstatt des VERA-Labors danke ich für die ungehinderte Nutzung ihrer Gerätschaften und die stets freundliche Hilfe.

Ein besonders herzlicher Dank geht an meine Arbeitsgruppe für die unkomplizierte und klaglose Unterstützung bei allen Aufgaben und die heitere Stimmung in allen Lebenslagen. Pascal Bohleber möchte ich u.a. für die tatkräftige Unterstützung bei der Bohrung auf dem Murtel und für alle kleinen und großen Diskussionen rund um den Colle danken, Michael Mommert für die vielen klaglosen und lustigen Stunden im Kältelabor, Christoph Elsässer für das Lesen so manches schwierigen Kapitels und all die hilfreichen Kommentare zu meiner Arbeit, Rainer Stempel für die ^{210}Pb Messungen am VCL Kern und die “erhellenden” Gespräche im Labor, Phil Stricker für den Aufbau und die Programmierung des DOCster, der mir gute Dienste geleistet hat, sowie Kira Rehfelder und Helga Baus für die vielen gemeinsamen Stunden im Labor.

Michael Sabasch danke ich, dass er meine oft sehr unerwartet auftretenden Proben gemessen hat.

Nicht vergessen werden sollen die stets freundlichen und hilfsbereiten Mitarbeiter der IUP Werkstatt, die mir bei allen großen oder kleinen Problemen immer schnell und unkompliziert geholfen haben.

Bei Frau Inge Clos-Lieffertz, Frau Thomas und Frau Weirich möchte ich mich besonders für die Hilfe im Verwaltungsdschungel bedanken. Ohne ihre Hilfe hätte sich so manche verwaltungstechnische Aufgabe zu einem Sysyphus-Projekt ausweiten können.

Allen die diese Arbeit gelesen und korrigiert haben und somit am Erfolg (oder Misserfolg) indirekt beteiligt sind, gilt an dieser Stelle besonderer Dank. Es war sicher nicht immer einfach.

All meinen früheren und gegenwärtigen Bürokollegen danke ich für die anregenden und vielseitigen, physikalischen und nicht-physikalischen Gespräche, die fröhliche Stimmung und die oft dringend benötigten Kaffeepausen. Es wird sicher nie wieder etwas vergleichbares geben.

Meinen langjährigen IUP Kollegen und Freunden Ronny Friedrich, Sam Hammer, Tobias Naegler, Felix Vogel, Alexandra Herzog, Martin Wieser, Sylvia Lorenz sowie allen “Mensarianern” danke ich für die vielen professionellen und verrückten Gespräche, das Lachen und den Spaßin den letzten vier Jahren.

Meinen Studienfreunden Juliet, Christine, Dominikus und Daniela, danke ich für die wundervolle gemeinsame Zeit. Es war wirklich schön dieses Abenteuer Studium mit euch zu teilen. Wer weiSS wie lange ich ohne euch durchgehalten hätte.

Und nicht zuletzt danke ich meinen Eltern und meiner gesamten Familie, die mich bei all meinen Entscheidungen stets unterstützt haben und mir ermöglicht haben diesen Weg zu gehen.